Isolation and Characterization of Extracellular Vesicles Using Microfluidic Technologies

by

Ting-Wen Lo

A dissertation submitted in partial fulfillment
of the requirements for the degree of
Doctor of Philosophy
(Chemical Engineering)
in the University of Michigan
2020

Doctoral Committee:

Associate Professor Sunitha Nagrath, Chair
Associate Professor Deepak Nagrath
Associate Professor Timothy Scott
Associate Professor Greg Thurber

Ting-Wen Lo

tingwen@umich.edu

ORCID ID: 0000-0002-2127-2000

DEDICATION

To my parents.

ACKNOWLEDGEMENT

I would like to thank my advisor, Prof. Sunitha Nagrath, whose passion and insight in research has inspired me for the past five years. She has been a great mentor during my PhD study. This work would not have been done without her constant support and guidance. Her positivity and dedication to research has encouraged everyone else around her to do the same. I also greatly appreciate the help and support from all the brilliant members of the Nagrath group. I feel blessed to have had the opportunity to meet and conduct research with such brilliant people.

I am thankful to my committee members Dr. Greg Thurber, Dr. Timothy Scott, and Dr. Deepak Nagrath for their valuable feedback and guidance on my research.

I would like to thank Ziwen Zhu for being such a great friend and colleague. Thank you for answering all my questions and I greatly enjoyed my time working and chatting with you. I learnt so much from you.

I would like to thank Dr. Claudia Figueroa-Romero for being such a great collaborator. Thank you for spending countless time with me to work our projects.

I also greatly appreciate all the help and support from Dr. Eva Feldman, Dr. Junguk Hur, Dr. Ebrahim Azizi, and Dr. Shamileh Fouladdel.

I am deeply grateful to the Lurie Nanofabrication Facility (LNF) and the Michigan Center for Materials Characterization ($(MC)^2$) at University of Michigan. I am also grateful for the Rackham Conference Travel Grant.

I would like to thank my friends in Ann Arbor –Yufei Wei, Xiaowen Zhao, Xingjian Ma, Tianhui Ma, and Shujie Chen. I will miss you all.

Finally, I would like to thank my parents, the most important people in my life. Their endless support and unconditional love gave me the strength to face my fears and doubts over the years.

Table of Contents

List of Tables

List of Figures

ABSTRACT

Extracellular vesicles (EVs) are a group of heterogeneous plasma membrane-bound vesicles that are secreted by almost all cell types into extracellular space. EVs contain selected nucleic acids, proteins and metabolites that modulate biological activities after their internalization by recipient cells. Considerable efforts have been devoted to the study of EV-mediated communication among the cells. Such studies have demonstrated the importance of EVs in the spread of diseases. Pathological molecular cargos such as miRNA and proteins are shuttled via EVs into the circulation and are now known to be key players in progression of diseases. Therefore, isolating and subsequently accessing these bioactive vesicles can provide great insights into the diagnosis and prognosis of a patient's pathological status. A critical caveat to the study of EVs is their extremely small size and the potential rarity of target EVs in a background of off-target EVs. The objective of this thesis is the study on the roles of EV in human disease and development of microfluidic technologies and protocols to advance the isolation and characterization of EVs

First, an immuno-affinity based microfluidic device was introduced to study the role of EVs in amyotrophic lateral sclerosis (ALS). The device was adapted to isolate EVs from three types of tissues, namely serum, frontal cortex, and spinal cord from ALS patients and healthy controls. We compared miRNA cargo from diseased tissues including postmortem spinal cord and frontal cortex to healthy controls. As a result, we identified 60 miRNAs that are significantly altered in the patient,

suggesting the possibility for use of EV miRNAs as biomarkers for ALS patients. The pathway analysis of miRNA targets also pointed the involvement of EV miRNAs in the ALS.

Secondly, a microfluidic device, OncoBean chip is modified and optimized for high throughput EV isolation from cell culture supernatant and human plasma. The OncoBean Chip is a previously reported microfluidic device for isolation of circulating tumor cells (CTCs) with bean-shape microposts functionalized with biotin-conjugated EPCAM antibody. We modified this chip with the antibodies against common EV surface markers to achieve high throughput EV isolation. The high surface area provided by the bean-shaped miroposts and radial flow design facilitate capture of EVs not only at high flow rate (up to 10 ml/hr), but also form larger volumes of media form cell culture supernatant. Through desthiobiotin antibody capture and biotin elution, the device is able to release functional EVs from the device for cell uptake and identification of surface markers.

Thirdly, to address the need for technologies for high-resolution analysis, we established a workflow for simultaneous mutation detection and gene expression profiling with low sample-input. We developed the workflow from analyzing circulating tumor cells (CTCs) at a single cell resolution, aiming a future application to EV analysis. By integrating microfluidic technologies including the Labyrinth and Fluidigm C1 system, single CTCs from patients can be isolated and profiled for multiple characteristics. The feasibility of the workflow was validated with six non-small-cell lung cancer (NSCLC) patient diagnosed with epidermal growth factor receptor (EGFR) mutation. The intra- and inter-patient heterogeneity observed in single lung CTCs from patients demonstrated the utility of the proposed workflow.

Chapter 1

Introduction

1.1 Extracellular vesicles

Complex and well-orchestrated molecular mechanisms facilitate cell-to-cell communication, which is essential for cell functioning and the disruption of these mechanisms lead to disease. In addition to hormones, the immune response, and neurotransmitters, extracellular vesicles are now recognized as an important source of cellular communication. Extracellular vesicles (EVs) are lipid-bilayer-enclosed vesicles of 30-2000 nm in size that are secreted by most cell types into the extracellular space.[1] These tiny vesicles are considered to be powerful mediators that carry the signaling machinery necessary to reprogram the functions and behavior of the recipient cells.[2,3] Many types of genetic information, including miRNA, mRNA, and DNA are found in EVs and have roles in many cellular functions.[4] The transfer of these material have been proven to maintain biological activities after internalization by recipient cells.[5,6] Furthermore, EV cargoes have proven to be involved in the pathological progression of various types of diseases, making them the new possible biomarkers and therapeutic targets.[7-9] Therefore, due to their potentials as biomarkers for disease and application for therapeutics, the biological roles and clinical applications of EV is now widely investigated.

Based on the size and biogenesis, EVs are commonly categorized into three major subtypes: exosomes, microvesicles, and apoptotic bodies (Figure 1.1). Exosomes are vesicles of 30-200 nm in size that are formed intracellularly by the inward budding of cellular compartments known as multivesicular endosomes (MVE) and released to the extracellular space by the fusion of MVE with the plasma membrane.[10,11] Microvesicles are shed by direct budding of the plasma membrane.[12] Apoptotic bodies are generated and released during programming cell death.[13] Notably, there are still controversies in the nomenclature and size definition of different population of EVs, especially for microvesicles and exosomes.[2] This arises from overlaps in the biophysical characteristics and protein markers among the subtypes of EV. Although the International Society for Extracellular Vesicles (ISEV) has published a Minimal Information for Studies on EVs (MISEV) guidelines, there is still not a well-defined classification that encompasses the heterogenous EV populations.[14]

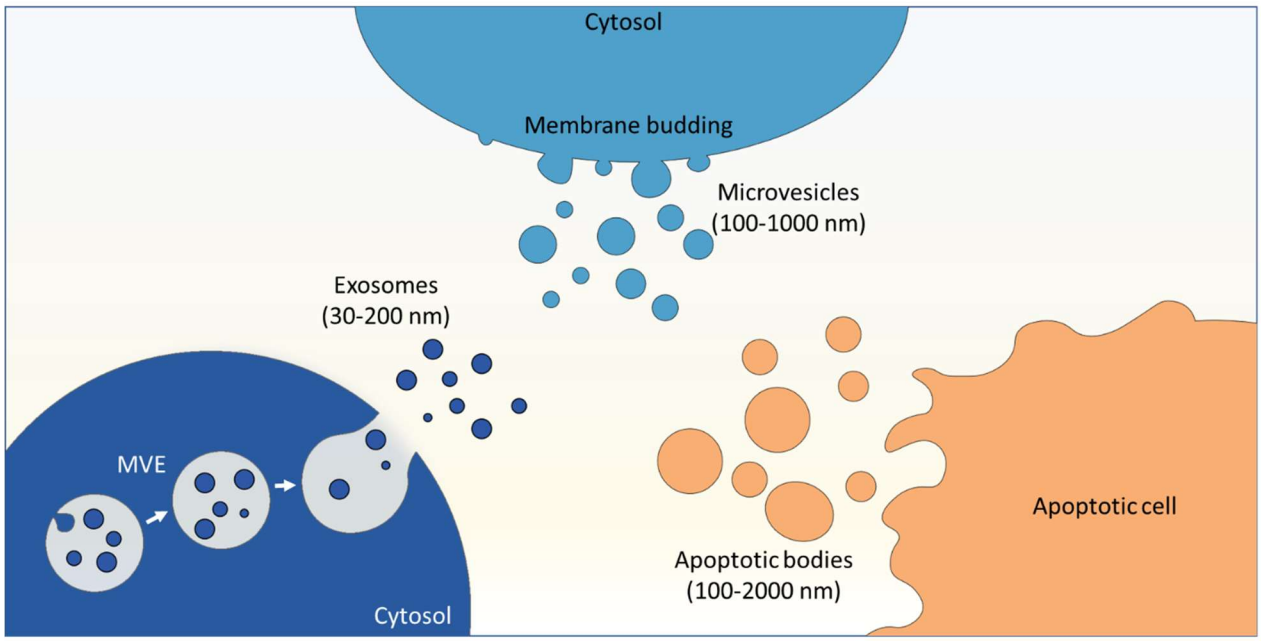

Figure 1.1 Schematic representation of extracellular vesicles.
Generally, EVs can be classified into three categories. Exosomes (30-200nm) are formed by the inward budding of multivesicular bodies (MVE). MVE can fuse with the plasma membrane of the

cell and release the exosomes into extracellular space. Microvesicles (100-1000nm) are formed by direct budding of the cell membrane. Apoptotic bodies (100-2000nm) are released from apoptotic cells

Technically, the study of EVs is not a new field. Several decades ago, EVs were discovered and were thought to serve as shuttles for cells to get rid of unnecessary proteins and nucleic acids that were not able to be degraded by the cell's lysosomal system.[3] However, accumulating evidence has shown that EVs contain specifically selected RNAs, proteins, and metabolites that are representative of their originating cells, suggesting an important role as mediators in cell-to-cell communication.[15-17] For instance, Valadi et al. demonstrated the presence of EV mRNAs, which can be transported to target cells where they are translated into proteins.[6] EVs are largely released in body fluids and taken up by the specific recipient cells where they release their cargo. These cargoes have proven to be involved in prognosis of tumors and other pathologies, such as neurodegenerative diseases.[18-20] Therefore, the identification and characterization of EV cargo can provide valuable information about biological function as well as the detection, characterization, and monitoring of disease progression.

1.2 EVs and their role in cancer

Accumulating evidence have demonstrated the vital roles of EVs as mediators between tumor and tumor environment.[21,22] Various biomolecules, including proteins, lipids, metabolites, RNA, and DNA, carried by EVs throughout the circulatory system can be involved in cancer growth, metastasis and dissemination.[23,24] Therefore, the ability of EVs to shuttle the tumorigenic information from one cell to another and alter the behavior of the recipient cells makes them a promising tool for understanding and uncovering molecular mechanisms to cancer biology. Zhao et al. demonstrated that EVs secreted from cancer-associated fibroblasts could be taken up by pancreatic adenocarcinoma cells and upregulate their proliferation by inhibiting mitochondrial

oxidative phosphorylation.[21] Furthermore, the rich supply of metabolites in found inside EVs from fibroblasts can also act as a pool to supply the nutrient for cancer cells.[21] Similar observations were also reported for other types of cancer. EVs derived from fibroblasts in breast cancer stroma enhance cancer motility and metastasis by alternating autocrine Wnt-planar cell polarity (PCP) signaling.[25] Khazaei et al. have shown that miR-451 transferred by EVs from cancer-associated fibroblasts contributes to the migration and progression of esophageal cancer.[26]

Additionally, tumor cells can also alter the microenvironment via EVs to promote tumor proliferation, angiogenesis and metastasis.[27,28] Transforming growth factor β transferred by mesothelioma-derived EVs was found to induce the myofibroblast differentiation.[29] MiR-1247-3p shuttled by the EVs secreted by high-metastatic hepatocellular carcinoma cells can alter inflammatory genes in fibroblasts, promoting lung metastasis.[30] Moreover, the influence of tumor-derived EV is not limited to local tumor microenvironment. Melanoma-derived EVs are able to promote vascular leakiness at future metastasis sites by influencing bone-marrow progenitors.[31] EVs secreted by pancreatic cancer cells can induce pre-metastatic niche formation in the liver.[32] In total, studying the role of EVs and their associations with tumorigenesis can really provide opportunities to analyze the biological principles underlying the progression of cancer.

In addition to the contribution of EVs in pathological development, studies have also highlighted the significance of EV as diagnostic tools for cancer. Due to the presence of EVs in virtually all types of body fluid, EVs are viewed as potential resources of easily-accessible biomarkers.[33,34] For example, EVs in peripheral blood has been extensively investigated for cancer detection. Melo et al. have shown that measuring the levels of tumor-derived EVs has a superior specificity and sensitivity as a diagnosis tool compared to the measurement of the levels of carbohydrate antigen 19-9 (CA19-9), the clinical standard pancreatic adenocarcinoma biomarker.[35] Fu et al. observed a

higher concentration of EVs in serum of gastric cancer patients comparted to healthy controls.[36] In addition to the total concentration, the proteomic and genomic cargos of EVs have gained significant interest as potential biomarkers. Fibronectin, one type of extracellular matrix protein, in EVs has been shown to be a sensitive marker to detect early stage of breast cancer.[37] Niu et al. demonstrated the diagnostic value of EV-derived alpha-2-HS-glycoprotein in serum for non-small cell lung cancer.[38] Hao et al. reported the high sensitivity of EV mRNA in serum to detect the kirsten rat sarcoma viral oncogene homolog (KRAS) and B-raf serine/threonine kinase proto-oncogene (BRAF) mutation in patients with colorectal cancer.[39] Notably, the miRNAs in EV have also attracted the attention in cancer biomarker. The dysregulation of EV-derived miRNA in body fluids has been identified in various types of cancer, including bladder, brain, pancreatic, breast, and lung cancer.[40,41] For instance, EV miR-21 in the CSF are found to be significantly upregulated in glioma.[42] Bryant et al. showed that the abnormal levels of miR-141 and miR-375 in serum-derived EV can be a marker for the metastasis in prostate cancer.[43] In total, it is believed that that studying the role of EV and their associations with tumorigenesis can provide opportunities to analyze the biological principles underlying the progression of cancer.

1.3 EVs and neurodegenerative diseases

Neurodegenerative diseases are a devastating class of diseases caused by the progressive loss of function or structure of neurons and, in most cases, no efficient cures and therapies are available. Several neurodegenerative diseases, including Parkinson's disease, Alzheimer's disease (AD), and Amyotrophic lateral sclerosis (ALS) are classified as proteopathies, meaning the neurodegeneration is associated the with overexpression or aggregation of misfolded protein.[44,45] Research has suggested that the misfolded proteins might trigger synaptic dysfunction and neuron

apoptosis, leading to neurodegeneration.[46] However, the propagation mechanism of these pathological proteins across the cells and tissues are still poorly understood.

Recently, the association between EV and neurodegeneration has attracted special interest in the field. EVs have been shown to transport biological molecules, including protein, DNA and RNA, throughout the human body, facilitating cell-to-cell communication over long distances. The cargo carried by EVs has been demonstrated to support crucial cellular functions in CNS such as neurite outgrowth, synaptic activity and immune functions.[47-49] Additionally, recent studies have shown the ability of EVs to transfer across the blood brain barrier, suggesting that they facilitate communication between the peripheral tissues and central nervous system (CNS).[50,51] In addition to normal cellular functions, accumulating evidence has also suggested the important roles of EVs in the spread of pathological proteins and nucleic acids related to neurodegenerative diseases.[19,52] Considerable efforts have been made to decipher the roles of EVs in various types of neurodegenerative diseases.

1.3.1 EVs and Alzheimer's disease

Alzheimer's disease (AD) is one of the most common type of neurological disorder in which the progressive death of brain cells causes cognitive and behavioral impairment.[53] Although the major causes of AD still remain unclear, it is widely accepted that neuron death in AD is the direct consequence of either the aberrant accumulation of amyloid-β or abnormally hyperphosphorylated tau protein.[54] Growing evidence have suggested that EVs are the mediators of these two pathological proteins, regulating the AD pathogenesis. It was recently shown that the amyloid-β are released to extracellular space brains via EVs.[55] Saman et al. reported that tau can be released by neuroblastoma cells through EVs.[56] Furthermore, they also found that EV-derived tau is the

major source of CSF tau in patients, suggesting the involvement of EV in abnormal processing of tau in AD pathogenesis. In addition to proteins, several studies have suggested the potential of dysregulated miRNAs in EV as AD biomarkers. Abnormal levels of miRNAs in EV are observed in pathogenesis of many diseases including AD.[53] For instance, using Illumina deep sequencing, Lugli et al. performed miRNAs profiling on the plasma EV. They identified 20 dysregulated EV miRNAs, and seven of them can predict AD status with 83–89% accuracy.[57] All these findings indicate the essential role of EVs in AD propagation as well as their diagnostic value.

1.3.2 EVs and Parkinson's disease

Parkinson's disease (PD) is another common neurodegenerative disease characterized by the progressive death of dopaminergic neurons in the substantia nigra of brain.[58,59] The loss of dopaminergic neurons can result in motor deficiency and cognitive impairment in PD patients.[60] The aggregation and misfolding of α-synuclein protein have been associated with the death of dopaminergic neurons.[61] Emerging evidence has pointed to the involvement of EVs in the spread of pathological α-synuclein between neurons.[62] For instance, Emmanouilidou et al. demonstrated the secretion of α-synuclein by EVs in cell cultures and confirmed their influence on the neighboring neurons.[63] The α-synuclein in EVs has also been identified in various types of body fluids in PD patients, such as CSF, saliva, and blood.[64-66] Stuendl et al identified the presence of α-synuclein in EVs from CSF of PD patients.[64] They also showed that the level of EV α-synuclein in CSF can be biomarker for PD and dementia. Furthermore, the altered miRNA cargos shuttled by EV have also been considered as potential biomarkers. Cao et al. analyzed the miRNA content in EV isolated from serum and identified significant dysregulations of miR19b, miR24 and miR195 in patients with PD.[67] Therefore, profiling and analyzing EV cargos can provide valuable information to elucidate the progression and to find the biomarkers for PD.

1.3.3 EVs and ALS

ALS is a phenotypically and genotypically heterogeneous, terminal neurodegenerative disease characterized by motor neuron death and muscle atrophy.[68] ALS is thought to develop as a non-infectious prion-like disease. The misfolded proteins, such as transactive response DNA binding protein 43 (TDP-43) and superoxide dismutase 1 (SOD1), are found to be aggregated in motor neurons before neurodegeneration.[68,69] Some of these misfolded proteins, which have the ability to propagate by inducing misfolding of normal proteins like a prion, and are speculated to be the main cause of ALS.[70] Clinical and molecular observations indicate that motor neuron death proceeds in a patterned manner and pathological protein aggregates are secreted and then taken by other neuron cells.[71,72] However, the mechanisms underlying these processes are not fully understood.

The ability of EVs to carry information from one cell to another and promote the transportation of biological molecules can provide great opportunities to understand this intracellular transfer in ALS. Furthermore, in the nervous system EVs transport molecules between neuronal and non-neuronal cells and the cargo shuttled via EVs are able to cross the blood-brain barrier.[73] The discovery of pathogenic molecules, such as misfolded SOD1 and TDP-43, and the small RNAs (miRNAs) in EVs strongly imply the involvement of these vehicles in pathogenesis of ALS.[70,74] Thus, it is engaging to investigate the biological role and clinical relevance of circulating EV in ALS

1.4 EV isolation

High-purity EV capture would facilitate studies in EV biology, ranging from diagnostic applications to physiological functions. Additionally, high purity will reduce noise from

contaminating protein aggregates, thus leading to highly specific protein analysis. Conversely, contamination with non-vesicular proteins or other extracellular vesicles can lead to generation of false data and incorrect conclusions.

Many studies have focused on the enrichment and identification of EVs from body fluids for downstream analysis. Each of them exploits EVs' biochemical properties or physical properties, such as size, density, surface charge, and surface marker to separate EVs from interfering components in the sample.[75] The ideal technology should exhibit high efficiency isolation and enable downstream analysis to characterize the size, quantity, and cargos of EVs. Although several methods have demonstrated the ability to isolate EVs, they have associated drawbacks that can be improved upon.

1.4.1 Conventional EV isolation

1.4.1.1 Ultracentrifugation and ultrafiltration

Ultracentrifugation is the most common technology used for concentrating EVs, often in combination with sucrose density gradient that allows the relatively low density EVs to separate from the pellet (Figure 1.2A). It is a proven method which is used extensively to isolate EVs from multiple sample types including urine, whole blood and CSF.[76] However, the procedure is quite lengthy and the cumbersome protocol, which includes a series of centrifugations, requires a high amount of labor.[76,77] Additionally, the yield is relatively low as a result of material loss during the processes.[78]

Due to the fact that EVs are much smaller than other extracellular vesicles, isolation of the EVs based on size like ultrafiltration is a reasonable option (Figure 1.2B). The commercial kit ExoMir launched by *Bioo Scientific* take advantage of this size difference and uses two syringe filters to

capture the EVs and extract the RNA.[79] After the serum is pushed through the filters, the first filter removes the apoptotic bodies and microvesicles while the second filter captures all vesicles of diameter greater than 30 nm. Compared to ultracentrifugation, this method is relatively fast and easier to operate. Although the RNA from the EVs can be extracted from the second filter by lysing the captured vesicles with the provided reagents, the method is not able to reclaim purified intact EVs.[79] Additionally, the yield can still suffer from the tendency of EVs to aggregate.

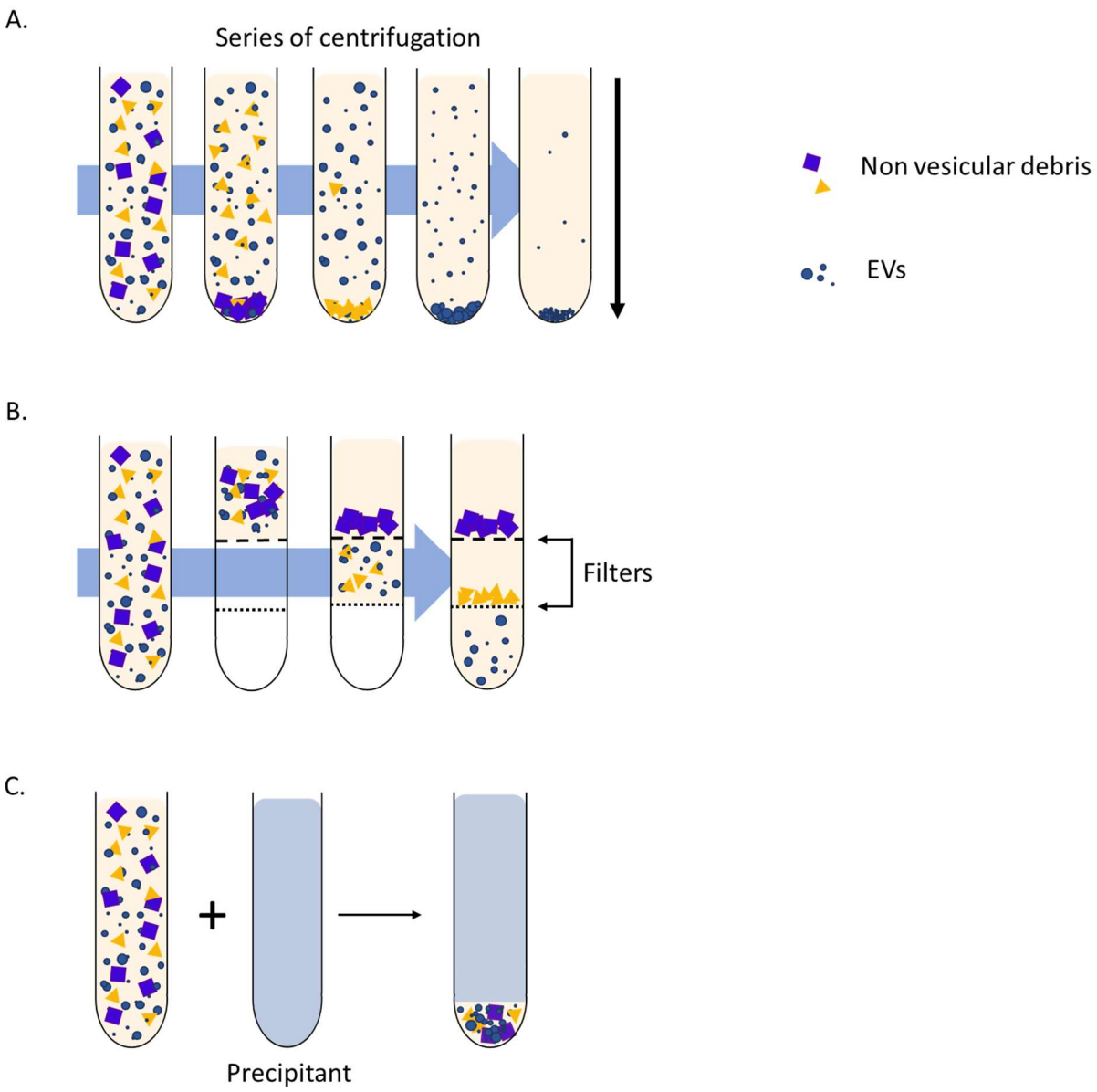

Figure 1.2 Conventional EV isolation techniques.
(A) Ultracentrifugation (UC) is the most common method for EV isolation. Series of centrifugation with increasing speed separates different size of EVs from the debris. **(B)** Ultrafiltration separates the EV by sizes. The non-vesicular debris are sieved from the EVs with filters. **(C)** Precipitation-based isolation ultlizes precipitants like PEG to concentrate all the particles in the samples. After adding the precipitants, the particles will sediment into pellets, which can be accelerated by centrifugation

1.4.1.2 Polymer-based precipitation

Precipitation-based technology is also commonly used for EV isolation. Typically, the introduction of the precipitant reduces the solubility of particles in the sample, and therefore the particles will sediment into pellets (Figure 1.2C). Although the application of this principle in isolating EVs is relatively new, commercial kits like ExoQuick and Total Exosome Isolation have demonstrated fast recovery of EVs from different body fluids.[80,81] Compared to the abovementioned techniques, these kits are easy to use and do not require advanced equipment. A complication is that the non-vesicular proteins can be co-isolated into the prep after precipitation, leading to contamination. It has been reported that although the yields of the RNA and proteins by precipitation is high, most of them are not from EV, which cause unwanted noise in the downstream analysis.[82] Therefore, an efficient and reproducible isolation method that supports the downstream analysis and clinical utilization of EVs is still necessary.

1.4.2 Microfluidic-based approaches s

In the past few years, microfluidic technologies have garnered special interest in their application to concentrate or isolate EVs. Microfluidic devices have enabled the development of unprecedented applications for medical diagnostics and body fluid analysis.[83,84] These devices have very small dimensions, facilitating minimized reagent volumes, isolation time, and procedural costs while enhancing the product purity and sensitivity.[83,84] Microfluidic isolation technologies are categorized by their use of i) physical or ii) chemical properties to isolate the EVs. The former isolates the EV based on their size, density, and surface charge while the latter relies on the expression of surface markers on EVs.

1.4.2.1 Physical-propertiy based approach

The use of EVs' physical properties allows for a label-free isolation, which overcomes biased EV selection based on specific biological properties. Furthermore, isolating EVs with label-free approaches typically avoid chemical binding to the surface of EVs, which permits greater flexibility for downstream characterization and use of EVs. Examples of these technologies include deterministic lateral displacement, microfilters, and nanowire trapping.

One such example was reported by Wunsch et al.[85] They devised a deterministic lateral displacement (DLD) device that enriched small EVs based on the size. The device was fabricated by silicon processes to produce a pillar array of uniform gap sizes, which determines a critical diameter Dc. Upon injection of the samples, particles with a diameter larger than Dc are displaced laterally and pushed to the side of the devices while the small EVs passed through device with streamlines of the fluid into the collecting channel. Similar system was also reported by Santana et al. Their DLD device can achieved high purity isolation of EVs (98.5 %), however with a low recovery efficiency. Although these devices demonstrated the isolation of selected size ranges EVs, they lacked performance evaluations with clinical samples to demonstrate the clinical applications. Wang et al. constructed a silicon nanowire with ciliated micropillar structures to trap vesicles ranging from 80 to 120 nm in diameter.[86] In operation, the porous microstructure of the pillar can capture the EVs while filtering out proteins and debris. Post capture, the immobilized EVs can be harvested by dissolving silicon nanowire with buffer solution. The authors demonstrated the ability of the device to isolate and harvest the small lipid vesicles (83 and 120 nm) from large polystyrene beads (500nm). However, the performance of the device was only validated with pre-purified vesicles and beads. Optimization with clinical samples and subsequent characterizations of the captured EVs are necessary for this approach.

Microfluidic filtration is another label-free EV separation technique. Generally, the microfluidic device is implemented with the nano-porous membrane with the pore size ranging between 100 and 1000 nm to separate different population of EVs from samples. For instance, Davies et al. developed a PMMA-based membrane sieve driven by pressure force applied by syringe pump to filter the EV from the blood sample.[87] In the cross-flow mode, the DC electrophoresis was used as an alternating driving force to push the particles across the membrane while sample and collection lines were injected at equal flow rates, preventing the clogging of pores. Liu et al. devised the Exosome Total Isolation Chip (ExoTIC), which targets small-sized EV.[88] The polyethersulfone (PES) filter sealed in the plastic gaskets separates the EVs from free nucleic acids, lipids, and other contaminating fragments. The clinical utility of the chip was also evaluated by applying different types of clinical sample, including plasma, urine, and lavage.

Although advancements in size-based and other physical separation approaches have allowed label-free isolation of EVs, they generally still suffer from limitations related to heterogeneity of EVs, the complexity of body fluids, and low throughputs. The contamination with cellular debris and proteins cause lower specificity and purity compared with the chemical properties-based systems. Moreover, these label-free technologies typically need pre-processing steps such as dilution and centrifugation prior the isolation, limiting their utilities in processing clinical samples.

1.4.2.2 Immuno-affinity approach

Immuno-affinity capture based microfluidic devices for EV capture serves as a superior approach for the specific isolation of target EVs. Typically, the immuno-affinity approach exploits selective antibody-antigen binding to capture vesicles based on surface antigens and extract them from body fluids, allowing for the specific and selective capture of extracellular vesicles of interest.[89,90] EVs from virtually all cell types are highly enriched in the tetraspanins family of proteins, including

CD9, CD63, CD81, and CD82.[91] The overexpression of these surface markers on EVs enables the capture of EVs with high selectivity by the corresponding antibodies.

Chen et al. led a pilot study that incorporated an immuno-affinity based microfluidic device for EV capture from plasma samples of pancreatic cancer patients.[90] The polydimethylsiloxane (PDMS) chamber of the chip was conjugated with anti-CD63 that captures EVs upon sample injection. The device allows for the recovery of RNA and protein cargo from EVs by injecting corresponding lysis reagent, demonstrating its potential for clinical application.(PMID: 20126692) This technology was further advanced by Kanwar et al who also used an anti-CD63 capture microfluidic device, but then also used fluorescent dye to stain the captured EVs to achieve an on-chip EV quantification.[89] Zhang et al. developed a microfluidic chip that contains 3D graphene oxide (GO)/polydopamine (PDA) microposts coated with capture antibodies. They demonstrated the use of the chip for studying EVs from ovarian cancer.[92] Chen et al. designed an integrated microfluidic system that isolates EVs directly from human whole blood with magnetic beads coated with anti-CD63.[93] The system incorporates a membrane-based filtration module for pre-isolation of the plasma from whole blood. This was followed by the introduction of magnetic beads to the plasma for subsequent purification of EV under a magnetic field. The system is also integrated with on-chip enzyme-linked immunosorbent assay for on-chip EV quantification.

Notably, EVs are heterogeneous collections of vesicles secreted by cells; based on the cell origin, each subgroup of EVs can have distinctive combination of surface markers. In addition to the tetraspanins family, different markers such as epithelial cellular adhesion molecule (EPCAM) and annexin have also been used for capturing specific EV populations. Dudani et al. designed a microfluidic platform that allows rapid isolation of EVs with magnetic beads coated with anti-EPCAM and anti-CD63. The device utilized the inertial lift forces induced by the rapid inertial

solution exchange to focus the EV-beads complex to collecting streamlines, achieving high-throughput enrichment of EVs from the waste components.[94] Kang et al. demonstrated the EV capture from blood of patients with non-small cell lung cancer (NSCLC) and melanoma using annexin V antibody.[95] They also showed that compared to CD63 antibody, annexin V antibody had a higher efficiency for EVs capture in non-small cell lung cancer.

In addition to surface protein, recent studies have shown that EVs have specific lipid composition signatures depending on their parent cells.[96] The enrichment of lipids, such as cholesterols, sphingomyelins and phosphatidylserine in EVs have been demonstrated.[97] Therefore, lipids on the plasma membrane of EVs have also been considered as potential targets for affinity-based isolation. Wataru et al. demonstrated the isolation of small EVs using magnetic beads conjugated with T-cell immunoglobulin mucin protein 4 (Tim-4) that captures the phosphatidylserine (PS) in the EV plasmas membrane.[98] With similar capture strategies, Huiying et al. devised a microfluidic platform, ExoPCD-chip, that isolates EVs with Tim-4 magnetic beads from serum.[99]

1.5 EV characterization

EV analysis offers valuable insights into pathogenesis and diagnosis of diseases. However, due to the extremely small size of EVs and the potential rarity of target EVs in a background of off-target EVs, such analysis can face technical and analytical challenges. With an increasing need for EV cargo characterization in biomedical research, numerous technologies have been developed for concurrent EV detection and cargo characterization. For instance, Ye Hu and colleagues describe a nanoparticle-enhanced scattering assay that enables the detection of EVs in blood plasma with high sensitivity and specificity and demonstrate its use in the diagnosis of pancreatic adenocarcinoma, with performance superior to the standard clinical biomarker.[100] Si-Yang Zheng

and colleagues report a lipid-nanoprobe approach that allows for the rapid, cheap and efficient isolation of nanoscale EVs, and that enabled the identification of DNA mutations in the genetic material of plasma-derived EVs isolated from non-small-cell lung cancer patients.[101]

Methods for characterizing EVs can be classified into biochemical and biophysical analysis approaches. Biophysical methods characterize the concentration, size distribution and morphology of EVs while the biochemical approaches analyze biological composition of EV and their contents including, nucleic acid, protein and lipids.

1.5.1 Biophysical approaches s

The biophysical analysis of EVs is typically done by nanoparticle tracking analysis (NTA), scanning/transmission electron microscopy, and atomic force microscopy.

1.5.1.1 Nanoparticle tracking analysis (NTA)

In NTA, the motion of EVs in the suspension is tracked by measuring the scatter of laser signals corresponding to EV motion. The NTA software analyzes the motion trajectories of the EVs and estimate the concentration and size based on the counts of particles per frame and Stokes–Einstein equation, respectively.[102] The detection range of NTA is between 10 and 1000 nm in diameter, which is suitable for EVs measurement. NTA is one of the most commonly used method to determine the concentration and size distribution of the EVs.[102,103] Commercial NTA instrument is available and easy to operate. However, NTA is not capable of discriminating EVs from other nanoparticles in the suspension. Although fluorescently labeling with antibody or membrane dye can be a possible solution, the measurement is still hindered by the noises from the excess dye.[103]

1.5.1.2 Scanning/transmission electron microscopy (SEM/TEM)

Electron microscopy (EM) is a commonly used technique for directly measuring the size and morphology of EVs. SEM accesses the specimen by scanning a focused electron beam onto the specimens. The interactions between the primary beams and the atoms on the surface of specimens results in the emission of secondary electrons. The images are then obtained by collected and translated these secondary electrons. Instead of detecting the secondary electrons, TEM depends on the transmitted electrons, the electrons that pass through the specimen, to produce an image. Since the wavelength of electrons is much shorter than visible light, SEM and TEM provide higher resolution than light-scattering techniques like NTA.[104] Moreover, EM coupled with immunogold labeling has proven to be useful to the identification of the markers, such as proteins and antigens, on EVs.[105] One of the limitations for EM is the sample preparation, which involves fixation and series of dehydration steps.[106] These steps can potentially alter the shape and size of EVs. Furthermore, EVs can be damaged by the high-voltage electron beams during the EM measurement.

1.5.1.3 Atomic force microscopy (AFM)

AFM is another powerful, high-resolution microscopy technique that allows for characterization of EV-sized nanoparticles.[107] AFM scans the interactions between a sharp probe tip at the end of a cantilever and the surface of specimen. The deflection of the probe tip caused by interaction forces is monitored by recording a laser beam reflected off the back of cantilever. The reflected laser beam is detected by a position sensitive detector to image the topology of the surface.[108] The most appealing feature of AFM is the ability to operate in normal conditions, such as air and liquids while EM requires vacuum condition for high-resolution imaging. Therefore, compared to EM, AFM prevents the fixation and drying procedure for sample preparation, which retains the shape

and surface structure of EVs. Like EM coupled with immunogold labeling, AFM is also able to examine the biochemical properties of EVs by introducing probe tips functionalized with antibodies. For instance, Sharma et al. reported the use of AFM to detect the CD63 antigens of EVs from saliva samples with probe tips functionalized with antiCD63.[109]

1.5.2 Biochemical approaches

Biochemical approaches analyze EVs to determine their protein or nucleic acid composition, either DNA or RNA. EVs harbor disease-related genetic and proteomic information, which can provide valuable insights to the disease progression

1.5.2.1 EV protein analysis

Flow cytometry

Flow cytometry is a commonly used technique that analyzes the surface protein markers expressed on EVs via fluorescent-conjugated antibodies.[110] Although flow cytometry provides high-throughput measurements and quantification of EV, it has a 300–400 nm limit of detection for sample diameter.[111] The scattering light signals of smaller-sized EVs are missed due to its overlap with background instrument noise. To overcome this limitation, beads coated with antibodies are often used to capture EVs and act as carriers for the flow cytometry analysis.[110] However, this method can potentially underestimate the concentration of EVs due to the multiple binding of EVs on the bead. Recent advance in flow cytometry have improved the detection limit, making the direct measurement on EVs possible. For instance, imaging flow cytometry (IFCM) has been shown to facilitate detection of EVs with sizes smaller than 300 nm.[112]

Immunoblotting and enzyme-linked immunosorbent assay (ELISA)

Immunoblotting, also known as western blotting, is an established technique for identification of EV proteins.[103] Typically, the lysis buffer containing protease inhibitors is used to lyse the plasma membrane of purified EVs and release the protein. After dilution with loading buffer and denaturation by heat, the protein lysate is separated by sodium dodecyl sulfate polyacrylamide gel electrophoresis (SDS-PAGE). The specific proteins can then be targeted with corresponding primary antibodies. The secondary antibody that recognized the host species of the primary antibody are then applied to bind the antigen of the primary antibody. The proteins are then identified by detecting the enzymes, such as alkaline phosphatase or horseradish peroxidase groups, conjugated on the secondary antibodies. Immunoblotting is a well-accepted method to verify the existences of EVs in the samples by detecting the presence of common EV markers such as CD9, CD63, CD81, Tsg101, and heat shock proteins.[113] Despite the simple procedure and reliable detection, immunoblotting requires potentially unachievably high concentrations to achieve detectable concentrations. This is a drawback in EV analysis since purification of EVs typically needs lots of samples and time. Furthermore, it lacks the ability to quantitatively analyze the proteins.

Enzyme-linked immunosorbent assay (ELISA) is a commonly used method to detect and quantify the proteins of EVs. The principle of an ELISA is similar to the immunoaffinity approach. The protein markers on the EVs are recognized and captured by the matching antibodies coated on the supporting substrates (usually polystyrene plates). These antibodies can be directly labelled with an enzyme or indirectly labelled with enzyme-conjugated secondary antibodies. The presence of EV proteins can then be verified by detecting the fluorescent or color change of the substrates triggered by these enzymes. Compared to immunoblotting, ELISA can provide a quantitative

information of the protein of interest. Furthermore, the ELISA is also a widely used technique to isolate EVs.[103] Commercial kits, such as ExoELISA and ExoQuant™, are available.

1.5.2.2 EV nucleic acid analysis

EVs harbor nucleic acids including DNA, RNA, and miRNAs that have been shown to be prognostic and diagnostic of many diseases, along with allowing for biological studies of EVs. Analyzing these cargos can be challenging, with the heterogeneity and limited amount making analysis extremely difficult. Technologies with high sensitivity and efficiency are required to examine the composition of nucleic acids in EVs.

Digital PCR

Digital PCR (dPCR) is a highly sensitive technology which enables detection and quantification of nucleic acid sequences. In dPCR, individual nucleic acid molecules are compartmentalized into an individual droplet through water-in-oil emulsion such that each droplet carry either no molecules or only a single molecule. Each droplet acts as an individual reaction vessel and the nucleic acid molecules are amplified and analyzed in parallel by performing standard PCR amplification (Figure 1.3). Unlike classical real-time PCR, the quantification of nucleic acids can be achieved solely by counting the fluorescence signals of each droplet using TaqMan or SYBR green assays, and thus producing highly sensitive mutation detection. Several studies have demonstrated the ability of dPCR to quantify and detect the nucleic acid cargos of EVs. For instance, Zhang et al. used dPCR to evaluate the performance of their microfluidic device by quantifying the mRNAs in captured EV.[114] Wang et al. compared the performance of dPCR and conventional qPCR with miRNAs of urinary EVs.[115] They reported that compare to conventional qPCR, dPCR has a higher sensitivity and consistency with diluted samples. Chen et al. demonstrated the use of dPCR to identify and quantify the mutated transcripts in EV mRNA from

CSF of glioma patients.[116] DPCR has been shown to be a fast and easy-to-use technique to detect the abundance in nucleic acid sequences with high sensitivity and specificity. However, dPCR is only able to detect known targets in the sample by choosing the corresponding assays. Furthermore, it is a low-throughput method as each test only allows for no more than 12 samples. Therefore, dPCR has been used as validating or monitoring method after the targets are determined by large-scale molecular technologies like sequencing.

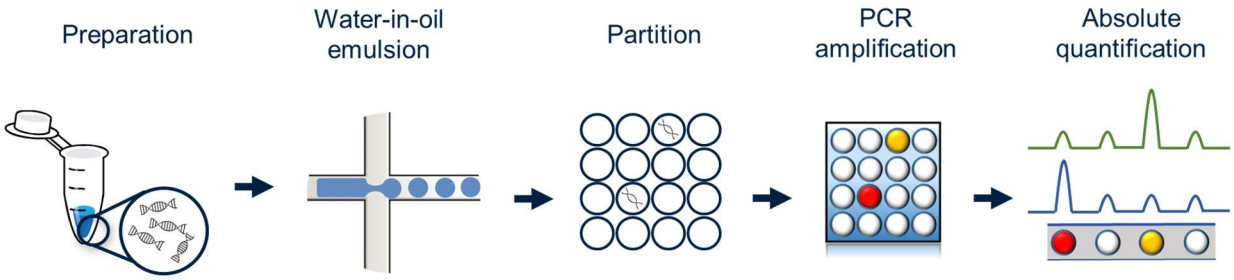

Figure 1.3 Schematic workflow of digital PCR (dPCR).
In dPCR, individual target molecules are compartmentalized into a individual droplet through water-in-oil emulsion such that each droplets carry either no molecules or only a single molecule. Each droplet acts as an individual reaction vessel and the target molecules are amplified and analyzed in parallel by performing standard PCR amplification. Unlike classical real-time PCR, the quantification of the target molecules can be achieved solely by discriminating the fluorescence signals of each droplet using probe assays such as Taqman and SYBR green.

Next generation Sequencing (NGS)

NGS is a high-throughput, reliable technique for quantitative characterization of mRNAs and miRNAs in EVs. It provides a comprehensive analysis on molecular signatures of mRNA and miRNA in EVs at single-base resolution. Typically, the small RNAs or miRNAs are reverse transcribed to cDNA molecules, followed by attaching the adapters or linkers to prepare the cDNA library with PCR amplification. The sequencing data are then generated with an NGS technology by aligning the sequences in the library with reference genome to determine the abundance of each

sequences in the sample. Several studies have demonstrated the use of NGS to identify aberrant mRNAs and miRNAs in EVs from various type of build fluids such as serum, urine, and CSF.[117] For instance, Rodríguez et al. isolated miRNAs from urinary EVs from prostate cancer patients and identified 5 dysregulated miRNAs using NGS.[118] Jin et al. identified several EV miRNA markers in serum for non-small cell lung cancer with NGS. They also demonstrated the diagnostic value of EV miRNAs to discriminate different subtypes of non-small cell lung cancer.[119] The main drawback of NGS is the potential bias caused by the amplification during the library construction. The bias between different library preparation protocols were also reported.[120] Furthermore, depending on the EV isolation method used, NGS can also be biased by non-vesicular contaminates remaining in the samples.[121]

Nanostring

NanoString is a digital counting technology that directly measures the expression levels of a broad range of mRNA or miRNA without cDNA synthesis and amplification.[122,123] It utilizes a pair of oligonucleotide probes, a capture probe and a reporter probe, that recognize and bind to the target genes (Figure 1.4). The reporter probes contain a barcode consisted of six fluorophores which can be four different colors. The biotin tag of the capture probe immobilizes the probe-gene complex on the slide coated with streptavidin through biotin-avidin binding, where the complexes are scanned by the fluorescent microscope. The genes are then quantified by directly counting the fluorescent barcodes, and therefore achieve absolute quantification without any amplification. The direct measurement prevents the bias induced by the amplification that is typically required for other PCR-based sequencing technologies. Therefore, NanoString can be a superior alternative for NGS to analyze low-abundance targets such as EV nucleic acid.

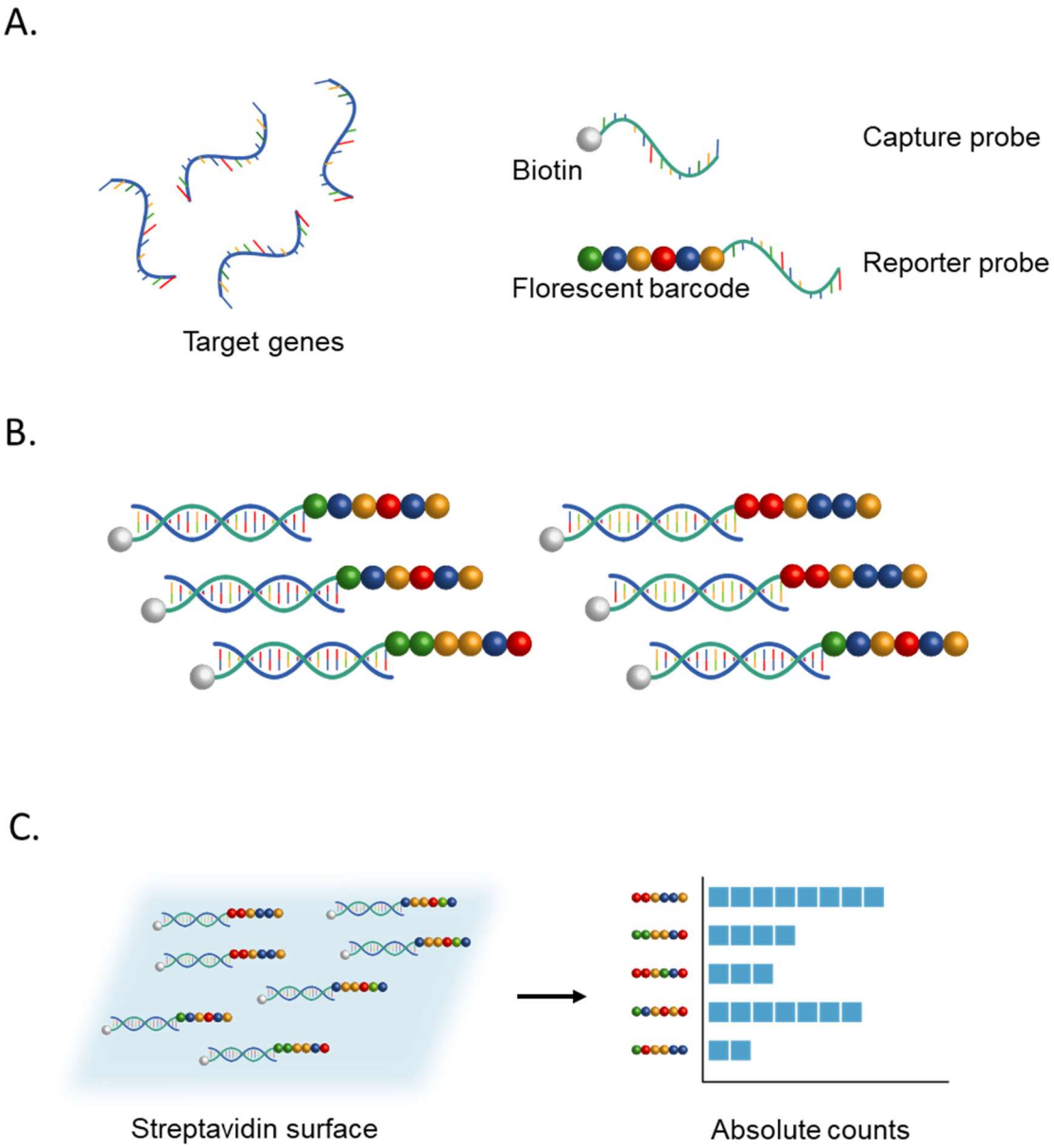

Figure 1.4 Principle of NanoString for nucleic acid quantification and profiling.
(A) The nucleic acid suspension is mixed with the capture probe and reporter probe. **(B)** The capture probes and reporter probes bind to the targets and form probe-target complexes. **(C)** The complexes are immobilized on the streptavidin surface through biotin-avidin binding for quantification. Subsequently, fluorescent barcodes are counted, getting the number of the corresponding target molecules

1.6 Summary

Over the past few decades, the field of EVs has been evolving rapidly. Significant efforts have been focused on investigating the role of EVs as mediators for disease progression and potential biomarkers. However, the study of EVs are still hampered by the lack of reliable and efficient methods for isolation and characterization. Microfluidic technologies have demonstrated great potential for isolating and characterizing EVs. Further studies and advancements of microfluidics technology will help broaden our understanding of EV function.

Chapter 2

Microfluidic Technologies for the Isolation and Characterization of Extracellular Vesicles and Evaluation of their Functional Role in Amyotrophic Lateral Sclerosis

2.1 Abstract

Amyotrophic lateral sclerosis (ALS) is a terminal neurodegenerative disease characterized by motor neuron death and muscle atrophy. Clinical and molecular observations suggest that ALS proceeds in a patterned and prion-like manner, perhaps driven by extracellular vesicles (EVs). EVs harbor, transfer, and spread molecules associated with ALS pathogenesis such as misfolded SOD1 and TDP-43 proteins as well as dysregulated microRNAs. However, the role of EVs cargo in ALS is still poorly understood. Immuno-affinity based microfluidic technologies have acquired special interest to concentrate and to isolate EVs. In this study, we investigated the EVs availability in ALS participants compared to healthy controls. Furthermore, we compared miRNA derived from EVs in frontal cortex, spinal cord and serum. We used an immuno-affinity-based microfluidic device, the ExoChip, for isolation and quantification of EVs. Furthermore, western blotting and electron microscopy were used for validation of vesicle isolation, and qPCR and NanoString profiling to evaluate EVs miRNA cargo. The pathway analysis of predicted miRNA target genes was performed to identify pathways that are commonly dysregulated among the frontal cortex,

spinal cord and serum. We demonstrated that miRNA cargo of circulating EVs may mirror the central nervous system disease state in ALS; therefore, EV miRNAs are potential biomarkers of ALS.

2.2 Introduction

Amyotrophic lateral sclerosis (ALS) is a heterogeneous terminal neurodegenerative disorder.[124-127] Neurodegeneration and voluntary skeletal muscle atrophy proceeds in a systematic manner resulting in respiratory failure and death within 3-5 years after symptoms onset.[128-130] The only interventions available for ALS include comprehensive patient care measures, Riluzole, and Edaravone.[131,132] However, these approaches provide limited improvement in patient survival due to unknow disease etiology and the lack of sensitive biomarkers for diagnosis, prognosis, and disease progression.[133]

Extracellular vesicles (EVs) are ubiquitously secreted membrane vesicles.[1,2] EVs contain molecular cargo from the releasing cell, they travel in the circulating system, and they are stable in various types of biological fluids and tissues.[134,135] In the nervous system, EVs may promote neurodegeneration by transporting and delivering aberrant molecules between neuronal and non-neuronal cells in a systematic and prion-like manner; therefore "spreading" the disease.[70,136-138] These tiny vesicles mediate cell function by carrying molecular machinery able change recipient cells behavior.[6,135] Genetic molecules, proteins, and metabolites are packaged in these vesicles and changes in their abundance are associated with health and disease in response to extracellular stimuli .[6,139,140]

Importantly, the cargo shuttled via EVs in the central nervous system is able to cross the blood-brain barrier; therefore, EVs and their cargo are attractive biomarker candidates for neurological

diseases.[141,142] Mobility, molecular mechanisms of action, and diagnostic implications of EVs and their cargo are not well understood in ALS. MicroRNAs (miRNAs) packaged in EVs have emerged as important biomarkers and pathophysiological candidates for neurodegeneration.[53,67,143] miRNAs are small noncoding RNAs that regulate gene expression post-transcriptionally by targeting and destabilizing multiple mRNAs; therefore, regulating physiological and pathological processes.[132,144-146] Dysregulated miRNAs levels in ALS biofluids and postmortem tissue suggest they have an important function in disease pathology.[147,148]

Microfluidic immunoaffinity technology has recently been developed to capture highly pure EVs using small amounts of bio-samples. This methodology utilizes an antibody that recognizes surface antigens on EVs to quickly and selectively isolate them from other sample components[84,90]. In this study, we optimized an immuno-affinity-based microfluidic device, the ExoChip[89] to isolate, characterize, and quantitate EVs and their miRNA cargo from ALS and control blood and frozen postmortem tissue. Our results indicate that miRNA cargo from circulating EVs reflect pathological signatures from diseased tissue.

2.3 Methods

2.3.1 Study participants and sample processing

ALS participants were recruited at the University of Michigan ALS clinic. The status of the ALS participants was determined by an ALS neurologist applying the revised EI Escorial Word Federation of Neurology criteria,[149] electromyography (EMG), and clinical and family history data. Age and sex-matched control participants. Control subjects were eligible to participate if (1) they did not have a diagnosis of ALS or other neurodegenerative condition, and (2) did not have family history of ALS in a first or second-degree blood relative. Participants older than 18 years of age

and/or next of kin provided informed consent. This research was approved by the University of Michigan Medical School Institutional Review Board.

Whole blood samples were drawn and collected in EDTA tubes. After centrifugation for 10 min at 2000 RCF, the top layer of plasma was collected. The plasma was mixed with an equal amount of Pacific Hemostasis Thromboplastin D (Thermo Scientific) and incubated at 37 °C for 15 min to coagulate plasma fibrinogen and clotting factors. The serum was obtained by collecting the supernatant and stored immediately at −80 °C.

For brain and SC, approximately 100 mg of motor cortex and 300 mg of SC were used to make tissue homogenates as previously reported.[150] Briefly, tissue was homogenized in 1ml of 1x PBS pH 7.4 supplemented with protease inhibitors (Roche Diagnostics, Mannheim, Germany; 1 tablet/10ml buffer) using a glass homogenizer (company). The tissue was sheered using a 26.5 gouge syringe and the homogenate was centrifuged at 300g for 10 min (max speed in microcentrifuge at 4 °C). The supernatant was filtered through a 0.2 um syringe filter (Millipore, Carrigtowhill, Cork, Ireland). A 1:10 dilution was used to determine protein concentration using BCA kit (Pierce/ThermoFisher, Waltham, MA USA).

2.3.2 Fabrication of SU-8 mold for the Exochip device

The mold for the polydimethylsiloxane (PDMS) device is formed from a negative photoresist SU-8 100 patterned silicon wafer using standard soft lithography techniques. SU-8 100 (Microchem. Corp., Newton, MA) was spin coated onto the silicon wafer at 2300 rpm for 60 seconds. This was followed by soft baking at 65 °C for 10 min and at 95 °C for 70 min. After UV exposure of the pattern onto the wafer for 12 sec using MA-6 aligner, the wafer was baked at 65 °C for 3 min and 95 °C for 10 min. The wafer was subsequently developed and rinsed with IPA to remove the

inactivated photoresist. The wafer was then hard baked for 3 min at 150°C. A post height of 50 μm was achieved.

2.3.3 Device fabrication and functionalization

The flow chamber of the chip was made from PDMS. Well-mixed PDMS and curing agent (10:1 ratio) were poured onto a SU-8 mold. The mold was then placed in a desiccator to remove bubbles. The polymer was solidified at 65 °C overnight in the oven. After baking, the polymer was peeled off from the mold and punched with tissue core for tubing. The PDMS chamber was bonded to a standard sized glass slide via plasma surface activation of oxygen. The device was immediately injected and incubated with 3-mercaptopropyltrimethoxysilane (Gelest) to make the surface hydrophilic. NeutrAvidin was conjugated to the chamber using the crosslinking agent GMBS (Pierce). The device was functionalized with the capture antibody immediately before capture by adding a biotinylated anti-CD63 (Ancell) the NeutrAvidin through biotin-avidin chemistry.

2.3.4 EV capture and on-chip quantification

EV isolation was based on the immuno-affinity approach reported by Kanwar et al in 2014. The functionalized devices was injected with biotinylated anti-CD63 solution in TBS containing 1% (w/ v) BSA to react with NeutrAvidin at room temperature for 1 hr. The devices were then blocked with 3% BSA-TBS solution infused at a flow rate of 50 μl/min for 10 min and then incubated for 20 min. Serum or homogenate of brain and SC samples (300~350 μl) derived from healthy volunteers or ALS patients were infused through the device at a flow rate of 6μl/min followed by a TBS rinse at a flow rate of 50 μL/min for 20 min. The device-immobilized EVs were stained with membrane dye for on-chip quantification or fixed for scanning electron microscope (SEM) or lysed for miRNA and protein extraction.

To label the captured EVs, the chambers were then flushed with fluorescent carbocyanine dye Vybrant™ DiO (Molecular Probes) at a flowrate of 20 µl/min for 10 min followed by incubation at 37 °C for 20 minutes for the DiO to stain the membrane of the EVs. Using BioTek-Synergy Neo multi-purpose plate reader, the fluorescent intensity can be measured at excitation wavelengths of 485 nm and emission wavelengths of 510 nm. The fluorescent intensities measured were normalized with the fluorescence intensity of background signals.

2.3.5 Scanning electron microscope (SEM) analysis of ExoChip captured EVs

EV immobilized within the device were fixed in 2% paraformaldehyde (PFA) in PBS for 20 min and then rinsed for 20 min with TBS. The samples were dehydrated in series of ethanol concentrations in distilled water (30%, 50%, 70%, 95%, and 100%) for 10 min at each step. For hexamethyldisilazane (HMDS) dry, the samples were immersed for 10 min in solution of 1:1 ethanol: HMDS and then transferred to 100% HMDS, followed by overnight air dry in the hood. The samples were then coated with gold by sputtering or carbon by thermal evaporation before imaging by FEI Nova 200 Nanolab Dualbeam FIB scanning electron microscope under low beam energies (2.0-5.0 kV) at the Electron Microscopy Analysis Lab (MC^2) at University of Michigan.

2.3.6 EVs size analysis

SEM micrographs were used to analyze EVs size. Image analysis was done using Metamorph (version 7.7.7. 0 Sab Jose, CA). Briefly, the threshold feature was used to identify EVs. After all objects were isolated, objects were verified using a filter for total area of EV and shape factor (0 indicates a straight line and 1 indicated a perfect circle). Objects smaller than 2000 nm^2 and with a shape factor smaller than 0.2 were discarded from the data set. Filtered data for total object area and shaper factor was logged in to excel and graphed. A linear mixed effect model with a random

patient intercept was used to take into account the correlated nature of the EV measurement (size) within patient. We evaluated difference in EV size between ALS and control patients using a likelihood ratio test.

2.3.7 Western blotting

To lyse the membrane of captured EVs, the chambers were flushed with radioimmunoprecipitation assay buffer (Sigma) at a flowrate of 20 μl/min and the protein will be collected from the outlet. The protein lysates were mixed with Laemmli sample buffer (Bio-Rad) and then heated at 95 °C for 3 min before separated by SDS-PAGE. The proteins were then transferred to the polyvinylidene difluoride (PVDF) membrane (Bio-Rad). The membranes were blocked with 5% milk/5% BSA in Tris-buffered saline containing 0.1% Tween-20 (TBST) for 1 hr at room temperature and then rinsed with TBST before incubated with primary antibodies diluted in TBST supplemented with 3% BSA. Subsequently, the membranes were washed with TBST and then incubated for 90 min with appropriate secondary antibodies diluted 1: 2000 with blocking buffer, as described above. After washing, the proteins were visualized using chemiluminescence and colorimetric detection kits (Bio-Rad).

2.3.8 RNA extraction and Nanostring miRNAs analysis

Total RNA from EVs was extracted from the device using Qiazol (QIAGEN). Qiazol eluted samples were vortexed for 15 min and incubated at room temperature for 5 min followed by the addition of chloroform (1/5 of Qiazol volume), vortexed for 15 sec, and incubated at room temperature for 3 min. The samples were centrifuged at 12k rpm for 15 min at 4 °C. RNA isolation was performed using Norgen columns (Norgen Biotek Corp., Thorold, ON, Canada) as indicated

by the manufacturer. The samples were eluted in 50 µl of DNAse and RNAse-free water and stored at -80 °C.

2.3.9 miRNA expression profiling and data analysis

EVs-contained miRNAs were profiled with the NanoString nCounter® Human v3 miRNA Expression Assay Kit (NanoString, Seattle, WA, USA) at the Genomics Shared Resource-Comprehensive Cancer Center at Ohio State University.[151] Each sample was scanned by the nCounter Digital Analyzer (NanoString) and expression data were extracted using the nCounter RCC Collector (NanoString).

For data analysis, overall quality of the expression data was assessed using nSolver™ Analysis Software v3.1 (NanoString) according to manufacturer's instruction. We performed principal component analysis (PCA) to visualize overall variation across samples. Then, two different software packages were used for DEmiRNA analysis: nSolver v3.1 from NanoString and NanoStringDiff, an R package specifically designed for NanoString nCounter data.[152] For nSolver analysis, nCounter data were normalized to the top 100 most highly expressed miRNAs and differential expression of miRNAs were examined using nSolver's differential expression testing menu between groups. Ratios of miRNAs between groups and statistical significance values (p-value) as well as False Discovery Rates (FDRs) were obtained. In the NanoStringDiff analysis, normalization of the data was done using positive controls, negative controls, and housekeeping genes embedded in the nCounter system. Differential analysis was also performed using NanoStringDiff and log fold-changes and multiple testing adjusted statistical significance values (q-value) were obtained. The significance cutoff for differential expression was FDR or q-value <

0.05. The dysregulated miRNAs identified by both nSolver and NanoStringDiff were deemed as DEmiRNAs in this study.

2.3.10 Pathway analysis

DIANA-miRPath v3.0 was employed to characterize the biological functions and pathways of the DEmiRNAs focusing on the Kyoto Encyclopedia of Genes and Genomes (KEGG) pathways.[153] KEGG pathways with FDR < 0.05 were determined to be significantly enriched among the DEmiRNAs from each tissue type (frontal cortex, spinal cord, and serum). To identify the overall theme of these enriched pathways, concept-similarity networks were generated based on their gene contents in these pathways using RichR, our in-house analysis R package (https://github.com/hurlab/RichR).

2.3.11 Statistical analyses

Fisher's exact test and student's t-test were used to determine demographic differences between cases and controls. Statistical analyses were done in GraphPad Prism v7 (GraphPad Software, La Jolla, CA, USA). Significance was defined as $P < 0.05$.

2.4 Results

2.4.1 Participants and samples

Frontal cortex (FC), spinal cord (SC), and serum were obtained from 15 ALS and 16 control participants (Table 2.1). For 11 of the ALS participants, all three tissues were collected from the same subject. ALS onset segment was limb for fourteen participants (93.33%) and bulbar for 1 participant (6.77%). In this study, we used a cohort of ALS subjects with no known familiar history of ALS or mutations in the *SOD1* gene or aberrant expansions in the *C9orf72* gene. Sex and age distribution were similar for ALS and control participants. All ALS participants were Caucasian,

while the control group consisted of fifteen Caucasian (93.75%) and 1 Back/African American (6.25%).

Table 2.1 Clinical characteristic of study participants

Characteristics		ALS group (n=15)	Control group (n=16)	*p*-value
Age (years)[a,b]		71.0, 64.4 ± 2.649, (47-80)	60, 66 ± 2.954, (49-85)	0.726[#]
Sex	Male	8 (53.33%)	9 (56.25%)	>0.99[¶]
	Female	7 (46.67%)	7 (43.75%)	
Onset	Bulbar	1 (6.67%)	-	
	Limb	14 (93.33%)	-	
PMI [b]*		13.73±2.11 h (n=11)	-	
Ethnicity	Caucasian	15 (100%)	15 (93.75)	
	Black/AA	-	1 (6.25%)	

(a) median; (b) mean ± standard error; (range); PMI, Postmortem Interval; *For autopsy tissue, no data available from one subject; AA, African American; [#]Student t-test, [¶]Fisher's exact test

2.4.2 Characterization of EVs captured by the ExoChip

The ExoChip integrates microfluidic technology and an immuno-affinity approach to isolate and characterize EVs. We previously demonstrated that the ExoChip is able to capture EVs from serum.[89] In this study, we refined the devise to compare EVs and their cargo from postmortem frozen FC, SC, and serum (Figure 2.1). Vesicle size and morphology of ExoChip captured EVs were assessed using scanning electron microscopy (SEM). EVs displaying typical spherical shape were observed with the anti-CD63 coated ExoChip, but not with the uncoated or PBS control; suggesting vesicle capture is specific (Figure 2.2A). The overall size of the captured vesicles from FC, SC, and serum ranged from 5.64 nm to 636.03 nm (213.78 ± 84.91 SD nm) in diameter.

Immunoblot analysis indicated that of ExoChip-captured EVs were positive for the EV marker CD9 (Figure 2.2C).

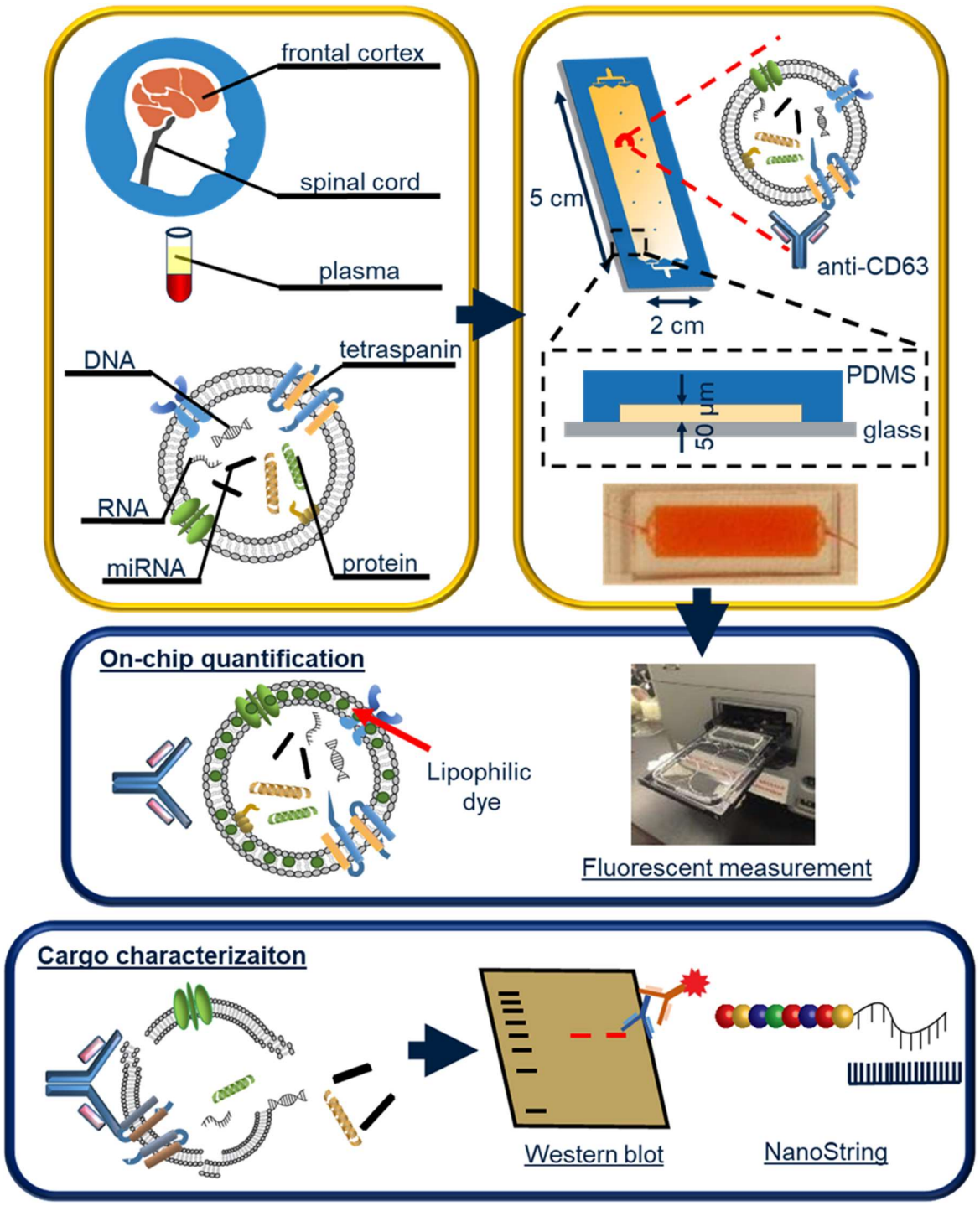

Figure 2.1 Workflow.
Extracellular vesicles (EVs) immobilization and characterization. EVs from FC, SC and serum from healthy or ALS subjects are captured by a CD63-antibody coated ExoChip. To quantify the captured EVs, the chip is processed with lipophilic (DiO) staining, and then measure the levels of fluorescently stained EVs by fluorescence intensity analysis. Immobilized EVs were analyzed by western blotting and EV cargo by NanoString.

2.4.3 EVs size and availability in sporadic ALS

We compared the EVs size from ALS and controls from frontal cortex, spinal cord and serum. The mean dimeter of EVs for FC was 255.07 ± 5.25 SEM nm for ALS and 245.86 ± 4.45 SEM nm for control; for SC, 193.92 ± 3.42SEM nm for ALS and 141.94 ± 2.59 SD nm for control and for serum, 187.12± 2.74 SEM nm for ALS and 247.33 ± 2.96 SEM nm for control (Figure 2.2B). Using a linear mixed model, we found significantly larger EVs in SC for ALS patients compared to control patients (P=0.03). This trend was reversed for serum, in which the size of EVs in ALS was smaller than that of controls (P=0.02). Finally, we did not detect a significant difference in size of EVs between ALS patients and controls in FC (P= 0.57).

To determine the abundance of EVs in ALS, we measured membrane associated lipids in EVs by fluorescence intensity assays. We observed a slight but no significant difference in the amount of EVs between ALS and controls (Figure 2.2D) in all samples, suggesting that the overall levels of EVs are not viable as biomarker for ALS.

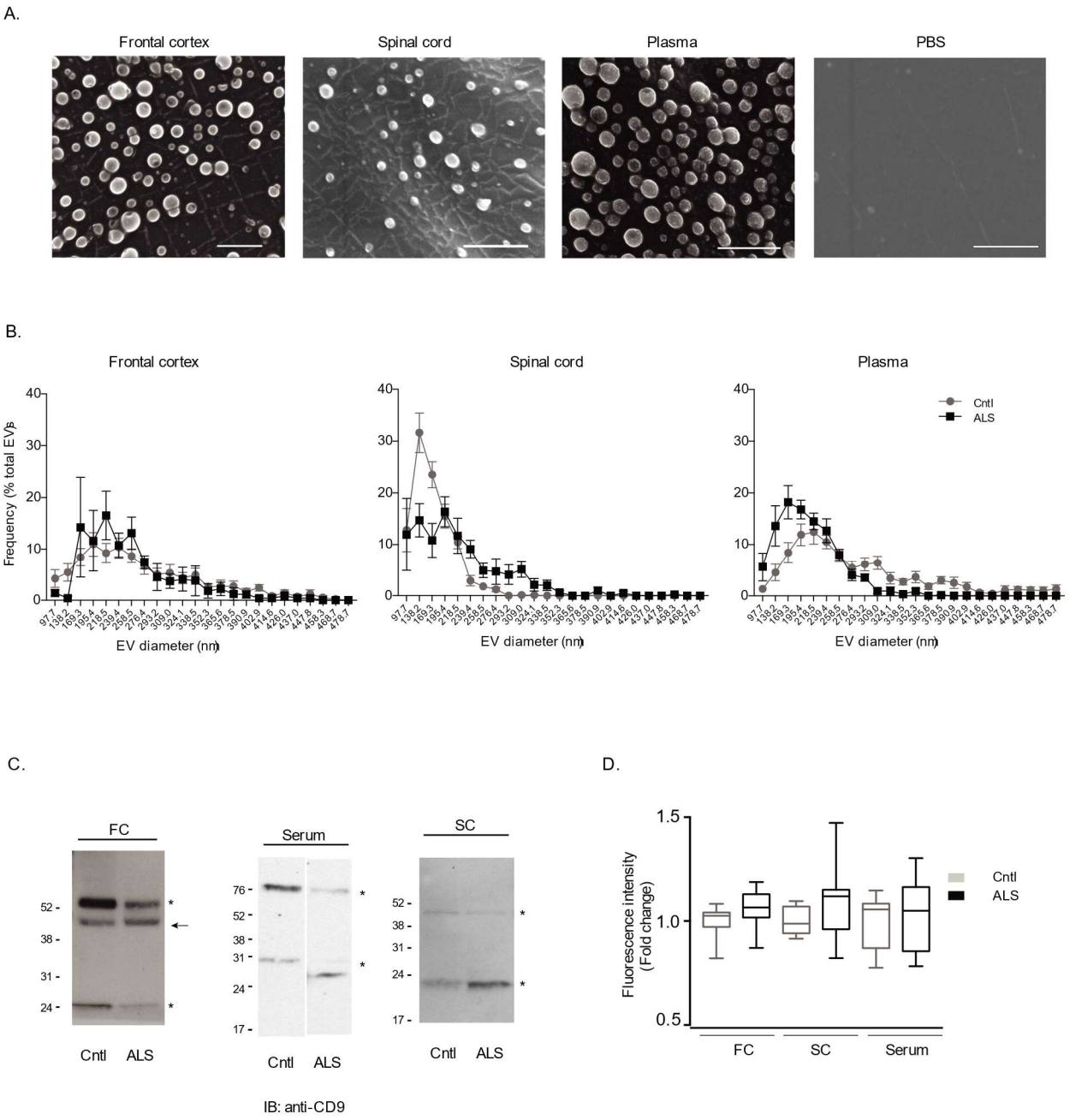

Figure 2.2 Characterization ExoChip captured EVs from frontal cortex (FC), spinal cord (SC), and serum of ALS and control (Cntl) subjects.

(A) Scanning electron micrograms (bars = 1 μm). **(B)** Size profile and frequency (%) by size (nm) of EVs measured with SEM images in **(A)**. ALS (black) and healthy controls (grey). **(C)** Protein characterization of ExoChip captured EVs from FC, SC, and serum using anti-CD9 antibody. **(D)** On-chip immobilized and purified EVs were labeled with a fluorescent lipophilic dye (DiO). The fluorescent intensity values obtained from the chip corresponding to healthy Cntls and cases were normalized against the background signal from the plate. Fold change is shown in a Min. to Max Wisker plot. FC (Cntl= 8, ALS=12), SC (Cntl= 6, ALS= 12), and Serum (Cntl= 9, ALS= 7).

2.4.4 EVs-contained miRNAs are dysregulated in ALS

Mature miRNAs contained in EVs from frontal cortex, spinal cord, and serum captured by the ExoChip were profiled by NanoString, which uses the probes conjugated with fluorescent barcodes and single molecule imaging to directly count miRNA copies.[154] Principal component analysis (PCA) indicates that EV-derived miRNAs from spinal cord and serum samples are clearly clustered by ALS or control, while frontal cortex EV-derived miRNAs are not (Figure. 2.3).

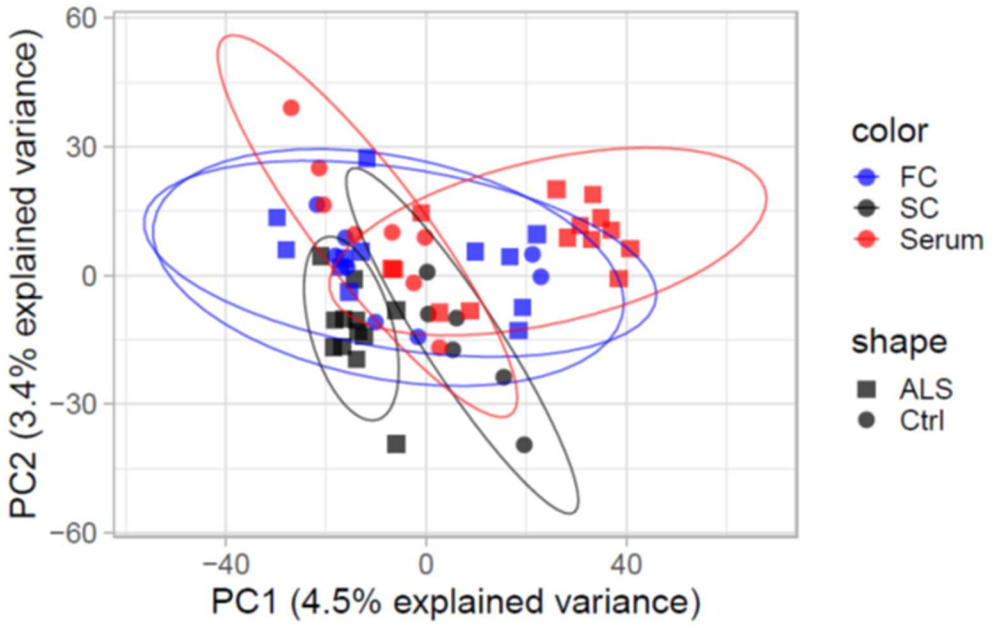

Figure 2.3 Principal component analysis (PCA).
The analysis was performed on EV miRNA data from spinal cord, frontal cortex and serum from ALS patients and healthy controls.

Significantly differentially expressed miRNAs (DEmiRNAs, $p<0.05$) in ALS compared to controls for each tissue were identified using a stringent pipeline in which DEmiRNAs overlapped with two independent platforms, nSolver and NanoStringDiff [152] (Figure 2.4A).

We observed an overall decrease in EV-derived miRNA levels in ALS frontal cortex and spinal cord compared to controls, while the opposite was observed for serum samples. In frontal cortex,

out of 11 dysregulated miRNAs, three of them show increased levels. In spinal cord, a total of 22 miRNAs were dysregulated with respect to control. The levels of 4 miRNAs were higher while 18 were lower in ALS. The opposite trend was observed in serum, where a total of 27 miRNAs had increased expression while 8 had decreased expression (Figure 2.4B-D). Five dysregulated miRNAs, miR-33b-5p, miR-122-5p, miR-664a-3p, miR-1268b, and miR-4286b, overlapped between serum and spinal cord; while only one miRNA, 185-5p was, dysregulated in both frontal cortex and spinal cord. Note that among all the 5 overlapped miRNAs, only miR-4286b is differentially expressed in the same direction in the tissues while the other four dysregulated in the opposite direction. We did not identify a common changing miRNA between the three tissues analyzed (Figure 2.4E).

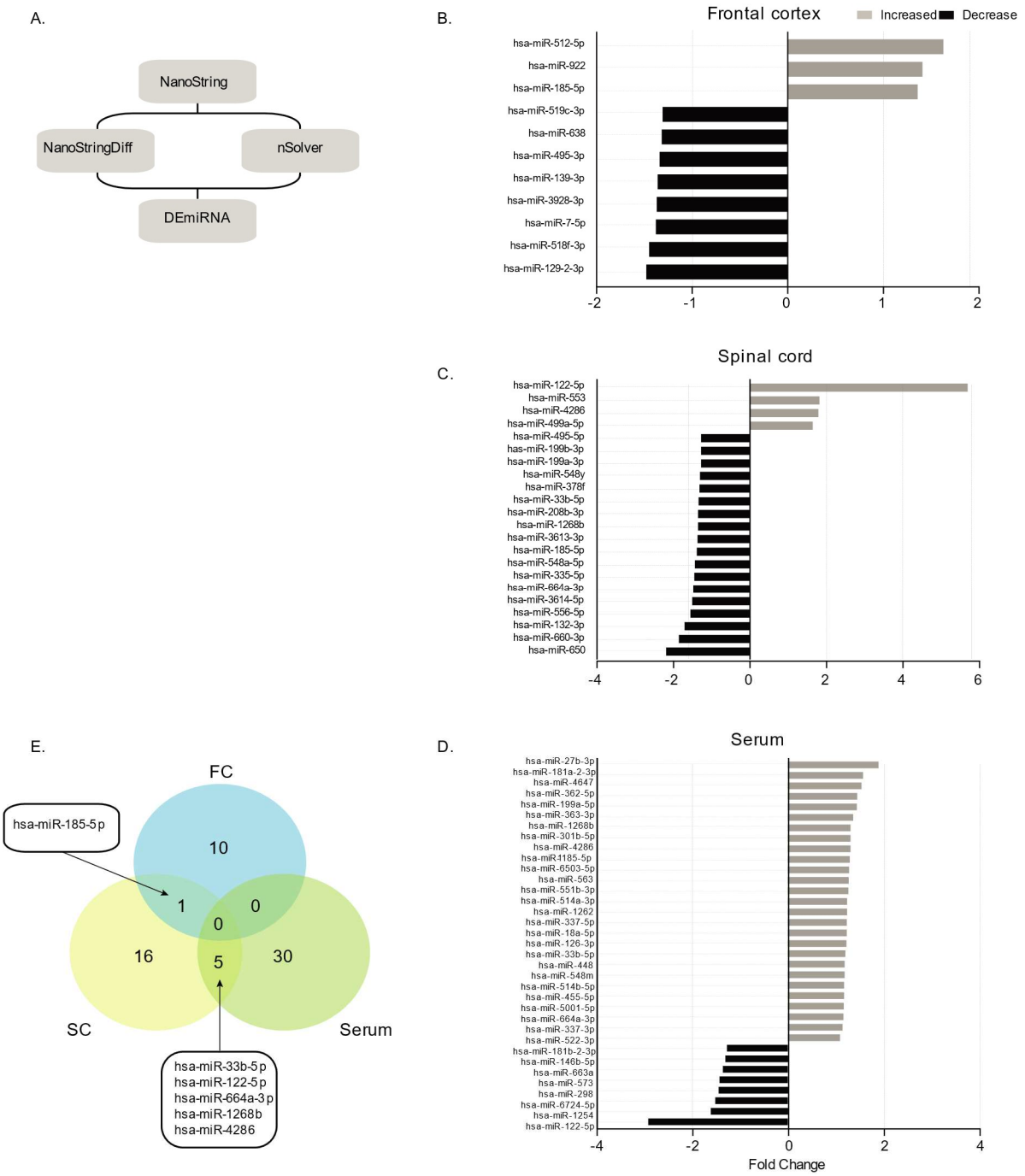

Figure 2.4 EV-contained miRNAs are dysregulated in frontal cortex, spinal cord, and serum in ALS.

(A) Schematic analysis workflow of EVs-contained miRNAs. The miRNAs were profiled using NanoString and normalized by nSolver and NanoStringDiff. Differentially expressed miRNAs overlapping with both methods are shown as DEmiRNAs. EV-derived DEmiRNA from **(B)** SC (n=12 for ALS and n=6 for healthy control), **(C)** FC (n=12 for ALS and n=8 for healthy control), and **(D)** plasma (n=7 for ALS and n=9 for healthy control**)** are shown to increase (yellow) or decrease (orange). Fold change of significant ($p<0.05$) mature miRNAs was determined between

ALS and control groups and the value from nSolver is shown. **(E)** Venn diagram showing common dysregulated EVs-derived miRNAs from different tissues in ALS.

2.4.5 Dysregulated EVs-contained miRNA in ALS.

To better understand the role of dysregulated EV-contained miRNAs in ALS pathology, we examined DEmiRNA predicted targets and their corresponding functional KEGG pathways for each tissue using DIANA-mirPath analysis.[153] A total of 81 KEGG pathways were significantly enriched (FDR<0.05). Of those pathways, 19 overlapped among all three tissues including "Axon guidance", Glutamatergic synapse", "GABAergic synapse", cAMP signaling", Oxytocin signaling", "Endocytosis", and cancer associated pathways (Table 2.2).

Table 2.2 KEGG pathway analysis for the predicted miRNA targets.

KEGG pathways	FC	SC	Serum	Overlap
	-log10 p-value			
Proteoglycans in cancer	8.4	5.5	5.6	Three tissues
Wnt signaling pathway	6.2	2.4	2.0	
Signaling pathways regulating pluripotency of stem cells	5.7	5.1	1.7	
Hippo signaling pathway	5.4	5.1	4.8	
TGF-beta signaling pathway	4.6	2.5	2.0	
ErbB signaling pathway	4.5	1.6	4.7	
Axon guidance	4.4	5.4	4.6	
Oxytocin signaling pathway	4.2	1.4	1.6	
Endocytosis	3.0	1.5	3.1	
Glutamatergic synapse	2.9	2.6	2.7	
Adrenergic signaling in cardiomyocytes	2.4	1.5	3.5	
FoxO signaling pathway	2.3	4.0	1.6	
Retrograde endocannabinoid signaling	2.0	1.7	3.4	
Circadian entrainment	1.7	1.4	2.9	
Focal adhesion	1.7	1.5	1.4	
Nicotine addiction	1.5	2.0	1.6	
Morphine addiction	1.4	3.6	6.7	
GABAergic synapse	1.4	2.7	4.6	
cAMP signaling pathway	1.4	2.6	2.8	

Phosphatidylinositol signaling system		2.3	2.5	Two tissues
N-Glycan biosynthesis		1.3	2.3	
Insulin secretion		1.5	1.9	
cGMP-PKG signaling pathway		4.1	1.8	
Transcriptional misregulation in cancer		3.1	1.6	
Neurotrophin signaling pathway		1.7	1.6	
Gap junction		1.9	1.5	
Prion diseases	7.5	5.3		
Thyroid hormone signaling pathway	5.4	5.3		
Pathways in cancer	5.4	3.5		
Adherens junction	5.4	2.2		
Glioma	5.4		1.8	
Ubiquitin mediated proteolysis	4.3	3.6		
Circadian rhythm	4.1	1.4		
AMPK signaling pathway	2.6		1.4	
Regulation of actin cytoskeleton	2.4	1.5		
Biotin metabolism	2.3	1.7		
Renal cell carcinoma	2.3	4.6		
Ras signaling pathway	2.2	1.5		
mTOR signaling pathway	2.1	1.7		
Bacterial invasion of epithelial cells	2.1	1.5		
Prostate cancer	1.9	2.2		
Insulin signaling pathway	1.9		1.5	
Sphingolipid signaling pathway	1.9		2.1	
Lysine degradation	1.8		3.1	
Dorso-ventral axis formation	1.7	1.9		
MAPK signaling pathway	1.7	1.5		
Amphetamine addiction	1.6		2.5	
Arrhythmogenic right ventricular cardiomyopathy (ARVC)	1.6	3.3		
Dopaminergic synapse	1.5		1.5	
Endocrine and other factor-regulated calcium reabsorption		3.1		No overlap
Glycosphingolipid biosynthesis - lacto and neolacto series		2.1		
mRNA surveillance pathway		1.7		
Aldosterone-regulated sodium reabsorption		1.6		
Rap1 signaling pathway		1.6		
Gastric acid secretion		1.5		

Long-term potentiation		1.5		
Inositol phosphate metabolism		1.5		
Colorectal cancer		1.4		
Mucin type O-Glycan biosynthesis			13.7	
Cell adhesion molecules (CAMs)			3.1	
Estrogen signaling pathway			3.0	
Calcium signaling pathway			2.9	
Cholinergic synapse			1.8	
Other types of O-glycan biosynthesis			1.8	
PI3K-Akt signaling pathway			1.4	
Amoebiasis			1.3	
Pancreatic cancer	4.3			
Oocyte meiosis	3.5			
Long-term depression	2.8			
Type II diabetes mellitus	2.3			
Melanoma	2.3			
Chronic myeloid leukemia	2.1			
Shigellosis	2.1			
GnRH signaling pathway	2.1			
Hedgehog signaling pathway	1.7			
Non-small cell lung cancer	1.6			
HIF-1 signaling pathway	1.6			
p53 signaling pathway	1.5			
Choline metabolism in cancer	1.5			
Hepatitis B	1.4			
Small cell lung cancer	1.4			

The inter-relationship among the identified pathways was visualized with Cytoscape[155] and the genes involved in these pathways were also predicted. The connection between the nodes (edges) denotes the degree of shared genes between the two pathways, and six densely connected clusters in the network were identified by MCODE,[156] (Figure 2.5) a Cytoscape app for network cluster analysis.

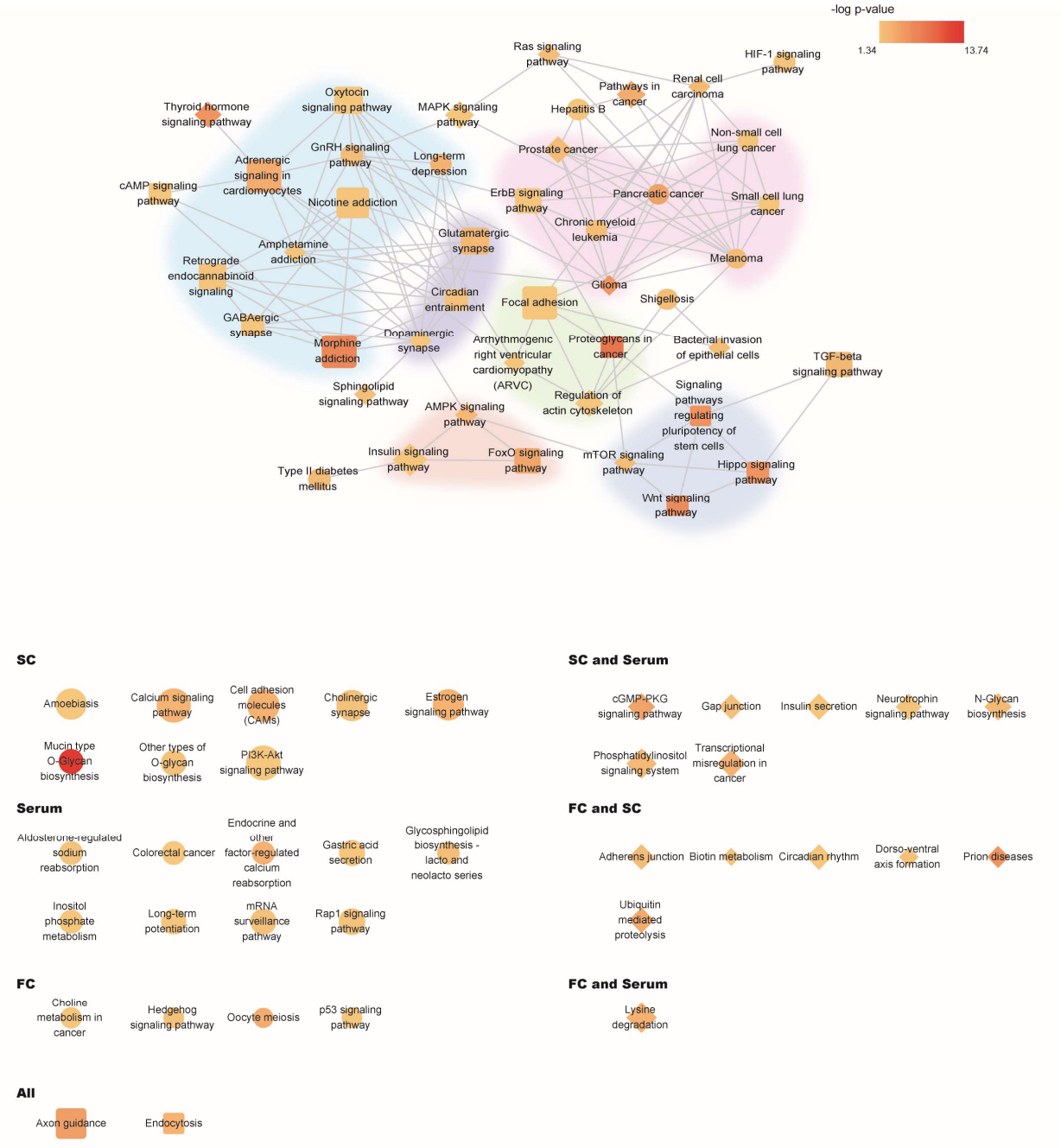

Figure 2.5 Association network of pathways in sALS human FC, SC, and serum.
Squares correspond to pathways identified in all three tissues, diamonds to pathways identified in either two types of the three tissues, and circles to pathways identified in just one type of tissue. The size of the nodes denotes the number of miRNAs in that pathway while the color gradient represents -log *p*-value (see color scale). Pastel colors delimit highly connected pathways clustered by MCODE Cytoscape[156] (Top panel). Non-clustered pathways are arranged by tissue (bottom

panel). For each pathway, -log p-values were calculated by averaging the -log p-values from each tissue.

2.5 Discussion

The lack of biomarkers limits early detection and effective treatment development for ALS. In the current study, we used microfluidic technology to determine whether circulating EVs availability and their cargo reflect pathological signatures from diseased tissue. Our approach provides an efficient, quick, and inexpensive alternative to extract and quantify EVs and their cargo from serum and postmortem tissues. We identified vesicle size differences and several dysregulated EV-contained miRNAs in frontal cortex, spinal cord, and serum associated with biological pathways related to neurodegeneration.

Availability of EVs and their cargo depend on the health and pathological state of the cell, thus serving as potential biomarkers to monitor disease progression and treatment outcome.[141,157 35,158] We did not observe significant difference in EVs abundance between ALS and control samples, regardless of tissue type. In parallel to reports in Parkinson's disease[159], our data suggest that EVs levels are not biomarker for neurodegenerative disease, contrasting with studies in cancer.[160] However, EVs concentration is influenced by many factors including age, sex, time of sample collection, and EV phenotype.[161,162] Although our case cohort was composed of only sporadic ALS patients, other clinical subgroups that define ALS patients, such as family history of neurodegeneration, site of onset, progression of the disease, age, and gender, may need to be taken in consideration in a larger cohort to detect significant altered levels of EVs in ALS. Notably, we observed EVs size difference between cases and controls in spinal cord and serum. EV size may define vesicle kind as well as content in disease.

EVs-contained miRNAs traveling from disease neuronal tissue to the blood stream may facilitate the identification of pathological events.[163-165] Dysregulated miRNAs are potential diagnostic and prognostic biomarkers for neurodegenerative diseases including ALS.[166] We identified common and unique EVs-contained dysregulated miRNAs form circulating and disease tissue, some of which are associated with distinct ALS pathology. For instance, miR-132-3p is decreased in sALS serum and patient-derived lymphocytes derived from patients with TDP-43 but not from lymphoblastoid cells with SOD1 mutations; This suggested the potential of miRNAs not only as markers for ALS in general but as an indicator for different forms of ALS.[167]

Among the 50 dysregulated EV-contained miRNAs identified, six overlapped between neuronal and blood tissues and they are associated with neuron survival and degeneration. For example, miR-122 inhibits neuronal cell death in ischemic stroke and together with miR-33, these miRNAs are important regulators of lipid metabolism.[168,169] ALS patients show a defined switch from glucose to lipid metabolism resulting in elevated lipid usage as energy fuel in neurons and increased oxidative stress, a pathological marker of ALS.[170] miR-185 protects against autophagy and apoptosis in cellular models of Parkinson's disease and it modulates DNA Methyltransferase 1 (DNMT1), therefore regulating global methylation, which is altered in ALS.[171-173]

Notably, only one of these EV-contained miRNAs was dysregulated in the same direction (upregulated). Opposite EV-miRNAs dysregulated direction is observed in breast cancer tumor tissue and plasma.[174] Whether this reflects EVs-contained miRNAs retention in disease tissues in such a way that the opposite result is observed in cargo from circulating EVs, needs to be determined. Although we did not observe high overlap between individual dysregulated miRNAs with FC, SC and serum, we identified pathways regulated by EV-contained DEmiRNA shared by the tissues. Many of the identified pathways are known to be associated with ALS pathology and

neuron degeneration. For instance, some of the shared identified pathways are related to metabolic dysfunction, including fatty acid oxidation and AMPK signaling pathways, which is consistent with hypermetabolism and hyperlipidemia observed in ALS patients.[175] Moreover, we identified EVs-contained dysregulated miRNAs highly enriched in pathways associated to neurodegeneration such as GABAergic synapse system and the Wingless-related integration site (Wnt) signaling pathway.[176-178] Alterations of the Wnt signaling pathway in neuronal and supporting cells contribute to motor neuron degeneration in ALS.[179,180] In addition, the transforming growth factor β (TGF- β), the core module of TGF- β signaling pathway, regulates motor neuron survival by modulating neuroinflammation and fibrosis.[181,182] Axon guidance plays essential roles in development of synaptic connections, thus dysregulation of axon guidance proteins such as Neuropilin and Semaphorin is observed in neurodegeneration.[183,184]

Notably, we identified a cluster of carcinogenesis pathways, such as prostate, melanoma, and brain cancer. These data parallel recent reports associating neurodegeneration and cancer. Depending on the cancer type, cancer patients present either higher or lower risk for neurodegenerative diseases.[185,186] Prostate cancer is inversely correlated to ALS onset, while the opposite trend is observed for melanoma and tongue cancers.[185,187] The Hippo signaling pathway is commonly recognized as a tumor suppressor pathway.[188,189] The mammalian sterile 20 (STE20)-like kinase 1 (MST1), one of the key components of this pathway is elevated in a mouse model of ALS and promotes motor neuron death.[190,191] Furthermore, we found that the mitogen-activated protein kinases (MAPK1) was the most common predicted target of EV-contained DEmiRNAs between the three different tissues. Dysregulation of the MAPK signaling pathway promotes drug resistance in cancer and leads to abnormal accumulations of neurofilaments in ALS.[192,193] Alteration of EV-contained miRNAs in cancer and ALS may regulate common biological mechanisms and signaling

pathways that control cell death and survival. In some cases, in a protective fashion, while in others with detrimental consequences.

2.6 Conclusion

The ability of EVs to ubiquitously carry molecular information from one cell to another provides an opportunity to assess proteomic and genetic information about neurodegenerative disease diagnostics.[194] The involvement of EVs in the progress of ALS is poorly understood. Our study implicates the role of EVs in ALS by identifying alterations of EV size and miRNA cargo in FC, SC, and serum. Using microfluidic technology, we identified EV miRNAs involved in biological pathways across tissues. These miRNAs may be potential biomarkers for screening onset or progression of the ALS.

Chapter 3

Microfluidic Device for High-Throughput Affinity-Based Isolation of Extracellular Vesicles

3.1 Abstract

Immunoaffinity based EV isolation technologies use antibodies targeting surface markers on EVs to provide higher isolation specificity and purity compared to existing approaches. One standing challenge for researchers is how to release captured EVs from the substrate to increase downstream and biological studies. The strong binding between the antibody and antigen or the antibody and substrate is commonly unbreakable without operating at conditions outside of the critical physiological range, making the release of EVs problematic. Additionally, immuno-affinity approaches are usually low-throughput due to their low flow velocity to ensure adequate time for antibody-antigen binding. To overcome these limitations, we modified the Oncobean chip, a previously reported circulating tumor cell isolation microfluidic device. The Oncobean chip is a radial flow microfluidic device with bean-shape microposts functionalized with biotin-conjugated EPCAM antibody through biotin-avidin link chemistry. It was demonstrated that the high surface area and varying shear rate provided by the bean-shaped posts and the radial flow design in the chip, enabled efficient capture of CTCs at high flow rate. We replace the anti-EPCAM with antibodies that recognize common EV surface markers to achieve high-throughput EV isolation. Moreover, by incorporating desthiobiotin-conjugated antibodies, EVs can be released from the

device after capture, which offers a significant improvement over the existing isolation. The released EVs were found to be functional by confirming their uptake by cells using flow cytometry and fluorescent microscopy. We believe the proposed technology can facilitate the both the study of EVs as cell-to-cell communicators and the further identification of EV markers.

3.2 Introduction

Extracellular vesicles (EVs) are a group of heterogeneous membrane-bound vesicles that include exosomes, microvesicles and apoptotic bodies, which are actively secreted by almost all cell types into extracellular spaces.[1,195] These vesicles have been widely investigated and are considered to be powerful mediators of cell-to-cell communications. They can travel across great distances within the human body through the circulation and release their cargos upon internalization by recipient cells.[2] Emerging evidence has shown that genetic information carried by these nanovesicles supports various biological functions such as activating anti-apoptosis, enhancing blood vessel formation and regulating immune response, to name a few.[2,134,196,197] Moreover, they have been shown to carry and transfer proteins and nucleic acids that are reflective of their originated cells.

The role of EVs and their cargo in promoting pathological processes in various kinds of disease, such as cancer and neurodegenerative diseases is becoming clearer, with many studies linking specific EV cargo to disease progression and outlook.[19,158,198,199] As such, proteomic and genomic analysis of EVs can potentially provide a valuable biomarker for the detection, characterization, and monitoring of disease progression. For instance, miRNA dysregulation in EVs have been detected in various types of cancer, such as brain and lung cancer.[42,200,201] The miRNAs carried by EVs released from the tumor or the tumor microenvironment have been shown to deeply influence

tumorigenesis and therapeutic response.[21,200] For example, miRNAs found in EVs secreted by lung cancer cells were shown to be promote tumor growth and metastasis through alternation of the immune response.[202] Furthermore, dysregulated miRNAs in EVs have also been considered as a diagnostic tool for many cancer types.[203,204] In addition to cancers, recent studies have shown that the cargos shuttled by EVs can be biomarkers for neurodegenerative disease, such as Alzheimer's and Parkinson's disease.[205,206] Thus, isolating and analyzing the contents of EVs can provide researchers and clinicians valuable information about a patient's diseases status, potentially even informing future diagnostic or prognostic tests.

Despite the valuable information housed in EVs, the lack of efficient isolation methods is still a major limitation for the study of EVs. The extremely small and heterogeneous size of EVs within a sample, 30-2000 nm, makes isolation technically challenge. The current standard isolation method is differential ultracentrifugation (UC), which is used to isolate EVs from various sample types including cell culture supernatant, blood, urine, and cerebral fluid.[76,207,208] Using UC, samples are processed through serial centrifugation steps with increasing speeds to remove cells and cellular debris and eventually pelleting the target population of vesicles. Sucrose density gradients are often utilized in combination with UC to further deplete any extracellular proteins, achieving better separation and purity. However, critical drawbacks such as lengthy processing time and inefficient yields make it challenging for EV studies where the sample volume is low or the target EVs are low in number.[78,83] Furthermore, several studies have shown that the high centrifugation force damages the membrane integrity of EVs and promotes EV rupture and coagulation, hindering potential downstream analysis. In a push to move away from ultracentrifugation, the need to reduce EV loss, increase purity, and preserve sample integrity has led the development of new isolation technologies to replace ultracentrifugation.[209]

One of the most promising alternative EV isolation techniques, immunoaffinity-based capture technologies, use antibodies to target surface markers of EVs. Common targets of immunoaffinity based captured are a group of proteins called the tetraspanins, specifically CD9, CD63, and CD81, which are broadly accepted EV markers.[91,209] For example, Koliha et al have demonstrated EV capture using magnetic beads coated with antibodies against EV markers, such as CD9, CD63, and CD81.[210] Since the molecular composition of EVs is also dependent on their parent cells, different markers such as epithelial cellular adhesion molecule (EPCAM) and epidermal growth factor receptor (EGFR) have also been used for capturing specific EV populations. For instance, magnetic beads coated with chondroitin sulphate peptidoglycan 4 antibody has been reported to isolate EVs from plasma to study melanoma cancer.[211]

Among the types of immunoaffinity isolation technologies, microfluidic platforms with antibody-coated surfaces have become a promising alternative EV isolation strategy. These devices have very small dimensions, facilitating minimized reagent volumes, isolation time, and procedural costs while enhancing the product purity and sensitivity.[83,90] For instance, Kanwar et al. developed a microfluidic platform, Exochip, that isolates EVs from plasma from pancreatic cancer patient using anti-CD63.[89] The device enables rapid EV quantification and facilitates EV protein and miRNA characterizations. Zhang et al. designed a device with graphene oxide nanoposts coated with CD81 antibody to detect and isolate EVs at low detection limit.[92].Vaidyanathan et al. fabricated a microfluidic device with functionalized gold electrodes coated with CD9, human epidermal growth factor receptor 2 (HER2) and prostate specific antigen (PSA) antibodies.[212] The capture of EVs is enhanced by nanoshearing between the electrodes induced by an alternating electric current. Zhang et al. devised a 3D-nanopatterned microfluidic chip with a porous herringbone mixer fabricated by assembled silica colloids to capture EVs from serum samples in

ovarian cancer.[114] They have shown that their device is compatible with downstream analysis including ELISA, western blotting and digital PCR. Although current immunoaffinity isolation technologies provide more specific EV enrichment and isolation, these technologies suffer from limitations of low throughput since the high flow rates would hinder the antigen-antibody interaction. Additionally, surface-antibody-EV binding is tight, making it challenging to release and retrieve viable EVs post isolation. Being unable to recover intact EVs is a critical drawback for studying the interaction between cells and EVs, hindering both in-vitro and in-vivo studies. Therefore, despite advances in the field, a need exists to further improve microfluidics platforms to isolate and harvest EVs.

Many immunoaffinity-based technologies for EV capture rely on the high-affinity binding of biotin-avidin to immobilize the capture antibodies on the micro/nano-structured surface or beads. Owing to the simple procedure and stable binding, biotin-conjugated antibodies have been used for antibody-based capture not just for EVs but also for other targets including cells, lipids, and enzymes.[213,214] However, the irreversibility of the biotin-avidin binding limits the use of captured EVs as the EVs would need to be lysed in some way for removal. Strategies to break biotin-avidin binding frequently operate at conditions outside of the physiological range, including extreme pH and high temperatures, which potentially reduce the integrity of the captured samples.[215,216]

The use of desthiobiotin, an analogue of biotin, has been reported to be an effective alternative to standard biotin.[215] Desthiobiotin has a lower binding affinity to avidin than regular biotin, meaning that samples captured by desthiobiotin-conjugated antibodies can be eluted from an avidin-coated surface using a biotin solution. This elution leads to the replacement of desthiobiotin with biotin, effectively releasing the sample from the capture surface and allowing for downstream applications.[101] This capture-release method has been used for the isolation and release cells and

proteins.[217] In the present study, we incorporated this desthiobiotin release method to achieve the release of intact EVs using a high throughput immunoaffinity based microfluidic device.

We have previously described the Oncobean chip, a radial flow microfluidic device with bean-shape microposts functionalized with biotin-conjugated anti-epithelial cell adhesion molecule (EpCAM) antibody through biotin-avidin link chemistry.[218] It was demonstrated that the high surface area and stable shear rate provided by the bean-shaped posts, as well as the radial flow design in the chip, enabled efficient capture of circulating tumor cells (CTCs) at high flow rates.[218,219] Here, we apply this chip with antibodies against common EV surface markers, CD9, CD63, and CD81, to achieve high throughput EV isolation. Our results showed that the device is well suited to process large volumes of samples, which is ideal for obtaining high concentrations of EVs for downstream analysis. Furthermore, by using desthiobiotin-conjugated antibodies instead of biotinylated ones, EVs can be released and harvested from the device after capture. The released EVs were shown to be functional by demonstrating their internalization by cells based on flow cytometry. One exciting application of releasing exosomes is to investigate the uptake of exosomes into distant cells. We performed initial experiments to first test the integrity of the EVs following release. To do so we performed immunofluorescent labeling of EVs for common EV proteins (CD81 and CD63) before demonstrating successful staining using flow cytometry. We then used fluorescently dyed EVs to perform an initial uptake experiment and demonstrated the uptake of released EVs by cells. We believe that this novel strategy can be used for high volume processing of samples for EV enrichment which will enable both systematic analysis of EV cargo and investigations into their interactions with recipient cells.

3.3 Methods

3.3.1 Oncobean fabrication and functionalization

The OncoBean Chip, a previously reported microfluidic device for isolating circulating tumor cells, was utilized for EV capture in the present study.[218] The device is made of a polydimethylsiloxane (PDMS) top bonded to a glass slide. The mold for the polydimethylsiloxane (PDMS) device is fabricated using a negative photoresist, SU-8 100, patterned silicon wafer using standard soft lithography techniques. Briefly, negative photoresist SU-8 100 (MicroChem Corp) was spin coated onto a silicon wafer at 2350 rpm before performing UV exposure, post exposure baking, developing, and feature measuring. Well-mixed PDMS and curing agent were poured onto a SU-8 mold at a ratio of 10:1 and degassed in a desiccator for 30 minutes to remove all bubbles. The polymer was cured at 65 °C overnight in the oven. After baking, the polymer was peeled off from the mold and cut for surface functionalization. The PDMS chamber was bonded to a standard sized glass slide via plasma surface activation of oxygen.

The completed device was processed with 3-mercaptopropyltrimethoxysilane (Gelest) in ethanol by syringe injection and incubated for an hour. This device was then washed with ethanol and treated with N-gamma-Maleimidobutyryloxy-Succinimide (GMBS) (ThermoScientific) for 30 min. This was followed by rinsing with ethanol and adding NeutrAvidin before incubating. The device was then stored at 4 °C for future use.

3.3.2 Sample preparation and EV isolation

Whole blood samples from healthy donors were drawn into EDTA tubes and were subsequently centrifuged at 2000 x g for 15 minutes to collect the top layer of plasma. The isolated plasma samples were kept at -80 °C until use.

3.3.3 Cell culture

Patu8988t pancreatic cancer cell line was cultured in DMEM medium with 10% FBS. Cultures were incubated at 37 °C in a humidified 5% CO2 incubator (Thermo Fisher Scientific, Waltham, MA). Cells were grown until they reached 70–80% confluence, at which time, they were subjected to experimentation.

3.3.4 EV capture and release

Before experiments, the device was functionalized with the capture antibody by injecting biotin or desthio-biotin conjugated antibody in 1% bovine serum albumin (BSA) (Sigma Aldrich) in phosphate buffered saline (PBS) and incubating for 60 minutes. After antibody immobilization and washing with 1mL of PBS at a flowrate of 50 µl/min, 3% BSA was processed at a flow rate of 50 µl/min for 10 min to block the excess reaction sites and prevent non-specific binding. Human plasma or cell culture medium were processed through the OncoBean Chip for EV capture, followed by washing with PBS at a flow rate of 50 µl/min for 20 min. The EVs captured by the desthiobiotin antiCD63 conjugated device were released from the device using a 0.5 mM biotin solution. The biotin solution was incubated for 1 hour in the device, followed by a wash with biotin solution and the collection of released EVs. The released EVs were either characterized by nanoparticle tracking analysis, NTA, using the NanoSight NS300 (Malvern Instruments, UK) to determine the size and concentrations, or proceeded to functional studies.

The EVs immobilized by the device using biotinylated antibodies were lysed for RNA and protein extraction.

3.3.5 Electron microscope (EM) analysis of captured EVs

A small portion of the PDMS top of the device after EV isolation was cut out using a biopsy punch. Each punched PDMS specimen was fixed in 2.5% glutaraldehyde in PBS at room temperature for one hour and then rinsed with PBS, followed by sequential dehydration with ethanol at concentrations of 50%, 70%, 90%, 95%, and 100% for 10 min each. The specimen was then immersed for 10 min in solution of 1:1 ethanol: hexamethyldisilazane (HMDS) and then transferred to 100% HMDS, followed by overnight air drying in the hood. The dehydrated specimen was then attached to carbon double sided tape and was mounted on a SEM stub before coating using gold sputtering. The EVs were examined by FEI Nova 200 Nanolab Dualbeam FIB scanning electron microscope under low beam energies (2.0-5.0 kV) at the Michigan Center for Materials Characterization (MC2) at University of Michigan.

3.3.6 Western blotting and protein quantification

To harvest the protein of the EVs captured, the device chamber was injected with RIPA buffer (Sigma) with 1% Halt protease inhibitor (Thermo) at a flowrate of 50 µl/min for 2 min, followed by a 10 min incubation on ice. This was followed by an injection of 70µL per device at the same rate and the effluent was collected. After another 10 min incubation, the remaining effluent in the devices was pushed out by pumping air manually. The collected samples were stored at -80 °C until used.

Total protein was measured by standard micro-BCA analysis according to the manufacturer's instructions (Thermo). Lysed protein was mixed with 4x Laemmli buffer with 2-mercaptoethanol

at a ratio of 4:1 and heated at 95 °C for 7 minutes. The protein samples were then loaded on a 10-lane 4-20% SDS gradient gel (BioRad) and run for 47 minutes at 120V in Tris-Glycine-SDS buffer (BioRad). The gel was then transferred to a methanol-activated PVFD membrane at 120V for 1hr using BioRad's Minigel wet transfer system. Following transfer, the membrane was rinsed with DI water before drying for 1 hour. The membrane was then reactivated with methanol, rinsed with DI water and submerged in tris-buffered saline with 1% Tween 20 (TBST) before blocking in 5% non-fat milk in TBST for 1 hour at room temperature on a rocker. Primary antibodies then incubated overnight in 4° on a rocker at a concentration of 1:1000 for both CD9 (Cell Signaling) and Beta-Actin (Cell Signaling). Primary antibodies were rinsed 6 times, 3 quick rinses and 3x 5 minutes on a rocker, in TBST before applying anti-rabbit HRP secondary at a concentration of 1:1500 (Cell Signaling) for 1.5 hrs on a rocker at room temperature. Secondary antibody was rinsed as previously described and Thermo's SuperSignal PICO Reagant was applied for 5 minutes before imaging using BioRad's ChemiDoc Imager.

3.3.7 RNA preparation, RT, and real-time qPCR

Total RNA from EVs was extracted using Qiazol (QIAGEN). After the EVs were immobilized within the device, 120 µl of Qiazol was flowed through the device at 50 µl/min, followed by 10 min incubation. The device was then processed with another 150 µl at the same flow rate while the effluent was collected. After another 10 min incubation, the remaining effluent in the devices was pushed out by pumping air manually. The collected samples were stored at -80 °C until used. SYBR Green-based real-time qPCR technique was performed for detection of miRNAs, as previously described.[220] Total RNAs were purified from isolated EVs using a Single Cell RNA Extraction Kit (Norgen). Purified RNA amount was measured by NanoDrop Lite

Spectrophotometer (Thermo Fisher Scientific). Reverse Transcription Kit (Thermo Fisher Scientific) was used to generate single-stranded cDNA from an equal amount of purified RNAs.

3.3.8 Flow cytometry

For directly exosome surface staining, EVs were incubated with pre-conjugated FITC mouse anti-human CD63 (BioLegend) and APC Anti-Human CD81 (BioLegend) for 30 min at room temperature. After incubation, the samples were washed with PBS, ultracentrifuged and then resuspended in PBS buffer. Stained samples were analyzed using ZE5 (Bio-Rad) flow cytometer and FlowJo software (Treestar).

3.3.9 Uptake of EVs

Following release from the capture device, EVs were labeled by PKH26 Red Fluorescent Cell Linker Kit (Sigma), and Exosome Spin Columns (MW 3000) (Thermo Fisher Scientific) were used to remove excess dye as previously described.[21] Patu8988t cells were seeded into a 6 well plate and allowed to settle and adhere for 48 hours before the dyed EVs were added for a 12 h incubation in a 37° cell culture incubator as previously described. Flow cytometry was performed to measure mean fluorescence intensity (MFI) of cells.

3.4 Results and discussion

3.4.1 Evaluation of EV capture with OncoBean chip

While previous work assessed the ability of Oncobean to isolate circulating tumor cells from blood samples, the present study explored the Oncobean's capture potential and throughput for isolating extracellular vesicles. Figure 3.1 schematically illustrates EVs being captured on the Oncobean's antibody-coated bean-shaped microposts. The increasing cross-sectional area in radial flow design

provides a decreasing flow velocity from inlet to outlet, which allows for higher flow rate compared to linear flow devices. The high surface area provided by the bean-shaped microposts also increases the contact of EVs with capture antibodies, thus enabling high capture at high flow rates.

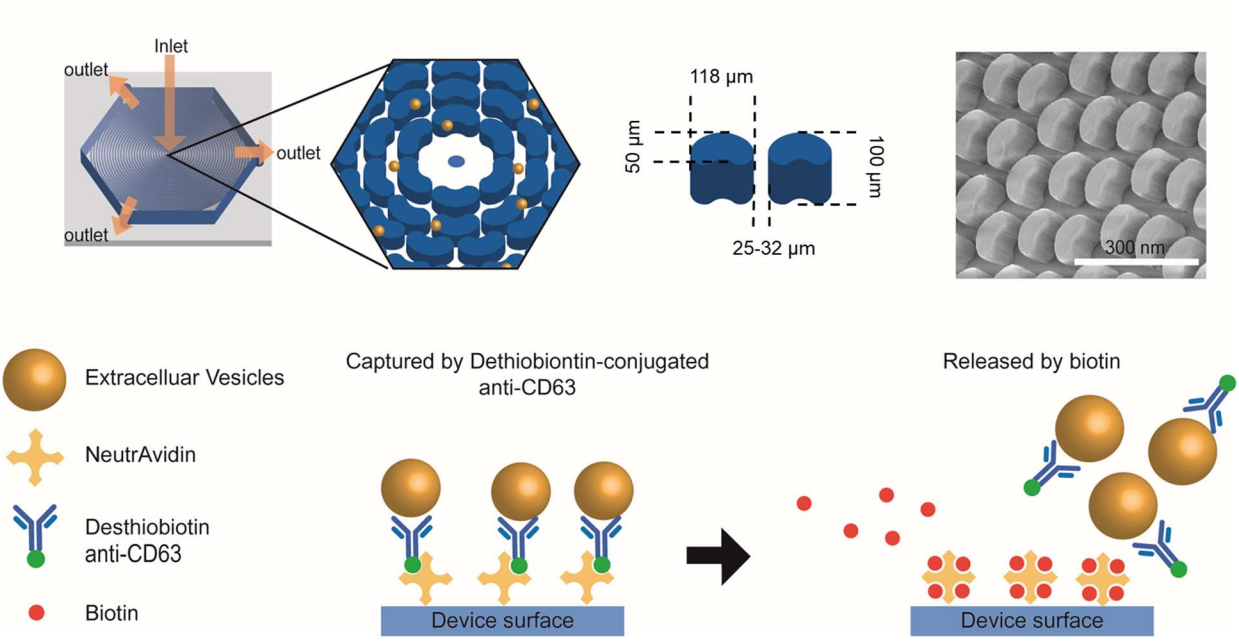

Figure 3.1 Schematic illustration of OncoBean Chip and EV isolation.
The design of the device can be seen in the previous report. In general, the bean posts are 50 µm in width, 118 µm along the longest axis, and 100 µm in height. The posts were placed 25-32 µm apart from each other. The device surface functionalized with Neutravidin can be coated with desthiobiotin-conjugated antibody that recognize surface markers of EVs. The EVs are captured by flowing samples through the chip. Compared to biotin, desthiobiotin has a lower binding affinity to avidin, thus facilitating a release mechanism for the EVs. Though the introduction of the biotin, the desthiobiotin-antibody-EV complex releases from the Neutravidin coated surface, allowing for EV collection.

To demonstrate the ability of the OncoBean chip to perform high-throughput isolation of EVs, we used the two most common sources of EVs: plasma and cell culture media. First, we used biotinylated CD63 and CD9 antibodies as capture antibodies to optimize the flowrate and sample volume for EV isolation. With the goal of minimizing the processing time, we fixed the processing time at 1 hour and tested the capture using varying sample volumes to determine the

capture capacity of the device. Protein was extracted by flowing RIPA extraction buffer through the device post EV capture. We used the protein concentration measured by microBCA kit to quantify the EVs captured. As can be seen in Figure 3.2A, when the volume of serum was increased to 1200 μl, the protein concentration reached the maximum value and further increasing the serum volume did not increase the protein concentration. For cell culture media, the chip was capable of processing up to 10 mL of culture media in an hour, demonstrating high throughput EV isolation (Figure 3.2B). However, the protein concentration decreased greatly at flow rates higher than 10 ml/hr. This could be caused by the limited contact time between the EVs and antibodies. Further, we performed Western blot analysis on the protein extracted from the chip to verify the EV capture, as shown in Figure 3.2C. The presence of CD9, a specific exosome marker, was confirmed in both culture media and plasma samples, and β-actin was used as a loading control. Additionally, immunofluorescence staining with CD81 and CD9 antibodies further demonstrated the capture of EVs by the bean posts (Figure 3.3).

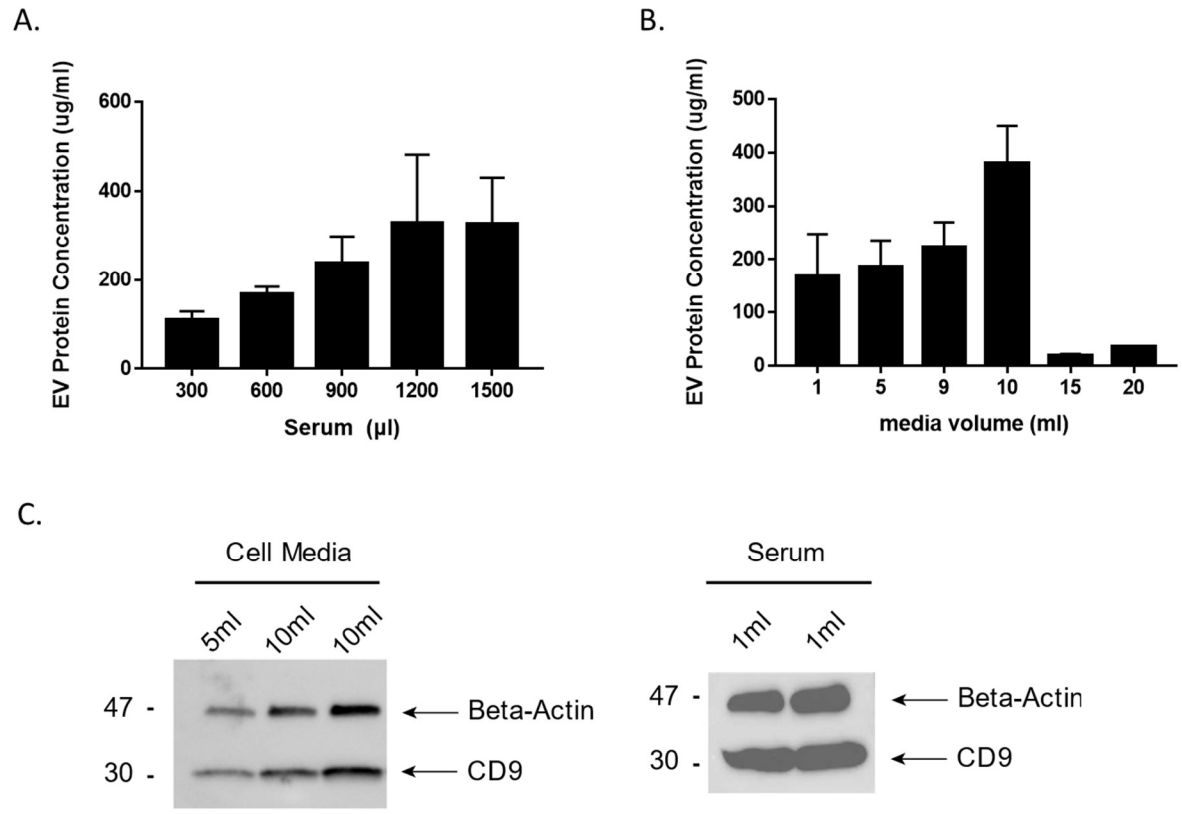

Figure 3.2 Characterization of EVs captured using OncoBean chip.
(A-B) Protein levels in EVs isolated from **A)** Serum and **B)** cell culture medium. (**C)** a representative western blot analysis of the proteins from EVs isolated from OncoBean using anti-CD81 and anti-CD63 and characterized for CD9 expression levels in plasma and cell culture medium.

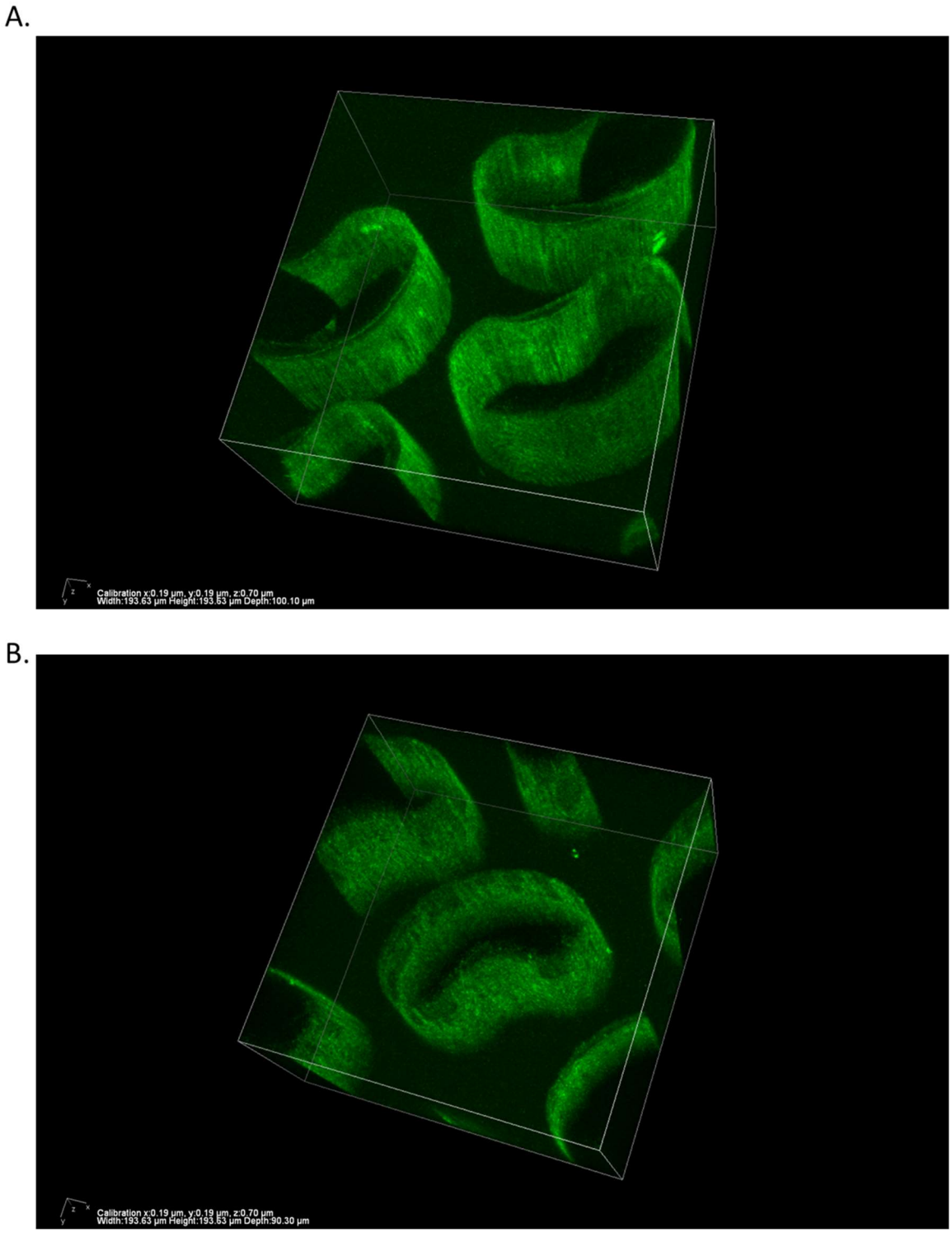

Figure 3.3 3D images by confocal scanning microscopy to confirm the capture of EVs with Oncobean chip.
The captured EVs were strained using **(A)** CD81 and **(B)** CD9 antibody conjugated with fluorescein isothiocyanate.

In addition to the protein analysis, we also evaluated our device for its applications in performing miRNA analysis of EVs. A variety of different types of RNA molecules have been identified in EVs. Messenger RNAs (mRNAs), long non-coding RNAs (lncRNAs), ribosomal RNA (rRNA), microRNAs (miRNAs) and the fragments of these intact RNA molecules have all been identified.[221] MiR-21, miR-155 and miR-200 have been shown to be enriched in EVs and their expression levels have been correlated with poor prognosis in pancreatic cancer.[222] To test the capabilities of our device to capture EVs for miRNA analysis, we performed RT-PCR to measure the level of miR-21, miR-155 and miR-200 in the EVs. Similar to the previously reported pancreatic cancer EVs, we observed enrichment of miR-21, miR-155 and miR-200 in the device isolated EVs (Figure 3.4). The characterization of EV protein and miRNA demonstrates the utility of the Oncobean Chip for downstream EV analysis after high throughput capture of both low and high sample volumes.

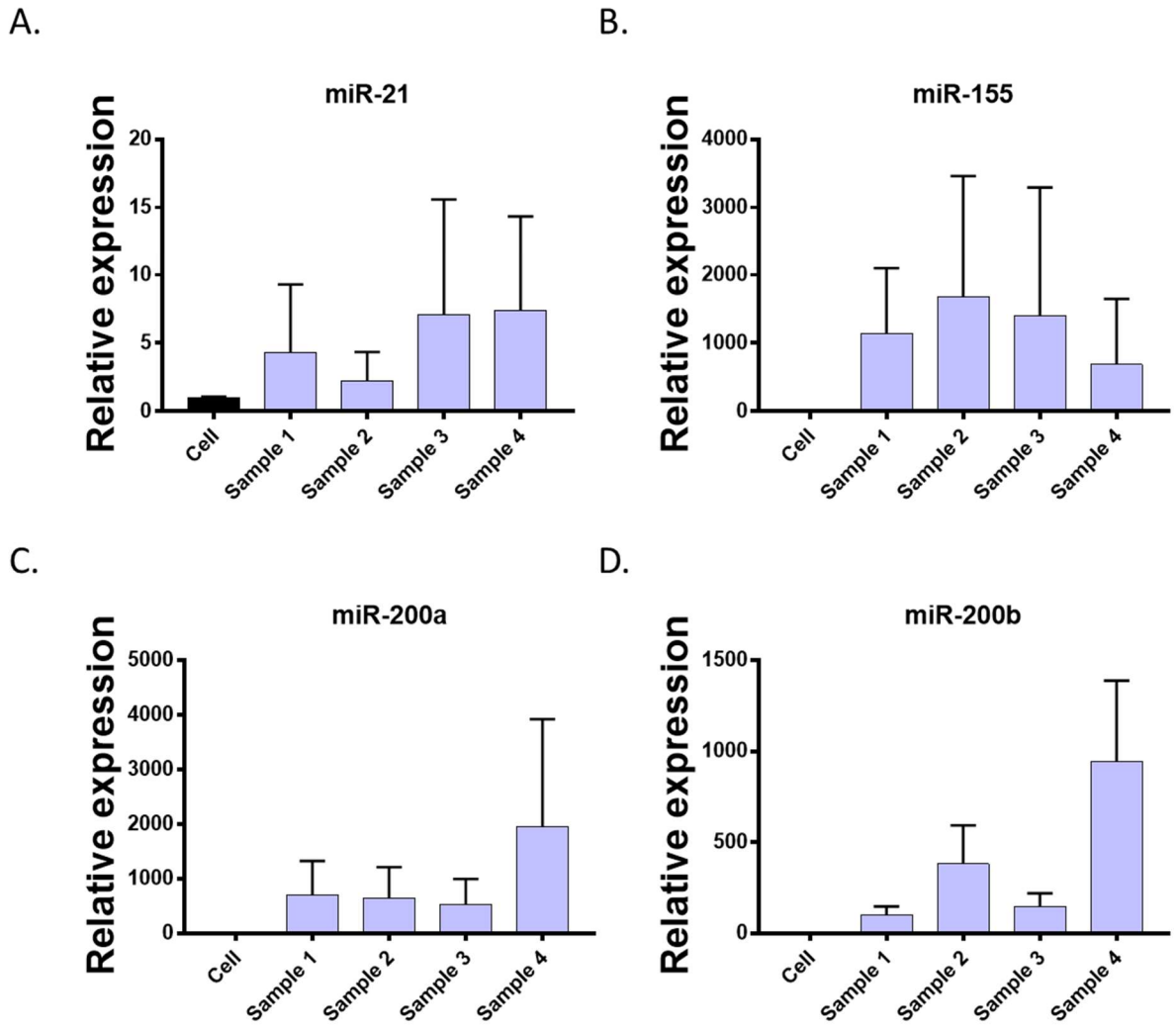

Figure 3.4 Real-time quantitative PCR analysis on captured EVs.
(A) miR-21, **(B)** miR-155, **(C)** miR-200a, and **(D)** miR-200b expressions from device isolated EVs. The RNA was obtained by lysing the captured EVs in the device and quantified using the real-time quantitative PCR (RT-qPCR). Individual miRNA expression levels are shown in bar graphs.

3.4.2 Release and harvest EVs from the device

A critical disadvantage of using biotin-conjugated antibodies for EV capture is the irreversible binding between biotin and avidin, hindering the harvest of intact EVs from the device. To overcome this challenge, we used desthiobiotin-conjugated anti-CD63 instead of biotinylated anti-CD63 to capture EVs. Compared to biotin-avidin binding, desthiobiotin-avidin binding can be

reversed in mild conditions because of the lower binding affinity between desthiobiotin and avidin. When we used desthiobiotin-conjugated antibody instead of biotinylated antibody, immobilized EVs within the device were released through exchange reactions as illustrated in Figure 3.1. The stronger affinity between the biotin and neutravidin causes the replacement of desthiobiotin with biotin, and thus enabling the release of the EVs from the neutravidin-coated surface.

Optimization studies were conducted in order to determine a reasonable biotin concentration that allowed for effective release of EVs from the device. Pre-purified EVs from healthy plasma (System Biosciences) were captured using desthiobiotin-conjugated anti-CD63 on the Oncobean chip and the released EVs were then quantified with NTA analysis. As shown in Figure 3.5A, the concentration of released EVs increased along with increasing concentrations of biotin and reached a maximum at a concentration of 0.5 mM. This result led us to use 0.5 mM for all further experiments to achieve effective release of EVs. In addition to the biotin concentration, we also evaluated the influence of biotin solution incubation time. However, as illustrated in Figure 3.5B, the incubation time was not a significant factor for EV release. Figure 3.5C and 3.5D shows the concentration of EVs collected after release from the outlet at different sample volumes using the 0.5mM biotin solution. These graphs showed that our device can harvest EVs from up to 900 µl of serum or 10 ml of cell culture medium. To the best of our knowledge, this is the highest throughput achieved on a microfluidic platform for EV isolation from culture medium reported to date.

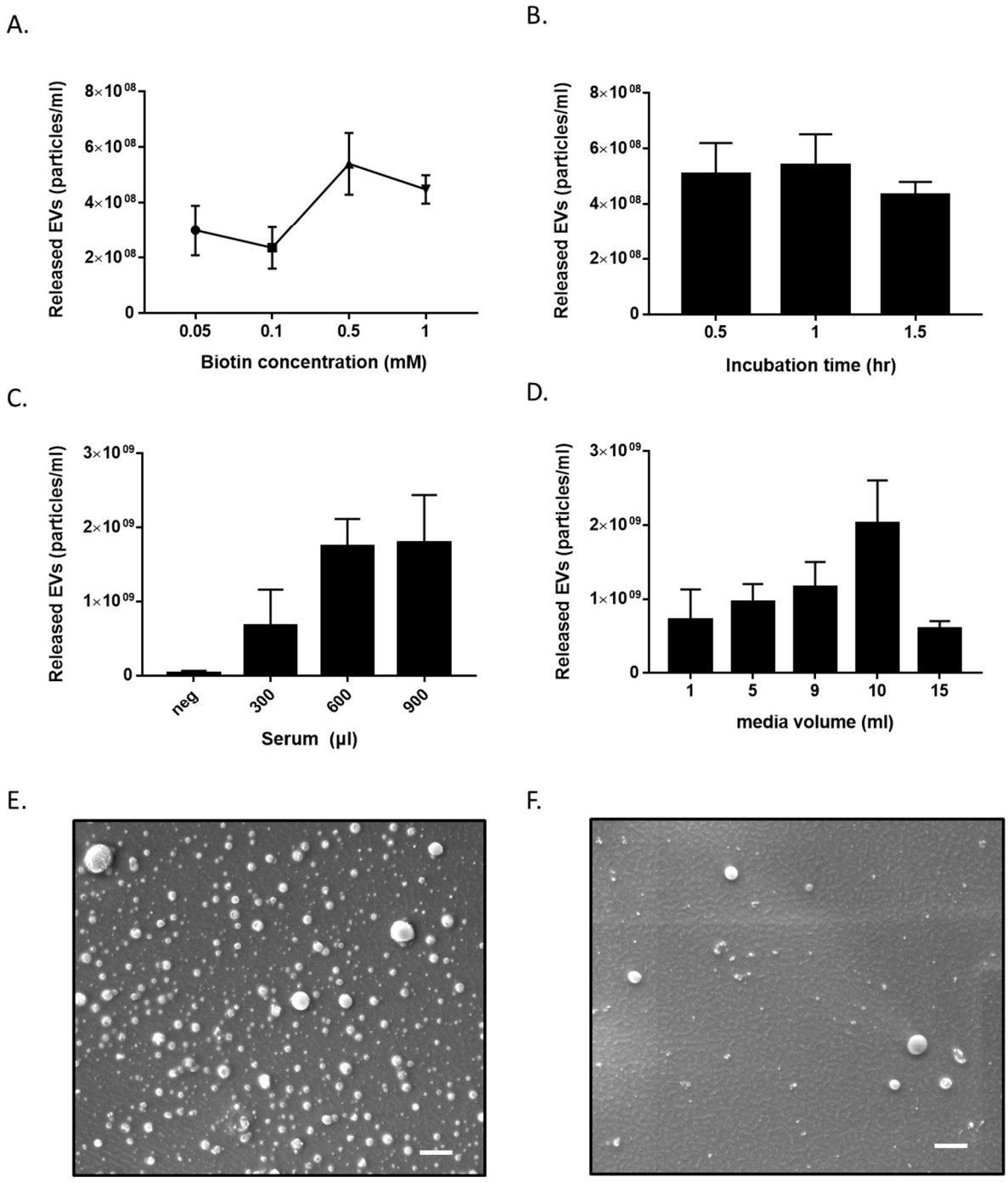

Figure 3.5 Characterization of EVs isolated using the OncoBean chip.
(A-B) NTA analysis of harvested EV with varying **(A)** biotin concentration and **(B)** incubation time for the release of EV using pre-purified EVs (System Biosciences). **(C-D)** NTA measurement of EVs harvested from **(C)** plasma and **(D)** cell culture media. **(E-F)** Electron microscope images showed the presence of EVs immobilizations **(E)** before and (**F)** after the biotin introduction (bars = 1 μm).

To confirm the successful release of EVs from the chip, SEM images were taken showing the device with and without the injection of biotin, or with and without EV release. The images clearly showed that most of the EVs captured on the chip were released after the biotin. (Figure 3.5E-F), and thus further validating our ability to capture and release EVs form microfluidic chip.

3.4.3 Characterization and cell uptake of harvested EVs

Accumulating evidence has shown that EVs can act as powerful mediators of cell-to-cell communication, facilitating various biological events. Importantly, EVs and their cargo have been shown to play important roles in disease progression. Therefore, harvesting EVs that are functional is important for in-vivo and in-vitro studies. To demonstrate that the captured and released EVs are functional and preserve their surface markers, we performed flow cytometry analysis to examine EV surface markers and cellular internalization of EVs.

We used direct flow cytometry to examine two common EV surface markers, CD63 and CD81, on EVs isolated using the Oncobean with release and ultracentrifugation. As shown in Figure 3.6A, the population of positive EVs from ultracentrifugation is found in the top right demonstrating the presence of both CD63 and CD81 on each EV. Similar to the ultracentrifuged EVs, device isolated and released EVs have more than 99% CD63 and CD81 positive populations (Figure 3.6B). This data not only demonstrated that these vesicles represent EVs but also highlighted a sensitive method for surface marker characterization of EVs using flow cytometry. Therefore, this approach can be used to differentiate and identify heterogenous populations of EVs, thus providing insights into identifying EV surface markers.

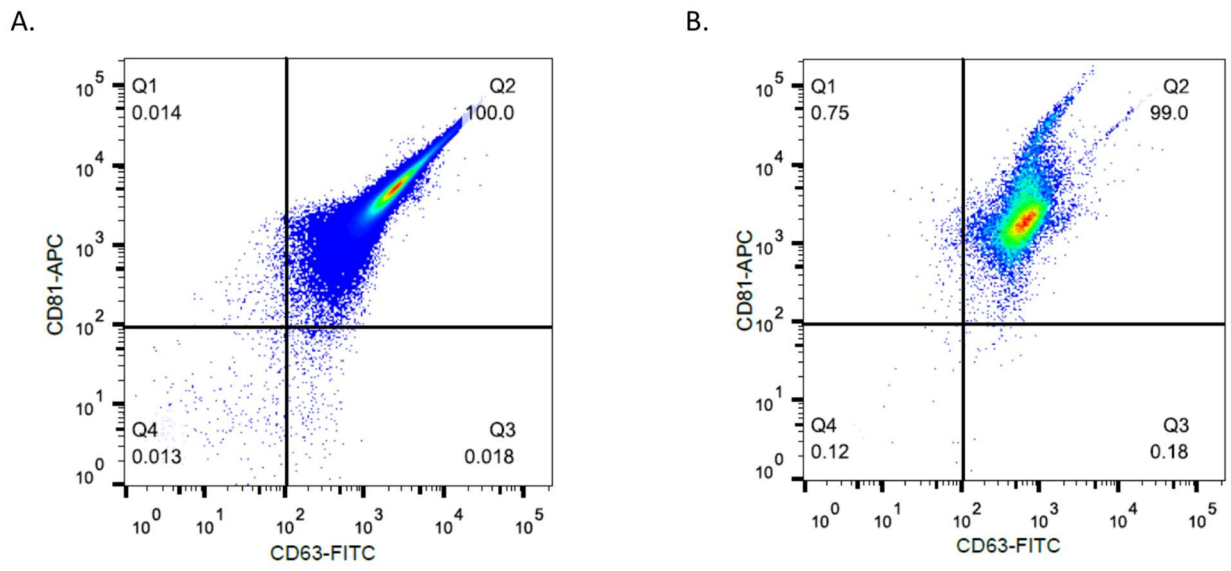

Figure 3.6 Flowcytometry analysis.
Flowcytometry analysis of **(A)** ultracentrifuged and **(B)** device isolated and released EVs. The anti-CD63 antibody conjugated with FITC and anti-CD81 antibody conjugated with APC were used to immunolabel the EVs.

The goal of recovering viable EVs from a sample is to study the influence of EVs on the behavior of recipient cells after internalization. In order to demonstrate the biological functionality of released EVs, we demonstrate that they can be internalized by cancer cells. To do this, we compared internalization between EVs isolated from cell culture media using both the Oncobean device and ultracentrifugation. To examine whether EVs are taken up by Patu8988t cancer cells, we pre-labeled isolated EVs with PKH green dye and incubated them with Patu8988t cells for 12h and analyzed their internalization into the cancer cells using flow cytometry. As indicated by the higher green peak, the ultracentrifuged sample had similar uptake to the device-released EVs while they both had markedly more uptake into cells than the no-EV negative control using only PKH dye. This demonstrated that EVs are indeed taken up by Patu8988t cancer cells. Additionally, we found that device isolated EVs were similarly functional compared to the ultracentrifuged ones (Figure 3.7A and Figure 3.7B).

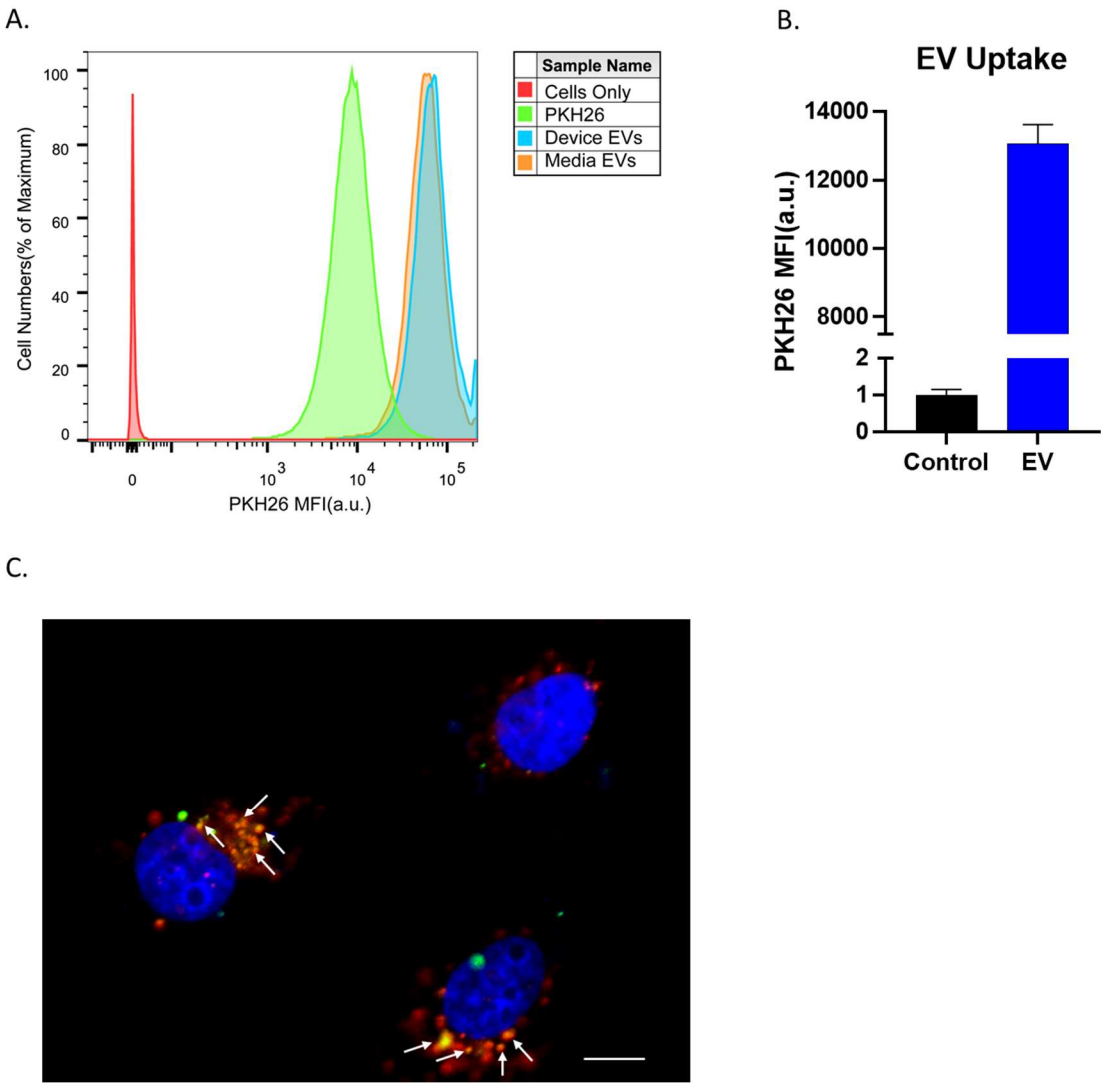

Figure 3.7 EV uptake by cells.
(A) Flow cytometry analysis shows uptake of device-derived and ultracentrifuged EVs by Patu8988t cells. The EVs were pre-labeled with PKH67 dye before the uptake. Two samples without added EVs were used as negative controls: one with PKH dye, one without PKH dye. **(B)** The comparison of mean fluorescence intensity (MFI) of cells treated with EVs to the negative control of cells with no EVs. **(C)** PKH67-labeled EVs (green) were trafficked to lysosomes labeled by Lysotracker (red). The traffic of PKH67-labeled EVs through lysosomes was confirmed by the colocalization of PKH67 and Lysotracker in Patu8988t cells, as indicated by arrowheads. The yellow regions indicate colocalization of green and red, or EVs and lysosomes.

We also studied the intracellular trafficking of internalized EVs to lysosomes in Patu8988t cells to further verify the EV uptake. Lysosomes are membrane-bound organelles found in nearly all animal cells. They are spherical vesicles which contain hydrolytic enzymes that can break down

many kinds of biomolecules. Simply stated, lysosomes are a type of vesicles with a specific composition of both its membrane proteins and proteins in its lumen. The lumen's pH (4.5–5.0) is optimal for the enzymes involved in hydrolysis.[223] Lysosomes are an essential part of the vesicular compartment and connect the outside medium with many classes of cellular targets in the cytosol, nucleus, mitochondria, endoplasmic reticulum, and Golgi.[224] EVs can reach the lysosome through endocytosis. The capture of EVs occurs through specific endocytic mechanisms according to the nature of the cargo. After uptake, the EVs are routed to early endosomes. From the endosomes, the EVs can either be recycled back to the plasma membrane or sorted and targeted for lysosomal degradation.

To verify the migration of EVs into lysosomes, cells were incubated with Lysotracker (red; to label lysosomes) and cocultured with PKH67-labeled (green) EVs from human serum and analyzed by confocal microscopy. PKH67 detected in lysosomes demonstrated the colocalization of EV and lysosomes (Figure 3.7C), demonstrating that the EVs from device are biologically active.

Using flowcytometry and fluorescent microscopy, we have shown the feasibility of using the immunoaffinity based Oncobean device for EV capture and release. We were then able to show the uptake of isolated and enriched EVs by cells and confirmed their surface markers using flow cytometry. We strongly believe this technology will facilitate studies into the role of EVs as cell-to-cell communicators.

3.5 Conclusion

In this study, we have successfully demonstrated the utility of the high-throughput Oncobean for EV isolation from cell culture supernatant and human plasma. The high surface area and radial flow design provided by the bean-shaped microposts facilitate capture of EVs not only at high

flow rate, but also from larger volumes of media form cell culture supernatant. Furthermore, our results indicate that the Oncobean chip facilitates the analysis of EV proteins and RNAs using western blot and qPCR. Most excitingly, through desthiobiotin antibody capture and biotin elution, we were able to release functional EVs from the device for cell uptake and identification of surface markers, which were verified using flow cytometry. We believe our microfluidic device can facilitate specific enrichment of EVs enabling the study of EVs in cell-to-cell communication.

Chapter 4

Simultaneous Single Cell Gene Expression and Mutation Profiling of Circulating Tumor Cells

4.1 Abstract

Tumor cell populations are known to be highly heterogeneous. An invasive tumor biopsy has the potential to miss these clones due to spatial heterogeneity, while bulk analysis can miss information from rare subpopulations. To investigate tumor cell heterogeneity, we developed a streamlined workflow to scrutinize rare cells, such as circulating tumor cells (CTCs), for simultaneous single cell mutation and gene expression profiles. This powerful workflow overcomes low-input limitations of single cell analysis techniques. Here we highlight the utility of this multiplexed workflow to unravel inter- and intra-patient heterogeneity in lung CTCs from six epidermal growth factor receptor (EGFR) mutant positive non-small-cell lung cancer (NSCLC) patients isolated using the high-throughput microfluidic technology, the Labyrinth.

4.2 Introduction

The power of targeted therapies, designed to target specific molecular vulnerabilities, was shown in non-small-cell lung cancer (NSCLC) patients with activating mutations in the epidermal growth factor receptor (EGFR) gene who responded favorably to tyrosine kinase inhibitors (TKIs) compared to patients with wildtype EGFR.[225] A patient's eligibility to receive targeted therapy is determined by molecular information obtained from tumor biopsies. However, false-negatives

resulting from spatial tumor heterogeneity and the risk of missing mutant tumor clones from regional tissue biopsies can occur. Alternatively, circulating tumor cells (CTCs) and circulating tumor DNA (ctDNA) present in the blood can be accessed through a routine blood draw, termed a "liquid biopsy", which may better capture tumor heterogeneity.[226] Both ctDNA and CTCs have been used to monitor disease progression and have shown clinical significance across many cancer types.[227-231] ctDNA, present in low levels in the blood, typically ranging from <0.1% to >10% of total cell-free DNA content[232], is frequently below the detection limit of technologies such as Sanger sequencing and quantitative PCR (qPCR), therefore many groups have focused on next-generation sequencing and more recently digital PCR (dPCR) to detect tumor-specific mutations.[232,233]

Currently, the Roche Cobas EGFR mutation test v2 is the only FDA-approved liquid biopsy test, used for screening EGFR mutations from ctDNA as a companion diagnostic. However, the sensitivity and specificity of the system is only 58.4% and 80.4% respectively for the T790M mutation.[234] Due to the relatively low efficiency of this test, it is used as a "rule-in" test, meaning if the mutation is not detected, it isn't considered absent, and rather a clinician may consider recommending a repeat tumor biopsy before modifying treatment.[234,235]

While ctDNA has shown promise, there is still debate about using ctDNA for tumor monitoring. ctDNA arises from lysed cells, and therefore represents a bulk snapshot of the tumor. Alternatively, CTCs may provide a real-time view of active disease status, and will likely be enriched for highly aggressive, treatment-resistant live cells. While CTCs are rare in the blood, typically on the order of tens of CTCs per milliliter of blood, many isolation techniques have been developed, most commonly using microfluidic technologies.[236-238] This enables whole cell analysis, which can include genomic, transcriptomic, or proteomic analysis.

Initial work in CTCs focused on enumeration and bulk analysis for gene expression using techniques such as qPCR or RNA sequencing (RNA-seq). This approach is limited to characterizing the sample as an aggregate of the bulk population, therefore missing rare phenotypes and may be biased by sample purity from leukocytes remaining in the sample.[236,239]

As a result, several groups have developed workflows for single cell analysis to study tumor cell heterogeneity, commonly through gene expression or genetic profiling. These analysis techniques tend to be labor intensive, time consuming, and expensive. Due to the low starting material many single cell analysis platforms require pre-amplification steps such as whole genome amplification (WGA) for genomic aberrations and whole transcriptome amplification (WTA). An inherent limitation of pre-amplification is the predisposition for PCR bias and gene dropout.[240] Nonetheless, single cell RNA-seq (scRNA-seq) has emerged as a common method for transcriptomic analysis, important in exploratory studies for prognostic markers. scRNA-seq has revealed intra-patient CTC heterogeneity and signatures of highly metastatic cells. Despite its promises, groups have reported many inefficiencies and technical limitations, leading to few recovered CTCs proceeding through the entirety of the workflow from recovery, library preparation, and sequencing.[240] It reported that after all these limitations, sequencing only achieves coverage of 15-50% of total transcripts.[240]

Alternatively, dPCR is a highly sensitive approach facilitating precise and accurate detection and quantification of specific nucleic acid target sequences without the requirement of pre-amplification. In dPCR, individual DNA segments are partitioned into discrete reaction droplets through a water-in-oil emulsion following the Poisson distribution. Each droplet acts as an individual reaction for PCR amplification. The fluorescent intensity of each droplet is then measured in parallel with end-point PCR analysis. This converts data analysis into a binary

positive/negative result based on fluorescent intensity, leading to easy data analysis without the need for standard curves for quantification, which could be quickly reported back to a treating physician.[241,242]

Here, we have established a workflow for rapid single cell profiling of CTCs for simultaneous gene expression and mutation detection to evaluate how tumor subpopulations evolve over time. We screened 58 CTCs from six NSCLC patients with known EGFR mutations and identified intra-patient heterogeneous mutation profiles in these CTCs.

4.3 Methods

4.3.1 Cell culture

Cells were maintained at 37 °C under normoxic conditions. Cells were grown to 70-80% confluence before subculturing using 0.05% Trypsin-EDTA (Gibco). H1975 (EGFR L858R/T790M mutant), H1650 (exon 19 deletion) and T47D (EGFR wildtype) cells were grown in RPMI-1640 (Gibco), and A549 (EGFR wildtype) were grown in F-12 (Gibco), each supplemented with 10% FBS (Sigma) and 1% Antibiotic-antimycotic (Gibco). Media was exchanged every 48-72 hours between subculturing. Cell lines were routinely tested and reported negative for mycoplasma contamination (Lonza).

4.3.2 RNA extraction & cDNA synthesis

For cell line experiments, total RNA was purified using miRNeasy mini kit (Qiagen) following the manufacturer's protocol. RNA concentration and purity were evaluated using a NanoDrop ND-1000 spectrophotometer. For each sample, 2000 ng of total RNA was loaded into each reverse transcription reaction. cDNA was synthesized using SuperScript IV VILO Master Mix with ezDNase Enzyme (Invitrogen) following the manufacturer's protocol. All purified RNA and

cDNA products were handled in a PCR workstation (AirClean Systems) to prevent nuclease contamination.

4.3.3 Experimental protocol for labyrinth (patient sample processing)

The experimental protocol was approved by the Ethics (Institutional Review Board) and Scientific Review Committees of the University of Michigan and all patients gave their informed consent to participate in the study. All patients had a diagnosis of EGFR mutant lung adenocarcinoma.

Briefly, blood samples were collected in EDTA tubes and processed through the Labyrinth within 2 hours of collection. RBCs in the blood samples were removed using density separation with Ficoll-Paque™ PLUS Media (GE Healthcare) following the manufacturer's protocol prior to processing in the Labyrinth.

The plasma and blood mononuclear cells (PBMCs) layers were collected and diluted with PBS (1:5). The diluted sample was then processed through the Labyrinth at 2500 μL/min, and the product from outlet 2 was collected. To achieve a higher purity, the second outlet's products of the Labyrinth (single) were processing through another Labyrinth (double).

4.3.4 Immunofluorescent staining and CTC enumeration

The product of single Labyrinth from outlet 2 was processed using a Thermo ScientificTM Cytospin Cytocentrifuge. A poly-lysine coated slide was placed into the cytospin funnel and 250 μL of sample was added to each cytospin funnel and cytocentrifuged at a speed of 800 rpm for 10 min. Samples were fixed on the cytoslides using 4% paraformaldehyde (PFA) and cytocentrifuged at the same conditions as described above. Slide samples were permeabilized by applying 0.2% Triton X-100 solution for 3 min. Slides were then washed with PBS (X 3) for 5 min and blocked using 10% donkey serum for 30 min at room temperature.

The panel of antibodies (anti-human CD45 (mouse IgG2a) (Bio-Rad), anti-human Pan-cytokeratin (CK) (mouse IgG1) (Bio-Rad), anti-human EpCAM, biotinylated (goat IgG) (R&D Systems), and anti-human vimentin (rabbit IgG) (Abcam) were used. The slides were then incubated with a cocktail of primary antibodies (anti-CD45, anti-PanCK, anti-EpCAM, and anti-Vimentin) overnight at 4˚C, followed by PBS wash (X 3) for 5 min the following day. Slides were incubated in the dark with secondary antibodies secondary antibodies goat anti-mouse IgG2a Alexa Fluor 488 (AF 488) (Invitrogen), goat anti-mouse IgG1 Alexa Fluor 546 (AF 546) (Invitrogen), goat anti-rabbit Alexa Fluor 647 (AF 647) (Invitrogen), and Stepavadin, Alexa Fluor 750 conjugate (Invitrogen) for 1.5 hour at room temperature. Finally, slides were washed with PBS (X 3) for 5 min and mounted using Prolong Gold Antifade Mountant with DAPI (Invitrogen). The stained slides were imaged using a Nikon TI inverted fluorescent microscope at 20X magnification for enumeration.

The tiled images generated from the scans were manually viewed and CTCs were determined based on their fluorescent signals in each channel. A CTC was counted as DAPI+/CK+ (AF 546)/CD45- (AF 488). The CTC phenotype was determined based on the presence/absence of phenotype markers. EpCAM was used an epithelial marker, and vimentin was used as a mesenchymal marker. CTCs (DAPI+/CK+/CD45-) were considered epithelial if EpCAM+/vimentin-, mesenchymal if EpCAM-/vimentin+, and EMT (epithelial to mesenchymal transition) if EpCAM+/vimentin+.

4.3.5 Fluidigm C1 & Biomark HD

Cell suspensions were loaded onto the C1 Single-Cell Auto Prep IFC for Preamp (10-17μm) (Fluidigm) following the company's protocol with on-chip cell staining. The cells were stained

with FITC pre-conjugated anti-human CD45 (Biolegend), as a negative marker. After loading, each cell capture site was manually imaged.

For targeted pre-amplification, a pre-designed panel of 96 genes implicated in cancer progression, phenotype, and aggressiveness was used to characterize the cells. After the C1 run was complete, the sample was diluted using C1 DNA dilution reagent. For the dPCR data generated using lung cancer cell lines, the C1 product was diluted to 28 μL, based on the manufacturer's protocol. For the lung CTC samples, the C1 product was diluted to only 12-15 μL to keep the sample more concentrated for dPCR testing. 2 μL of this sample was further diluted to 4 μL using the C1 DNA dilution reagent and was used for gene expression analysis on the Biomark HD system (Fluidigm) following the manufacturer's protocol, while the remainder was used for mutation detection.

4.3.6 Mutation detection using dPCR

The RainDrop system (RainDance Technologies) was used for dPCR mutation detection. In brief, the PCR mix was prepared using TaqMan SNP Assay (Life Technologies), TaqMan Genotyping Master Mix (Applied Biosystems), and droplet stabilizer (RainDance Technologies). cDNA was mixed with the PCR mix in PCR tubes to generate 25 μL reactions and loaded onto the Source Chip (RainDance Technologies). The PCR reaction is emulsified with Carrier Oil (RainDance Technologies) into approximately 4 million, 5 pL sized droplets with single molecule loading, and collected into an 8-tube PCR strip (Axygen). After droplet generation, the PCR tubes were transferred to the thermocycler for 45 rounds of PCR amplification. The TaqMan SNP assays contain two probes, one for wildtype EGFR sequence the other for the mutant EGFR sequence, with VIC and FAM probes, respectively. The TaqMan exon 19 deletion assay contains probes for 19 common exon 19 deletion variants, all with a FAM probes. The PCR tubes containing the

amplified samples were then transferred onto the Sense Machine (RainDance Technologies) where the endpoint fluorescence intensity of each droplet is measured. Gating templates were generated using positive and negative cell line controls.

4.4 Results and discussion

4.4.1 Single cell co-analysis workflow

The development of a highly sensitive approach could overcome the limitations of liquid biopsies, such as rarity of the targets and low volume constraints, facilitating early detection of resistance mutations. Here, our workflow is optimized for ultra-low input and can consistently detect the presence of these EGFR mutations at the single cell level (Figure 4.1). To interrogate CTCs with single-cell resolution, we integrated our previously developed inertial microfluidic isolation technology, the Labyrinth and the commercial Fluidigm integrated fluidic chip (IFC).[243] First, CTCs are enriched from peripheral blood using the Labyrinth, a high-throughput, label-free technology, that isolates CTCs from blood cells based on cell size. The microfluidic device incorporates curved channels and sharp corners to efficiently focus both CTCs and white blood cells (WBCs) into separate streamlines, and has been previously shown to yield >90% recovery of CTCs and >90% WBC removal.[243] To improve CTC purity and facilitate better compatibility with current single cell isolation technologies, the remaining WBCs are depleted using an immunoaffinity capture microfluidic device functionalized with a cocktail of antibodies against common WBC targets including CD45, CD15, and CD11b. Finally, the ultra-pure CTC suspension is loaded onto the Fluidigm IFC, which streamlines on-chip single-cell capture, lysis, reverse transcription (RT), and targeted PCR pre-amplification of up to 96 single cells. For pre-amplification and gene expression, we chose a targeted analysis because it has been previously

reported single cell PCR offers all the benefits of bulk qPCR analysis including high sensitivity, specificity, and reproducibility.

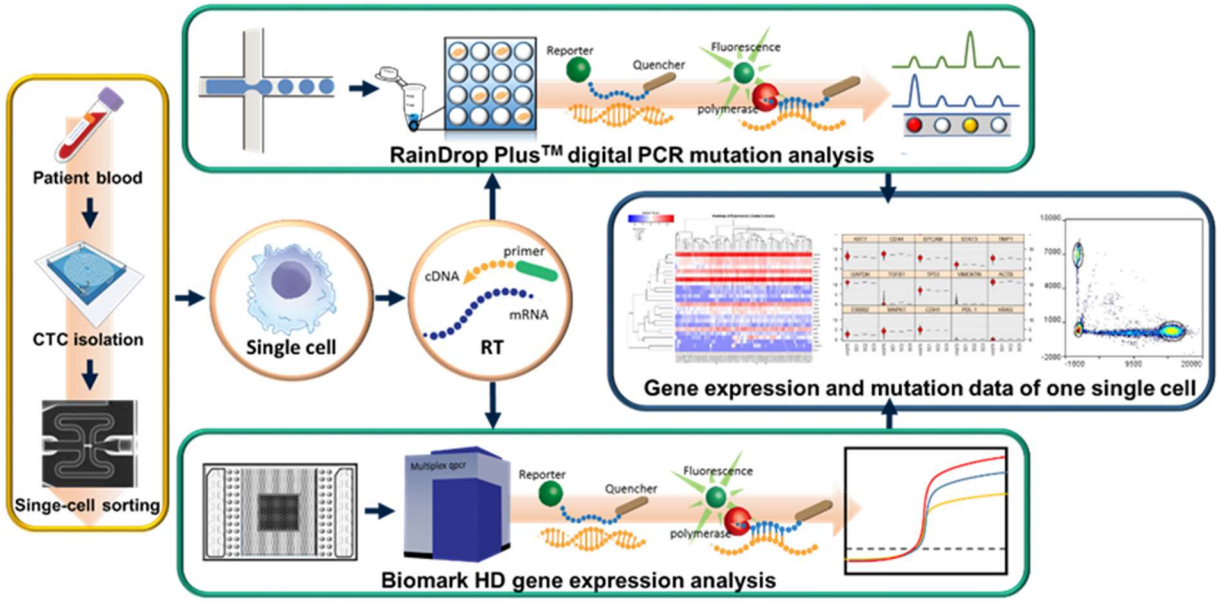

Figure 4.1 Circulating tumor cell sample processing schematic overview for single cell analysis.
Blood is collected from EGFR mutant NSCLC patients and. The blood sample is process through the Labyrinth, a size-based sorting microfluidic technology to isolate CTCs (~15-20µm) from WBCs (~10-12µm). The CTC sample is loaded onto the Fluidigm C1 for single cell capture and processing. The resultant single cell sample is then used for gene expression and EGFR mutational profile co-analysis.

Due to the C1 processing protocol, the generated complementary DNA (cDNA) is fragmented due to RT with random primers. This is optimal for the gene expression and EGFR mutation co-analysis because it allows for better coverage of the entire transcript. The pre-amplification on the C1 IFC is a targeted gene panels and occurs only within the region of interest for gene expression (Table 4.1), while the regions of the EGFR mutations (exons 19-21) remain un-amplified. This leaves an untampered view of not only the EGFR mutational burden but the relative transcription of wildtype and mutant alleles.

Table 4.1: Lung cancer 96 gene panel used for Biomark HD qPCR

Lung Cancer 96 Gene Panel											
GAPDH	CD133	KRT5	MMP2	JUP	ELF3	SERPINB6	TMPRSS2	IL6	CXCR1	MKI67	CD3D
ACTB	ALDH1A1	KRT7	MMP9	EVPL	CHP1	DSP	CXCL16	IL8	IGFBP5	XIST	CD11B
EPCAM	ALDH1A3	KRT8	TIMP1	NTRK2	PKP2	MLPH	ETV1	MTOR	ERCC1	HOTAIR	CD20
VIMENTIN	CDH1	KRT14	TIMP2	MUC1	CDH11	TROP2	ERG	ALK	KLF4	SPARC	CD33
ERBB2	CDH2	EMP2	PD-1	PSME3	BCL-xL	CTNND1	KLK3	EGFR	MAPK1	CCND1	CD34
CD24	TGFB1	TP53	PDL-1	XBP1	XIAP	CTNNA1	FOLH1	BMi1	STAT3	COL3A1	CD45
CD44	ABCG2	PTEN	COL1A2	FOXC1	CASP3	NFKB1	PTCH1	PIK3CA	ZEB1	SNAI1	CD146
CD44v6	CTNNB1	RB1	LGALS3BP	FOXC2	UBB	AR	PTPRN2	KRAS	ZEB2	SNAI2	FGF18

To achieve the simultaneous gene expression and mutation detection from a single cell, a small portion of the pre-amplified cDNA was used for gene expression profiling of the pre-designed, targeted 96 gene panel with highly multiplexed qPCR via the Biomark HD Dynamic Array (Fluidigm, USA).[243] The remaining single cell sample is analyzed for mutations using a duplex assay for the wildtype and mutant-specific sequences on the RainDrop dPCR system (RainDance Technologies, USA).

4.4.2 Validation of EGFR mutation detection using digital PCR (dPCR)

Three major EGFR driver mutations, L858R, T790M and exon 19 deletions, were chosen for this study because of their implications on patient sensitivity to TKI therapy. NSCLC patients harboring activating mutations, L858R or exon 19 deletions, in EGFR have a dramatic response to TKI therapy, but develop resistance after about 10 months through a secondary mutation, most commonly T790M.[233,244,245] To validate the performance of the dPCR platform, we detected and quantified the mutant transcripts of bulk cDNA derived from H1975 (L858R and T790M) and H1650 (exon 19 deletion) cell lines. The cDNA was analyzed for the presence of EGFR L858R, T790M and exon 19 deletions at loadings ranging from 0.05ng-50ng (Figure 4.2). For the point mutations, L858R and T790M, discrete mutant and wildtype gates were generated based on the positive controls. For the exon 19 deletion, the TaqMan assay contains a pool of 19 common exon 19 deletion variants, which caused a larger population spread, even in control cell lines, and

required a quadrant-based gating, as shown in Figure 4.2A. Linear regression analysis of the fraction of positive droplets versus cDNA loading exhibited a linear relationship (R^2=0.99), demonstrating a large dynamic range (Figure 4.2B).

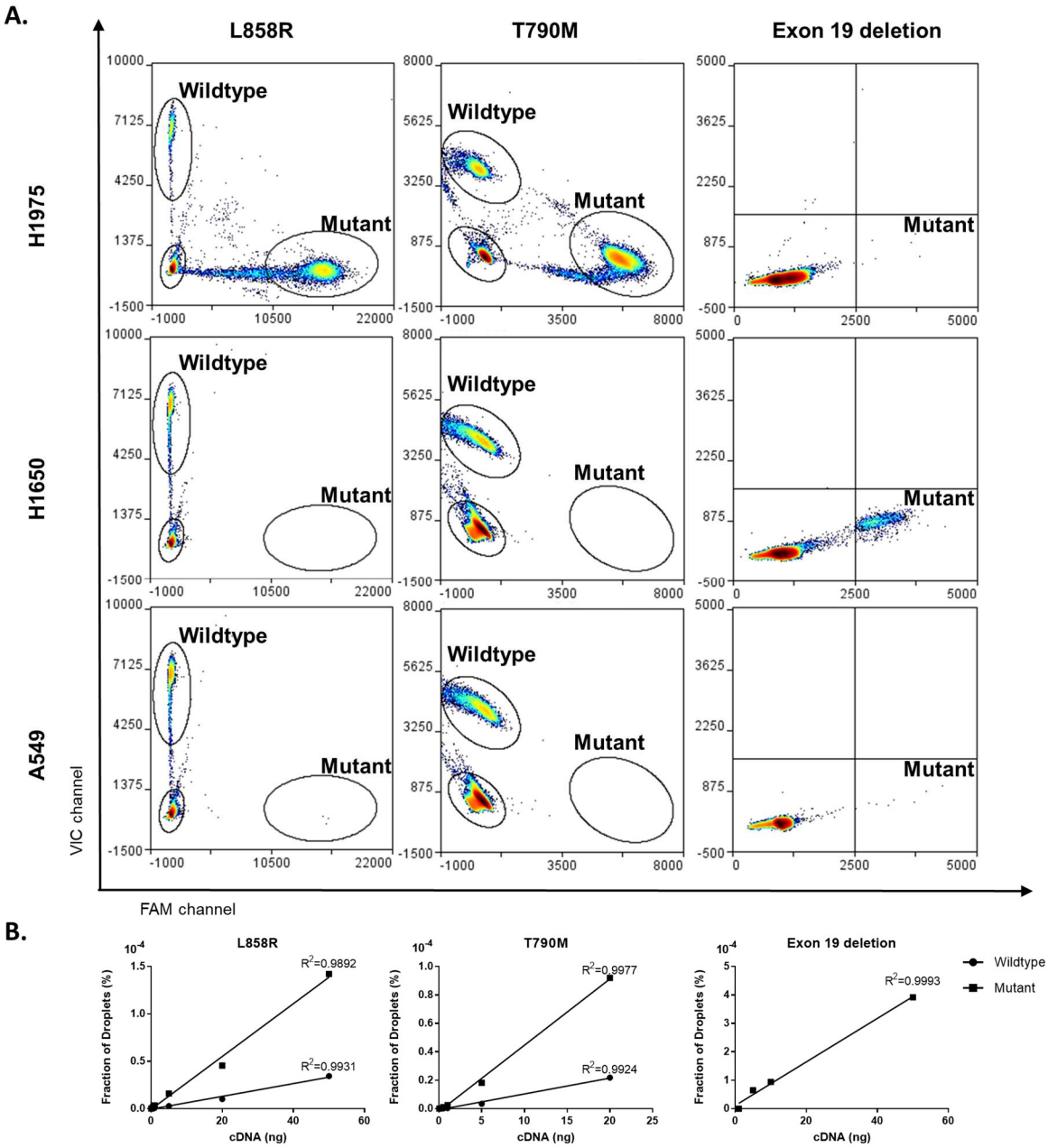

Figure 4.2 Validation of EGFR mutation detection using RainDance dPCR system.
(A) Representative dPCR plots of lung cancer cell line controls, H1975 (L858R/T790M), H1650 (exon19 deletion) and A549 (wildtype), for the three tested EGFR mutations, L858R (left), T790M (middle), and exon 19 deletion (right). For the point mutations (L858R and T790M, Taqman assays detect the wildtype (VIC channel) and mutant (FAM channel) variants. For exon 19 deletion, the assay screens for 19 common deletions (FAM channel). **(B)** Dynamic linear range of positive droplet counts using serial dilutions of cDNA for L858R (left), T790M (middle) and Exon 19 deletion (right) (Range = 0.05ng-50ng). Droplets counts for L858R and T790M results used cDNA generated from H1975 cells and exon 19 deletion results used H1650 cells.

4.4.3 Establishing robust single cell gene expression and EGFR mutation co-analysis

To establish the single cell co-analysis workflow, H1975 and H1650 cells were processed on the aforementioned C1 IFC chip followed by multiplexed qPCR and dPCR analysis (Figure 4.3A). Figure 4.3B shows consistent detection of EGFR wildtype and mutant transcripts at the single cell level in H1975 cells. A heterogeneous expression of total EGFR was observed in H1975 cells with an average of 57 EGFR droplets per cell (range 17-88) for the L858R mutant duplex assay and 41 positive EGFR droplets per cell (range 13-72) for the T790M mutant duplex assay. The H1650 cells tested with the exon 19 deletion assay showed an average of 11 positive droplets per cells (range 3-14). Figure 4.3C shows that the mutant population contained approximately 5 times higher droplet counts than the wildtype population (ratio range 2.5-9.3) in both the L858R and T790M duplex assays. The variations in the mutation-wildtype ratio demonstrate cell-to-cell heterogeneity, highlighting the utility of single cell analysis. The average of the H1975 single cells matched the bulk population for both mutation assays (Figure 4.3C). This higher expression of the mutant transcript is consistent with an increased EGFR mutant copy number in H1975 cells.[246]

Even within a cell line, heterogeneous gene expression profiles (Figure 4.3E) and EGFR transcript counts based on dPCR were observed (Figure 4.3B), highlighting the need to dissect heterogeneity of tumor cells at a single-cell resolution. As can be seen, the expression of common NSCLC phenotype markers, such as EGFR, CD44, and EPCAM, showed cell to cell variability in each H1975 and H1650 single cells and could be used to characterize phenotypic subpopulations. Moreover, there was a strong concordance between EGFR gene expression measured by qPCR and absolute EGFR droplet count in H1975 single cells (Figure 4.3F), further confirming the accuracy of the results and highlighting their complementarity.

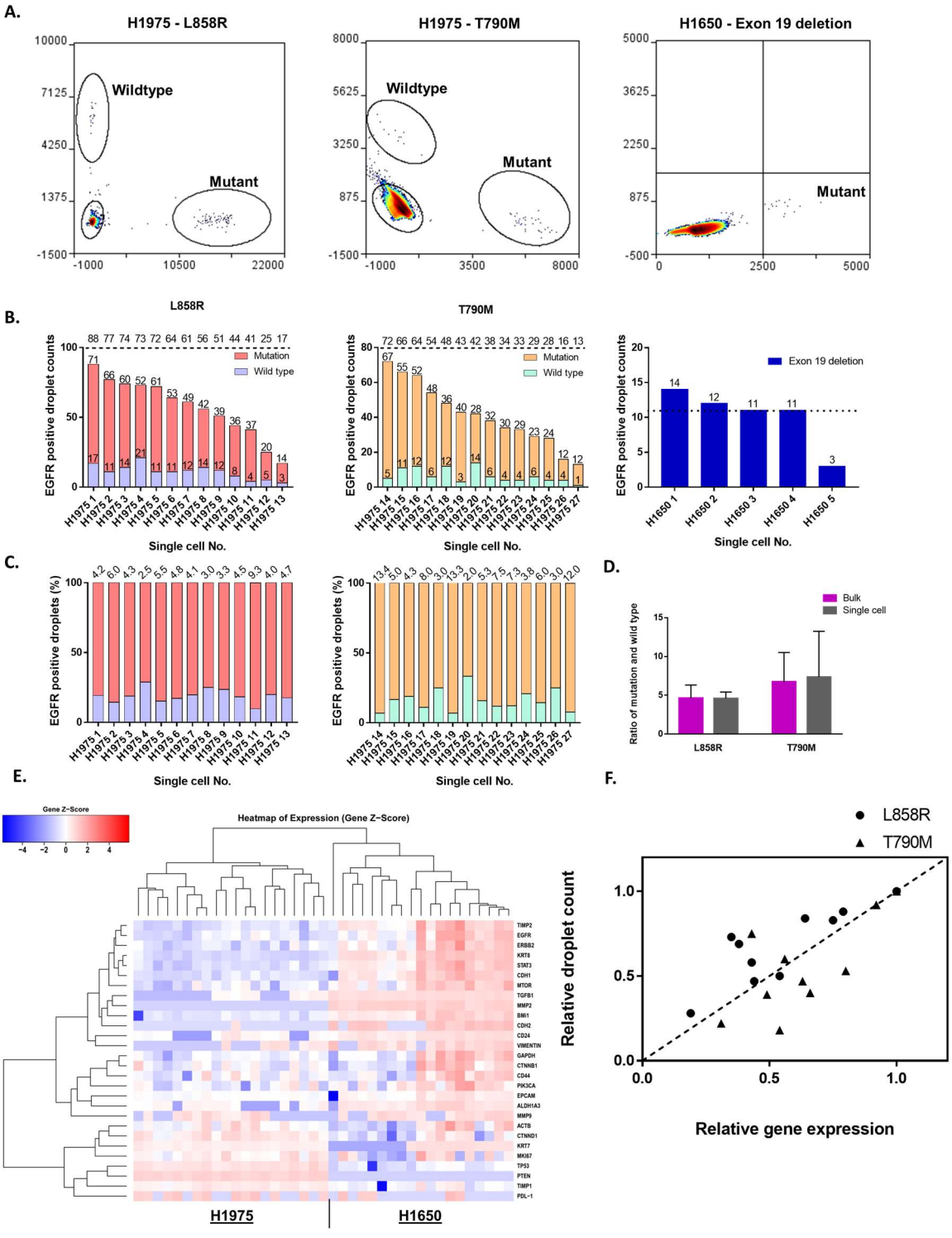

Figure 4.3 Validation of single cell workflow for gene expression and EGFR mutation analysis using lung cancer cell lines.

(A) Representative dPCR plots of H1975 and H1650 single cells for EGFR L858R and T790M point mutations and exon 19 deletion, respectively. (**B)** Single cells express heterogeneous total EGFR levels based on the combined mutant and wildtype droplet counts. Positive droplet counts

for each cell are shown. L858R: n= 13 H1975 cells. T790M: n= 14 H1975 cells. Exon 19 deletion: n= 5 H1650 single cells. Due to the noise of the exon 19 deletion assay, a threshold for positive detection is shown. (**C)** Comparison of relative mutant and wildtype EGFR expression in single droplet counts in H1975 single cells. Ratio of mutant:wildtype droplet counts shown above each cell. L858R: n=13 H1975 cells. T790M: n=14 H1975 cells. (**D)** The average ratio of mutant:wildtype droplet counts in H1975 single cells was compared to bulk cells in the L858R and T790M assays. L858R - bulk: n=12, single cells: n= 13. T790M - bulk: n=9. single cells: n= 14. (**E)** Heatmap of H1975 and H1650 single cells of 28 genes shows heterogeneous gene expression within each cell line. (**F)** The correlation between gene expression and total droplet counts of mutation and wildtype in the same single cells. Each data point denotes a single cell. The gene expression and mutation droplet count data of each single cell are normalized to a cell that has the highest gene expression and mutation droplet counts.

4.4.4 Single cell characterization of NSCLC CTCs

After establishing this single cell workflow, CTCs isolated from NSCLC patients were evaluated. NSCLC patients were enrolled at the University of Michigan Rogel Cancer Center, under an IRB approved protocol and contained known EGFR mutations based on primary tumor characterization.

CTCs were isolated from six metastatic NSCLC patients positive with known EGFR mutations (Figure 4.4B). CTCs were isolated using the previously described Labyrinth microfluidic technology.[243] A small portion of the CTC sample was used for enumeration with immunocytochemistry (ICC) (Figure 4.4A). CTCs were identified as being cytokeratin (CK) positive and CD45 negative (Figure 4.4A) and had highly heterogeneous expression of EMT markers. Some CTCs showed the expression of epithelial marker, EpCAM, while others showed expression of mesenchymal marker, vimentin (vim). A subset of CTCs showed dual expression of EpCAM and vim, suggesting an intermediate state within EMT (Figure 4.4A). We observed a wide range of CTC numbers across the patients (range 38.5-201.4 CTCs/mL blood), and it was noted that the patients who were progressing at the time of blood draw tended to have higher CTC numbers than those who have stable disease (Figure 4.4B,C).

From these six patients, the remainder of the CTC sample was used for single cell analysis via the C1 platform. The sample was stained on the IFC for CD45, and only CD45 negative cells were processed for mutation screening. Individual CTCs were tested for the presence of tumor tissue-matched EGFR mutations (Figure 4.4B, 4.5A). In 5/6 patients, we were able to identify the presence of these EGFR mutations (Figure 4.5A, C-E) in at least one CTC. In patients 1 and 3-6, the CTCs contained patient-matched EGFR mutations, whereas for patient 2, dPCR signal was within the level of uncertainty to confidently classify the CTCs as containing exon 19 deletion. We did not observe any correlation between the CTC number and the percent of CTCs that tested positive for EGFR mutations. Nor was it observed that the percent of EGFR mutation positive CTCs trended with patient status.

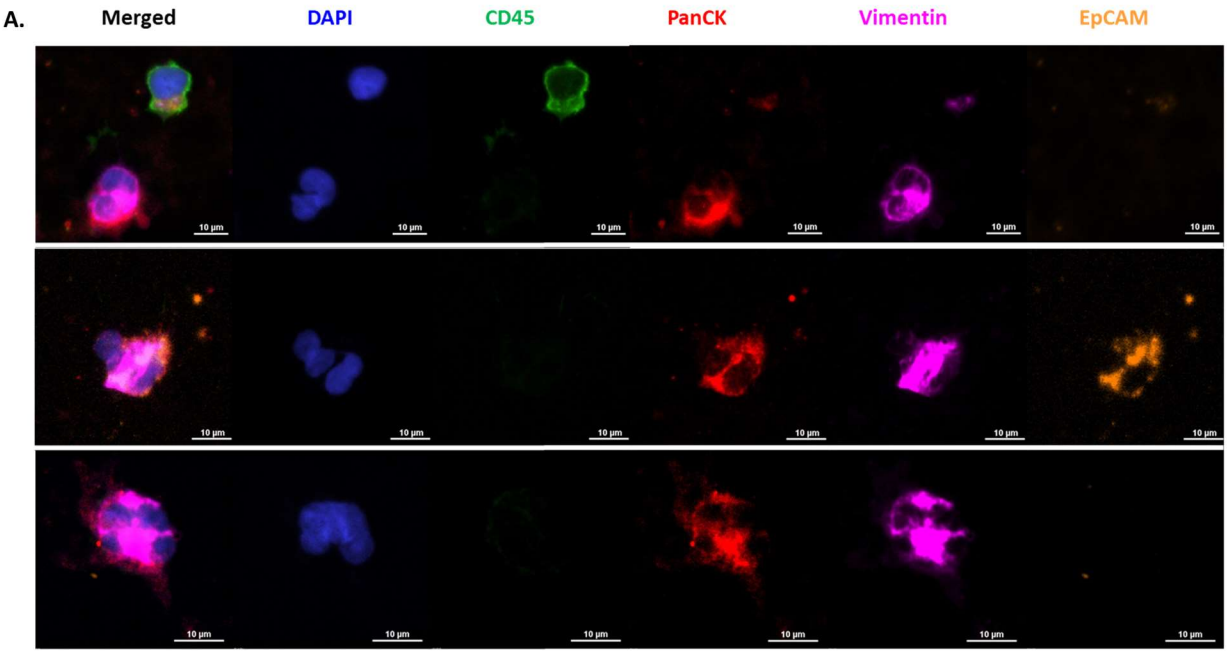

B.

Patient	EGFR Mutation	Treatment at time of blood draw	Status
P01	T790M	Osimertinib	Stable
P02	Exon 19 deletion	Osimertanib	Stable
P03	L858R, T790M	Pemetrexed	Progressing
P04	Exon 19 deletion	Afatinib	Progressing
P05	Exon 19 deletion, T790M	Osimertinib	Progressing
P06	Exon 19 deletion	Osimertinib	Stable

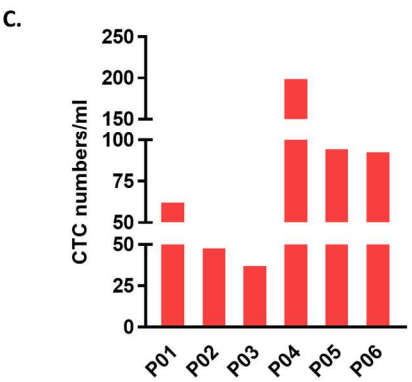

Figure 4.4 Patient characteristics and CTC analysis.
(A) Representative images of heterogeneous CTCs and different EMT phenotypes based on EpCAM (epithelial) and vimentin (mesenchymal) ICC. **(B)** Patient mutation based on tumor profiling and treatment regimen. **(C)** CTC enumeration across the 6 patients based on immunofluorescent staining. (Range = 38.5-201.4 numbers/ml).

For the subset of patients with the point mutations, L858R and T790M, in all CTCs we exclusively observed a heterozygous EGFR mutation expression, with variable mutation to wildtype expression ratios. For all tested cells, there was a higher abundance of wildtype expression compared to the mutant allele. This could be caused by the altered copy number variation profiles within the CTCs or differential gene expression regulation. Our data demonstrated the significance of single cell analysis to identify homozygous and heterozygous mutations, which would be lost

in bulk analysis. Further, with single cell analysis we could also evaluate the relative expression of each allele.

The remaining portion of the single cell sample was used for gene expression of the pre-designed 96-gene panel. dPCR was able to detect the presence of EGFR transcripts that was below the limit of detection on the multiplexed qPCR system (Figure 4.5B). Interestingly, the genes most commonly expressed in the CTCs were regulators of cell proliferation, such as estrogen receptor 1 (ESR1) and anti-apoptosis, such as BCL2, or differentiation, such as TGFβ1. It has been shown that ESR1 expression and EGFR mutations tends to occur more frequently together in NSCLC.[247,248] ESR1 expression in lung cancer has been associated with poor patient prognosis, while ESR2 correlation with patient prognosis appears to be dependent on cellular localization. Estrogen, through estrogen receptor signaling, can activate the signaling pathway downstream of EGFR, PI3K/AKT. This can lead to EMT and promote cancer metastasis.[248] Additionally, there have been clinical trials evaluating the efficacy of EGFR TKI therapy in combination with estrogen receptor antagonists and in a pilot study treatment was well tolerated and showed efficacy.[248]

TGFβ1, known to be involved in EMT, expression showed a positive correlation with the expression of ER in the CTCs. Interestingly, the CTCs with the highest ER and TGFβ1 also had has BCL2 expression, an inhibitor of apoptosis.[249]

EGFR expression was below the limit of detection on the qPCR analysis but was detected using the dPCR (Figure 4.5). Notably, for patient P06, a subset of the CTCs demonstrated a high level of exon 19 deletion EGFR expression, and also exhibited a gene expression profiles consistent with an aggressive phenotype.

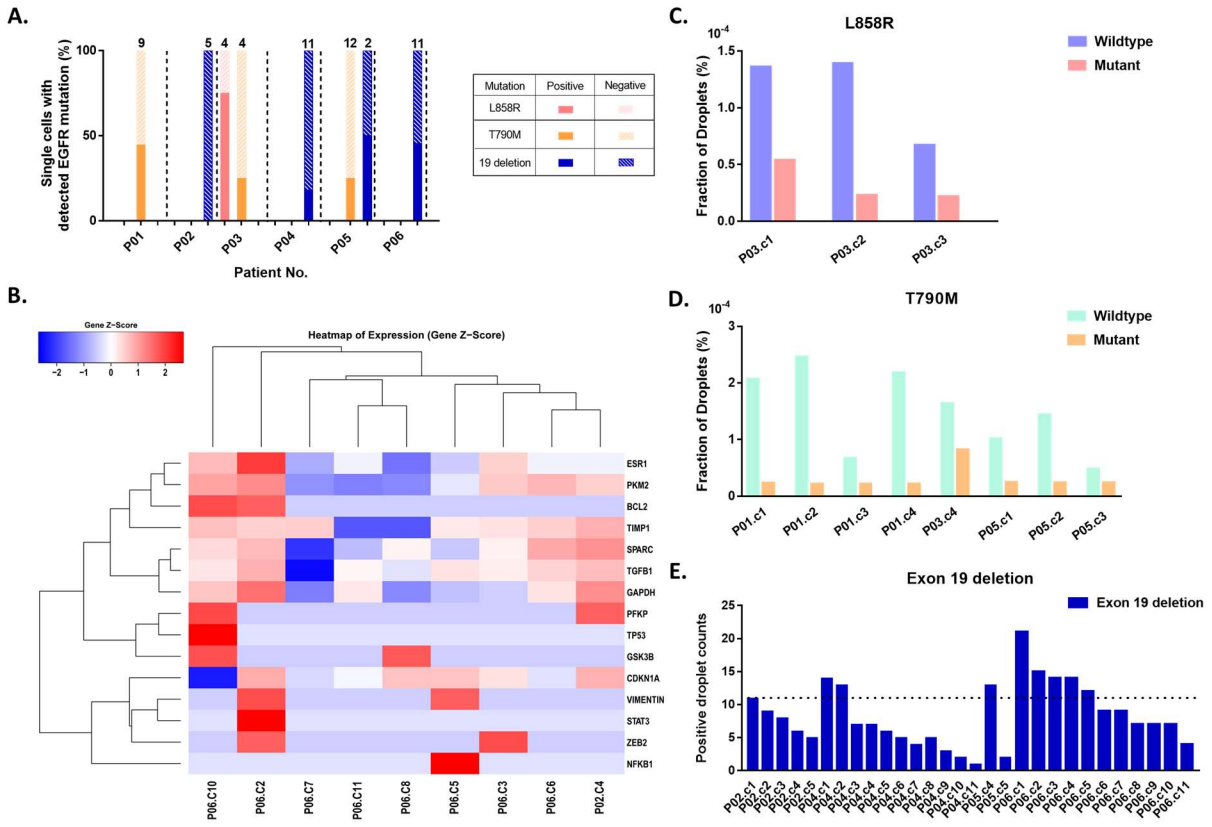

Figure 4.5 Patient tumor-matched mutations detected in CTCs.
(A) Summary of mutant single CTCs identified in each of the 6 patients (n=58). **(B)** Heatmap showing heterogeneous gene expression of single CTCs from two NSCLC patients (n=9). **(C-E)** Primary tumor matched mutations detected in patients' single CTCs for (**C)** L858R (n=3), **(D)** T790M (n=8), and **(E)** Exon 19 deletion (n=8).

4.5 Conclusion

In conclusion, we described a multiplexed, single-cell analysis method targeting gene expression and mutation detection from single circulating tumor cells. Compared to current clinical testing, this multiplexed method enables rapid turnaround from sample collection to result. By integrating ultra-sensitive technologies, a single cell can be profiled for multiple characteristics. We demonstrated the feasibility of our method to simultaneously quantify mutant transcripts and profile the gene expression of a single cell. To the best of our knowledge, this is the first use of dPCR for single cell analysis in CTCs, and we have highlighted the clinical relevance of this work. Due to the genetic instability and dynamic changes a tumor undergoes throughout treatment, real-time CTC monitoring of tumor evolution could help continually optimize a patient's treatment plan, improving patient outcome. The single-cell resolution enables the early detection of emerging rare clones that could lead to therapeutic resistance from a routine blood draw, allowing for more predictive analysis of targeted therapy response. In the case of NSCLC, co-analysis could reveal if specific clones harboring EGFR mutations are primarily utilizing EGFR-related pathways, or if another driver mechanism may be being utilized. The coupled gene expression and mutation profiling using a simple workflow that doesn't require complex computational analysis could be easily integrated into a clinical setting, enabling real-time monitoring and could ultimately facilitate more timely treatment modification.

Chapter 5

Conclusions and Future Directions

5.1 Summary of research

5.1.1 Microfluidic technologies for the isolation and characterization of circulating extracellular vesicles and evaluation of their functional role in amyotrophic lateral sclerosis

Amyotrophic lateral sclerosis (ALS) is a terminal neurodegenerative without an adequate biomarker to detect the disease. The study of EVs have offered valuable information to find new diagnostic and prognostic biomarkers for neuron degenerative diseases. In this study, we explored the potential of EV miRNAs as biomarkers of ALS. We used an immuno-affinity-based microfluidic device, the Exochip, for isolation and quantification of EVs from blood and tissues, including spinal cord and frontal cortex of ALS patients and healthy controls. The western blot and electron microscopy validated the vesicle isolation, and NanoString profiling was used to evaluate EVs miRNA signatures. Although there were no significant differences in EV concentrations between the ALS and control subjects, a total of 60 EV miRNAs were observed to be significantly dysregulated. The pathway analysis of predicted miRNA target genes also suggested the involvements of these miRNAs in ALS and neuron degeneration. This study showed the potential of EV miRNAs as novel biomarkers for ALS. Further studies on these miRNAs with

larger cohorts of patients may contribute to an understanding of the pathological mechanisms underlying ALS progression.

5.1.2 Microfluidic device for high-throughput affinity-based isolation of extracellular vesicles

Immuno-affinity approaches for EV isolation utilize the antibodies targeting the surface markers of EVs, providing higher specificity and purity over the existing physical approaches. However, the immuno-affinity methods suffer from certain limitations including low-throughput and the inability to release the EVs from the capture substrate. To overcome these limitations, we reprogramed the Oncobean chip, a immuno-affinity based microfluidic device that was developed to capture circulating tumor cells. The radial flow design and bean-shaped microposts functionalized with CD9, CD63, and CD81 antibodies allow for high-throughput isolation of EVs from plasma and culture media. Furthermore, by using the desthiobiotin antibody, the captured EVs can be released from the device with biotin elution. The cell uptake and intercellular migration of EVs verified by flow cytometry and confocal microscopy demonstrated that the released EVs are functional. We believe the proposed technology can facilitate the studies on the role of EVs as cell-to-cell communicators and identification of EV markers.

5.1.3 Simultaneous single cell gene expression and mutation profiling of Circulating Tumor Cells (CTCs)

Dissecting tumor cell heterogeneity is critical for understanding the tumor progression and resistance to therapies. However, the cellular heterogeneity and diversity are usually overlooked in bulk cell analysis, and thus missing important information from rare subpopulations. Here, we developed a workflow for rapid single cell profiling of CTCs for simultaneous gene expression and mutation detection. We demonstrated the feasibility of our method to simultaneously quantify mutant transcripts and profile the gene expression of a single cell with lung cancer cell lines. Our

data showed that there is cell-to-cell variation in gene expression and mutation transcript counts even in the homogenous cell population. Moreover, we demonstrated the utility of the workflow to study intra-patient heterogeneity by analyzing 58 CTCs from six NSCLC patients with known EGFR mutations.

5.2 Future directions and limitations

5.2.1 EV in ALS

In this thesis work, miRNA signature in EVs derived from tissues were profiled using NanoString technology. By comparing the miRNA profiles of ALS patients and healthy control, a total of 60 dysregulated EV miRNAs were identified, suggesting the potential of EV miRNAs as biomarkers for ALS. However, there were some limitations in this study.

One of the major limitations is the reliance on CD63 for EV capture. Using our technology, we were able to isolate only CD63 positive EVs. However, studies have demonstrated the presence of CD63 negative EVs. Isolation solely based on CD63 may exclude important populations of EV. Method to address such concerns is using a cocktail of antibodies that are also common markers for EVs, such as CD9 and CD81. Furthermore, antibodies that targets specific EV populations can also be incorporated. For instance, L1 cell adhesion molecule antibody could be used to target EVs of neuronal origin.

Another limitation is the relatively small size of patient cohort (<15 for each tissue). Due to the limited availability of brain and spinal cord tissues, cohorts selected in this study were mainly based on availabilities, and all patients are sporadic ALS. To generate data that can have significant conclusions on implications of EV miRNA in ALS, the data should be verified in larger cohorts. Additionally, the uncertainty in the sample collections is also a limitation. The plasma samples

were collected from the patients at various stages of ALS while the spinal cord and frontal cortex tissues were collected postmortemly, which only reflects the terminal stage of ALS. To address such limitations, the dysregulated miRNAs identified in postmortem tissues can be validated with samples from central nervous system of patients at different ALS stages, such as CSF.

Finally, although the pathway analysis in the current study suggested the potential involvement of EV miRNAs for neuron degeneration, the influence of EV miRNAs on ALS pathology was not experimentally verified. It is important to examine the correlation of transfer of miRNAs via EVs with ALS pathology. The future investigation should focus on how the miRNAs regulate the cellular functions in CNS through EVs and verify their involvements in ALS pathogenesis. Furthermore, to evaluate the utility of EV miRNAs as diagnostic biomarkers, the correlation of ALS progression and status with the changes in EV miRNA will also be investigated in the future.

5.2.2 High throughput capture and release of EVs using OncoBean chip

In the past two decades, the advancements in microfluidic technologies for EV isolation has profoundly improved the understanding of mechanisms involved cancer and neurodegeneration diseases. The microfluidic EV isolation can be classified into immuno-affinity approach and physical approach. The immune-affinity approach coupled with microfluidic technologies have shown higher purity and specificity enrichment of EV. The microfluidic device introduced in this report (Chapter 3) made further advancements by incorporating the radial flow microfluidic chip with desthiobiotin-biotin release strategy to increase the throughput and harvest the intact EVs. To more broadly apply such technology, some potential future steps are worth to be mentioned.

Although we have demonstrated the ability of the device to capture and release EV from culture media and healthy plasma at high throughputs, the Oncobean device should be tested with clinical

samples to further validate its application. Optimization will require continued testing on the device with other types of samples such as CSF, tissue homogenates, and urine. Body fluids have different physical properties and non-vesicular components that requires different operation conditions for the device to maintain the yields with reliable quality. The performance of the chip with different body fluids should be evaluated by analyzing the quantity, size, and purity of released EV. Moreover, further work should involve examining the feasibility of performing other downstream analysis on genomic and proteomic contents of these EVs, such as NGS, ELISA, and dPCR.

More importantly, the major reason for releasing EVs is to facilitate the study on how the EVs change the genotype and phenotype of the cells after their internalization. Therefore, to apply the device for such studies, the device should be tested and optimized with other desthiobiotin-conjugated antibodies that target EVs with different cell origin. More studies also need to be done to further evaluate the influences of uptake of released EVs by analyzing the genomic and proteomic alterations in the recipient cells. Characterizing the uptake and the intracellular tracking of these EVs in different cells can provide valuable information in EV biogenesis. We believed further development of this chip and its application will hold promise to enable the study of EVs on their composition, properties, and functions in various cell types.

5.2.3 Single cell analysis

In chapter 4, we presented a workflow integrated different microfluidic technologies to achieve the CTC isolation and characterization at the single cell level. Although the described workflow demonstrated the ability to assess the heterogeneity among CTCs with high sensitivity, the workflow is not yet perfect. Some limitations of the proposed workflow need to be addressed.

Another major limitation that needs to be improved is the challenge of the contaminating leukocytes. The proposed workflow utilizes a previously developed microfluidic device, the Labyrinth, to concentrate the CTCs from patient blood. After 88% WBCs are sorted out from the sample by the Labyrinth, we used a microfluidic device with cocktail of antibodies, including CD45, CD11b, and CD15, to further remove the WBCs. However, the remaining WBCs in the suspension still cause the low recovery of single CTCs in C1 chip. In the future, other technologies should be incorporated to further enhance the WBC deletion.

The other potential area of improvement will be the workflow is multiplex dPCR. Although the dPCR mutation analysis workflow provide precise and sensitive quantification of mutation transcripts, it only detects up to two targets within a single reaction. It is a critical shortcoming when working with large sample numbers and low availability of sample volume, which is typical for single cell analysis. To increase analytic capacity, future studies should focus on the implementation of multiplex dPCR that enables simultaneous mutation analysis on multiple targets without compromising the sensitivity and specificity. Optimization of multiplex dPCR protocol is currently underway in our lab.

Finally, another critical goal of a future study could be to extrapolate the proposed workflow to EV molecular analysis. Similar to single cell analysis, molecular analysis of EVs is also facing hurdles in retrieving and analyzing RNA from small sample inputs. Given the successful implementation of the workflow for sorting and characterizing CTCs at a single-cell resolution, future efforts should adapt and further optimize the single cell analysis workflow to EV studies. This can be accomplished by incorporating technologies and protocols for EV isolation and then optimizing their compatibilities with current workflow.

5.3 Conclusion

Overall, the current thesis work performed has developed new technologies and approaches to analyze CTCs and EVs at molecular level. Further improvement will help the transition of these technologies from laboratory research into clinical application, thus facilitating the development for personalized precision medicine.

Bibliography

1 Willms, E. *et al.* Cells release subpopulations of exosomes with distinct molecular and biological properties. *Sci Rep* **6**, 22519, doi:10.1038/srep22519 (2016).

2 Raposo, G. & Stoorvogel, W. Extracellular vesicles: exosomes, microvesicles, and friends. *J Cell Biol* **200**, 373-383, doi:10.1083/jcb.201211138 (2013).

3 Thery, C. Exosomes: secreted vesicles and intercellular communications. *F1000 Biol Rep* **3**, 15, doi:10.3410/B3-15 (2011).

4 Zaborowski, M. P., Balaj, L., Breakefield, X. O. & Lai, C. P. Extracellular Vesicles: Composition, Biological Relevance, and Methods of Study. *Bioscience* **65**, 783-797, doi:10.1093/biosci/biv084 (2015).

5 Yanez-Mo, M. *et al.* Biological properties of extracellular vesicles and their physiological functions. *J Extracell Vesicles* **4**, 27066, doi:10.3402/jev.v4.27066 (2015).

6 Valadi, H. *et al.* Exosome-mediated transfer of mRNAs and microRNAs is a novel mechanism of genetic exchange between cells. *Nat Cell Biol* **9**, 654-659, doi:10.1038/ncb1596 (2007).

7 Gezsi, A., Kovacs, A., Visnovitz, T. & Buzas, E. I. Systems biology approaches to investigating the roles of extracellular vesicles in human diseases. *Exp Mol Med* **51**, 33, doi:10.1038/s12276-019-0226-2 (2019).

8 Lane, R. E., Korbie, D., Hill, M. M. & Trau, M. Extracellular vesicles as circulating cancer biomarkers: opportunities and challenges. *Clin Transl Med* **7**, 14, doi:10.1186/s40169-018-0192-7 (2018).

9 Vlassov, A. V., Magdaleno, S., Setterquist, R. & Conrad, R. Exosomes: current knowledge of their composition, biological functions, and diagnostic and therapeutic potentials. *Biochim Biophys Acta* **1820**, 940-948, doi:10.1016/j.bbagen.2012.03.017 (2012).

10 Otake, K., Kamiguchi, H. & Hirozane, Y. Identification of biomarkers for amyotrophic lateral sclerosis by comprehensive analysis of exosomal mRNAs in human cerebrospinal fluid. *BMC Med Genomics* **12**, 7, doi:10.1186/s12920-019-0473-z (2019).

11 Goran Ronquist, K. Extracellular vesicles and energy metabolism. *Clin Chim Acta* **488**, 116-121, doi:10.1016/j.cca.2018.10.044 (2019).

12 Contreras-Naranjo, J. C., Wu, H. J. & Ugaz, V. M. Microfluidics for exosome isolation and analysis: enabling liquid biopsy for personalized medicine. *Lab Chip* **17**, 3558-3577, doi:10.1039/c7lc00592j (2017).

13 Caruso, S. & Poon, I. K. H. Apoptotic Cell-Derived Extracellular Vesicles: More Than Just Debris. *Front Immunol* **9**, 1486, doi:10.3389/fimmu.2018.01486 (2018).

14 Thery, C. *et al.* Minimal information for studies of extracellular vesicles 2018 (MISEV2018): a position statement of the International Society for Extracellular Vesicles and update of the MISEV2014 guidelines. *J Extracell Vesicles* **7**, 1535750, doi:10.1080/20013078.2018.1535750 (2018).

15 Tetta, C., Ghigo, E., Silengo, L., Deregibus, M. C. & Camussi, G. Extracellular vesicles as an emerging mechanism of cell-to-cell communication. *Endocrine* **44**, 11-19, doi:10.1007/s12020-012-9839-0 (2013).
16 Puhka, M. *et al.* Metabolomic Profiling of Extracellular Vesicles and Alternative Normalization Methods Reveal Enriched Metabolites and Strategies to Study Prostate Cancer-Related Changes. *Theranostics* **7**, 3824-3841, doi:10.7150/thno.19890 (2017).
17 Deng, J. *et al.* Neurons Export Extracellular Vesicles Enriched in Cysteine String Protein and Misfolded Protein Cargo. *Sci Rep* **7**, 956, doi:10.1038/s41598-017-01115-6 (2017).
18 Becker, A. *et al.* Extracellular Vesicles in Cancer: Cell-to-Cell Mediators of Metastasis. *Cancer Cell* **30**, 836-848, doi:10.1016/j.ccell.2016.10.009 (2016).
19 Thompson, A. G. *et al.* Extracellular vesicles in neurodegenerative disease - pathogenesis to biomarkers. *Nat Rev Neurol* **12**, 346-357, doi:10.1038/nrneurol.2016.68 (2016).
20 Coleman, B. M. & Hill, A. F. Extracellular vesicles--Their role in the packaging and spread of misfolded proteins associated with neurodegenerative diseases. *Semin Cell Dev Biol* **40**, 89-96, doi:10.1016/j.semcdb.2015.02.007 (2015).
21 Zhao, H. *et al.* Tumor microenvironment derived exosomes pleiotropically modulate cancer cell metabolism. *Elife* **5**, e10250, doi:10.7554/eLife.10250 (2016).
22 Kahlert, C. & Kalluri, R. Exosomes in tumor microenvironment influence cancer progression and metastasis. *J Mol Med (Berl)* **91**, 431-437, doi:10.1007/s00109-013-1020-6 (2013).
23 Quail, D. F. & Joyce, J. A. Microenvironmental regulation of tumor progression and metastasis. *Nat Med* **19**, 1423-1437, doi:10.1038/nm.3394 (2013).
24 Azmi, A. S., Bao, B. & Sarkar, F. H. Exosomes in cancer development, metastasis, and drug resistance: a comprehensive review. *Cancer Metastasis Rev* **32**, 623-642, doi:10.1007/s10555-013-9441-9 (2013).
25 Luga, V. & Wrana, J. L. Tumor-stroma interaction: Revealing fibroblast-secreted exosomes as potent regulators of Wnt-planar cell polarity signaling in cancer metastasis. *Cancer Res* **73**, 6843-6847, doi:10.1158/0008-5472.CAN-13-1791 (2013).
26 Khazaei, S., Nouraee, N., Moradi, A. & Mowla, S. J. A novel signaling role for miR-451 in esophageal tumor microenvironment and its contribution to tumor progression. *Clin Transl Oncol* **19**, 633-640, doi:10.1007/s12094-016-1575-0 (2017).
27 Ringuette Goulet, C. *et al.* Exosomes Induce Fibroblast Differentiation into Cancer-Associated Fibroblasts through TGFbeta Signaling. *Mol Cancer Res* **16**, 1196-1204, doi:10.1158/1541-7786.MCR-17-0784 (2018).
28 O'Loghlen, A. Role for extracellular vesicles in the tumour microenvironment. *Philos Trans R Soc Lond B Biol Sci* **373**, doi:10.1098/rstb.2016.0488 (2018).
29 Webber, J., Steadman, R., Mason, M. D., Tabi, Z. & Clayton, A. Cancer exosomes trigger fibroblast to myofibroblast differentiation. *Cancer Res* **70**, 9621-9630, doi:10.1158/0008-5472.CAN-10-1722 (2010).
30 Fang, T. *et al.* Tumor-derived exosomal miR-1247-3p induces cancer-associated fibroblast activation to foster lung metastasis of liver cancer. *Nat Commun* **9**, 191, doi:10.1038/s41467-017-02583-0 (2018).
31 Peinado, H. *et al.* Melanoma exosomes educate bone marrow progenitor cells toward a pro-metastatic phenotype through MET. *Nat Med* **18**, 883-891, doi:10.1038/nm.2753 (2012).

32 Costa-Silva, B. *et al.* Pancreatic cancer exosomes initiate pre-metastatic niche formation in the liver. *Nat Cell Biol* **17**, 816-826, doi:10.1038/ncb3169 (2015).
33 Huang, T. & Deng, C. X. Current Progresses of Exosomes as Cancer Diagnostic and Prognostic Biomarkers. *Int J Biol Sci* **15**, 1-11, doi:10.7150/ijbs.27796 (2019).
34 Verma, M., Lam, T. K., Hebert, E. & Divi, R. L. Extracellular vesicles: potential applications in cancer diagnosis, prognosis, and epidemiology. *BMC Clin Pathol* **15**, 6, doi:10.1186/s12907-015-0005-5 (2015).
35 Melo, S. A. *et al.* Glypican-1 identifies cancer exosomes and detects early pancreatic cancer. *Nature* **523**, 177-182, doi:10.1038/nature14581 (2015).
36 Fu, H. *et al.* Exosomal TRIM3 is a novel marker and therapy target for gastric cancer. *J Exp Clin Cancer Res* **37**, 162, doi:10.1186/s13046-018-0825-0 (2018).
37 Moon, P. G. *et al.* Fibronectin on circulating extracellular vesicles as a liquid biopsy to detect breast cancer. *Oncotarget* **7**, 40189-40199, doi:10.18632/oncotarget.9561 (2016).
38 Niu, L. *et al.* Tumor-derived exosomal proteins as diagnostic biomarkers in non-small cell lung cancer. *Cancer Sci* **110**, 433-442, doi:10.1111/cas.13862 (2019).
39 Hao, Y. X. *et al.* KRAS and BRAF mutations in serum exosomes from patients with colorectal cancer in a Chinese population. *Oncol Lett* **13**, 3608-3616, doi:10.3892/ol.2017.5889 (2017).
40 Salehi, M. & Sharifi, M. Exosomal miRNAs as novel cancer biomarkers: Challenges and opportunities. *J Cell Physiol* **233**, 6370-6380, doi:10.1002/jcp.26481 (2018).
41 Kinoshita, T., Yip, K. W., Spence, T. & Liu, F. F. MicroRNAs in extracellular vesicles: potential cancer biomarkers. *J Hum Genet* **62**, 67-74, doi:10.1038/jhg.2016.87 (2017).
42 Shi, R. *et al.* Exosomal levels of miRNA-21 from cerebrospinal fluids associated with poor prognosis and tumor recurrence of glioma patients. *Oncotarget* **6**, 26971-26981, doi:10.18632/oncotarget.4699 (2015).
43 Bryant, R. J. *et al.* Changes in circulating microRNA levels associated with prostate cancer. *Br J Cancer* **106**, 768-774, doi:10.1038/bjc.2011.595 (2012).
44 Robinson, J. L. *et al.* Neurodegenerative disease concomitant proteinopathies are prevalent, age-related and APOE4-associated. *Brain* **141**, 2181-2193, doi:10.1093/brain/awy146 (2018).
45 Sweeney, P. *et al.* Protein misfolding in neurodegenerative diseases: implications and strategies. *Transl Neurodegener* **6**, 6, doi:10.1186/s40035-017-0077-5 (2017).
46 Ghavami, S. *et al.* Autophagy and apoptosis dysfunction in neurodegenerative disorders. *Prog Neurobiol* **112**, 24-49, doi:10.1016/j.pneurobio.2013.10.004 (2014).
47 Antonucci, F. *et al.* Microvesicles released from microglia stimulate synaptic activity via enhanced sphingolipid metabolism. *EMBO J* **31**, 1231-1240, doi:10.1038/emboj.2011.489 (2012).
48 Wang, S. *et al.* Synapsin I is an oligomannose-carrying glycoprotein, acts as an oligomannose-binding lectin, and promotes neurite outgrowth and neuronal survival when released via glia-derived exosomes. *J Neurosci* **31**, 7275-7290, doi:10.1523/JNEUROSCI.6476-10.2011 (2011).
49 Janas, A. M., Sapon, K., Janas, T., Stowell, M. H. & Janas, T. Exosomes and other extracellular vesicles in neural cells and neurodegenerative diseases. *Biochim Biophys Acta* **1858**, 1139-1151, doi:10.1016/j.bbamem.2016.02.011 (2016).
50 Saeedi, S., Israel, S., Nagy, C. & Turecki, G. The emerging role of exosomes in mental disorders. *Transl Psychiatry* **9**, 122, doi:10.1038/s41398-019-0459-9 (2019).

51 Paolicelli, R. C., Bergamini, G. & Rajendran, L. Cell-to-cell Communication by Extracellular Vesicles: Focus on Microglia. *Neuroscience* **405**, 148-157, doi:10.1016/j.neuroscience.2018.04.003 (2019).
52 Lee, J. Y. & Kim, H. S. Extracellular Vesicles in Neurodegenerative Diseases: A Double-Edged Sword. *Tissue Eng Regen Med* **14**, 667-678, doi:10.1007/s13770-017-0090-x (2017).
53 Gui, Y., Liu, H., Zhang, L., Lv, W. & Hu, X. Altered microRNA profiles in cerebrospinal fluid exosome in Parkinson disease and Alzheimer disease. *Oncotarget* **6**, 37043-37053, doi:10.18632/oncotarget.6158 (2015).
54 Ittner, L. M. & Gotz, J. Amyloid-beta and tau--a toxic pas de deux in Alzheimer's disease. *Nat Rev Neurosci* **12**, 65-72, doi:10.1038/nrn2967 (2011).
55 Rajendran, L. *et al.* Alzheimer's disease beta-amyloid peptides are released in association with exosomes. *Proc Natl Acad Sci U S A* **103**, 11172-11177, doi:10.1073/pnas.0603838103 (2006).
56 Saman, S. *et al.* Exosome-associated tau is secreted in tauopathy models and is selectively phosphorylated in cerebrospinal fluid in early Alzheimer disease. *J Biol Chem* **287**, 3842-3849, doi:10.1074/jbc.M111.277061 (2012).
57 Lugli, G. *et al.* Plasma Exosomal miRNAs in Persons with and without Alzheimer Disease: Altered Expression and Prospects for Biomarkers. *PLoS One* **10**, e0139233, doi:10.1371/journal.pone.0139233 (2015).
58 Surmeier, D. J. Determinants of dopaminergic neuron loss in Parkinson's disease. *FEBS J* **285**, 3657-3668, doi:10.1111/febs.14607 (2018).
59 Lindvall, O. Dopaminergic neurons for Parkinson's therapy. *Nat Biotechnol* **30**, 56-58, doi:10.1038/nbt.2077 (2012).
60 Michel, P. P., Hirsch, E. C. & Hunot, S. Understanding Dopaminergic Cell Death Pathways in Parkinson Disease. *Neuron* **90**, 675-691, doi:10.1016/j.neuron.2016.03.038 (2016).
61 Wills, J. *et al.* Elevated tauopathy and alpha-synuclein pathology in postmortem Parkinson's disease brains with and without dementia. *Exp Neurol* **225**, 210-218, doi:10.1016/j.expneurol.2010.06.017 (2010).
62 Tofaris, G. K. A Critical Assessment of Exosomes in the Pathogenesis and Stratification of Parkinson's Disease. *J Parkinsons Dis* **7**, 569-576, doi:10.3233/JPD-171176 (2017).
63 Emmanouilidou, E. *et al.* Cell-produced alpha-synuclein is secreted in a calcium-dependent manner by exosomes and impacts neuronal survival. *J Neurosci* **30**, 6838-6851, doi:10.1523/JNEUROSCI.5699-09.2010 (2010).
64 Stuendl, A. *et al.* Induction of alpha-synuclein aggregate formation by CSF exosomes from patients with Parkinson's disease and dementia with Lewy bodies. *Brain* **139**, 481-494, doi:10.1093/brain/awv346 (2016).
65 Cao, Z. *et al.* alpha-Synuclein in salivary extracellular vesicles as a potential biomarker of Parkinson's disease. *Neurosci Lett* **696**, 114-120, doi:10.1016/j.neulet.2018.12.030 (2019).
66 Zhao, Z. H. *et al.* Increased DJ-1 and alpha-Synuclein in Plasma Neural-Derived Exosomes as Potential Markers for Parkinson's Disease. *Front Aging Neurosci* **10**, 438, doi:10.3389/fnagi.2018.00438 (2018).
67 Cao, X. Y. *et al.* MicroRNA biomarkers of Parkinson's disease in serum exosome-like microvesicles. *Neurosci Lett* **644**, 94-99, doi:10.1016/j.neulet.2017.02.045 (2017).

68 Feiler, M. S. *et al.* TDP-43 is intercellularly transmitted across axon terminals. *J Cell Biol* **211**, 897-911, doi:10.1083/jcb.201504057 (2015).
69 Soto, C. & Estrada, L. D. Protein misfolding and neurodegeneration. *Arch Neurol* **65**, 184-189, doi:10.1001/archneurol.2007.56 (2008).
70 Ding, X. *et al.* Exposure to ALS-FTD-CSF generates TDP-43 aggregates in glioblastoma cells through exosomes and TNTs-like structure. *Oncotarget* **6**, 24178-24191, doi:10.18632/oncotarget.4680 (2015).
71 Joyce, P. I., Fratta, P., Fisher, E. M. & Acevedo-Arozena, A. SOD1 and TDP-43 animal models of amyotrophic lateral sclerosis: recent advances in understanding disease toward the development of clinical treatments. *Mamm Genome* **22**, 420-448, doi:10.1007/s00335-011-9339-1 (2011).
72 Ludolph, A. C. & Brettschneider, J. TDP-43 in amyotrophic lateral sclerosis - is it a prion disease? *Eur J Neurol* **22**, 753-761, doi:10.1111/ene.12706 (2015).
73 Pascua-Maestro, R. *et al.* Extracellular Vesicles Secreted by Astroglial Cells Transport Apolipoprotein D to Neurons and Mediate Neuronal Survival Upon Oxidative Stress. *Front Cell Neurosci* **12**, 526, doi:10.3389/fncel.2018.00526 (2018).
74 Ferrara, D., Pasetto, L., Bonetto, V. & Basso, M. Role of Extracellular Vesicles in Amyotrophic Lateral Sclerosis. *Front Neurosci* **12**, 574, doi:10.3389/fnins.2018.00574 (2018).
75 Xu, R., Greening, D. W., Zhu, H. J., Takahashi, N. & Simpson, R. J. Extracellular vesicle isolation and characterization: toward clinical application. *J Clin Invest* **126**, 1152-1162, doi:10.1172/JCI81129 (2016).
76 Thery, C., Amigorena, S., Raposo, G. & Clayton, A. Isolation and characterization of exosomes from cell culture supernatants and biological fluids. *Curr Protoc Cell Biol* **Chapter 3**, Unit 3 22, doi:10.1002/0471143030.cb0322s30 (2006).
77 Guo, S. C., Tao, S. C. & Dawn, H. Microfluidics-based on-a-chip systems for isolating and analysing extracellular vesicles. *J Extracell Vesicles* **7**, 1508271, doi:10.1080/20013078.2018.1508271 (2018).
78 Jayachandran, M., Miller, V. M., Heit, J. A. & Owen, W. G. Methodology for isolation, identification and characterization of microvesicles in peripheral blood. *J Immunol Methods* **375**, 207-214, doi:10.1016/j.jim.2011.10.012 (2012).
79 Zeringer, E., Barta, T., Li, M. & Vlassov, A. V. Strategies for isolation of exosomes. *Cold Spring Harb Protoc* **2015**, 319-323, doi:10.1101/pdb.top074476 (2015).
80 Taylor, D. D., Zacharias, W. & Gercel-Taylor, C. Exosome isolation for proteomic analyses and RNA profiling. *Methods Mol Biol* **728**, 235-246, doi:10.1007/978-1-61779-068-3_15 (2011).
81 Tang, Y. T. *et al.* Comparison of isolation methods of exosomes and exosomal RNA from cell culture medium and serum. *Int J Mol Med* **40**, 834-844, doi:10.3892/ijmm.2017.3080 (2017).
82 Taylor, D. D. & Shah, S. Methods of isolating extracellular vesicles impact down-stream analyses of their cargoes. *Methods* **87**, 3-10, doi:10.1016/j.ymeth.2015.02.019 (2015).
83 Liga, A., Vliegenthart, A. D., Oosthuyzen, W., Dear, J. W. & Kersaudy-Kerhoas, M. Exosome isolation: a microfluidic road-map. *Lab Chip* **15**, 2388-2394, doi:10.1039/c5lc00240k (2015).

84 Gholizadeh, S. *et al.* Microfluidic approaches for isolation, detection, and characterization of extracellular vesicles: Current status and future directions. *Biosens Bioelectron* **91**, 588-605, doi:10.1016/j.bios.2016.12.062 (2017).
85 Wunsch, B. H. *et al.* Nanoscale lateral displacement arrays for the separation of exosomes and colloids down to 20 nm. *Nat Nanotechnol* **11**, 936-940, doi:10.1038/nnano.2016.134 (2016).
86 Wang, Z. *et al.* Ciliated micropillars for the microfluidic-based isolation of nanoscale lipid vesicles. *Lab Chip* **13**, 2879-2882, doi:10.1039/c3lc41343h (2013).
87 Davies, R. T. *et al.* Microfluidic filtration system to isolate extracellular vesicles from blood. *Lab Chip* **12**, 5202-5210, doi:10.1039/c2lc41006k (2012).
88 Liu, F. *et al.* The Exosome Total Isolation Chip. *ACS Nano* **11**, 10712-10723, doi:10.1021/acsnano.7b04878 (2017).
89 Kanwar, S. S., Dunlay, C. J., Simeone, D. M. & Nagrath, S. Microfluidic device (ExoChip) for on-chip isolation, quantification and characterization of circulating exosomes. *Lab Chip* **14**, 1891-1900, doi:10.1039/c4lc00136b (2014).
90 Chen, C. *et al.* Microfluidic isolation and transcriptome analysis of serum microvesicles. *Lab Chip* **10**, 505-511, doi:10.1039/b916199f (2010).
91 Andreu, Z. & Yanez-Mo, M. Tetraspanins in extracellular vesicle formation and function. *Front Immunol* **5**, 442, doi:10.3389/fimmu.2014.00442 (2014).
92 Zhang, P., He, M. & Zeng, Y. Ultrasensitive microfluidic analysis of circulating exosomes using a nanostructured graphene oxide/polydopamine coating. *Lab Chip* **16**, 3033-3042, doi:10.1039/c6lc00279j (2016).
93 Chen, Y. S., Ma, Y. D., Chen, C., Shiesh, S. C. & Lee, G. B. An integrated microfluidic system for on-chip enrichment and quantification of circulating extracellular vesicles from whole blood. *Lab Chip* **19**, 3305-3315, doi:10.1039/c9lc00624a (2019).
94 Dudani, J. S. *et al.* Rapid inertial solution exchange for enrichment and flow cytometric detection of microvesicles. *Biomicrofluidics* **9**, 014112, doi:10.1063/1.4907807 (2015).
95 Kang, Y. T. *et al.* Isolation and Profiling of Circulating Tumor-Associated Exosomes Using Extracellular Vesicular Lipid-Protein Binding Affinity Based Microfluidic Device. *Small*, e1903600, doi:10.1002/smll.201903600 (2019).
96 Brzozowski, J. S. *et al.* Lipidomic profiling of extracellular vesicles derived from prostate and prostate cancer cell lines. *Lipids Health Dis* **17**, 211, doi:10.1186/s12944-018-0854-x (2018).
97 Skotland, T., Hessvik, N. P., Sandvig, K. & Llorente, A. Exosomal lipid composition and the role of ether lipids and phosphoinositides in exosome biology. *J Lipid Res* **60**, 9-18, doi:10.1194/jlr.R084343 (2019).
98 Nakai, W. *et al.* A novel affinity-based method for the isolation of highly purified extracellular vesicles. *Sci Rep* **6**, 33935, doi:10.1038/srep33935 (2016).
99 Xu, H., Liao, C., Zuo, P., Liu, Z. & Ye, B. C. Magnetic-Based Microfluidic Device for On-Chip Isolation and Detection of Tumor-Derived Exosomes. *Anal Chem* **90**, 13451-13458, doi:10.1021/acs.analchem.8b03272 (2018).
100 Liang, K. *et al.* Nanoplasmonic Quantification of Tumor-derived Extracellular Vesicles in Plasma Microsamples for Diagnosis and Treatment Monitoring. *Nat Biomed Eng* **1**, doi:10.1038/s41551-016-0021 (2017).
101 Wan, Y. *et al.* Rapid magnetic isolation of extracellular vesicles via lipid-based nanoprobes. *Nat Biomed Eng* **1**, doi:10.1038/s41551-017-0058 (2017).

102 Dragovic, R. A. *et al.* Sizing and phenotyping of cellular vesicles using Nanoparticle Tracking Analysis. *Nanomedicine* **7**, 780-788, doi:10.1016/j.nano.2011.04.003 (2011).
103 Hartjes, T. A., Mytnyk, S., Jenster, G. W., van Steijn, V. & van Royen, M. E. Extracellular Vesicle Quantification and Characterization: Common Methods and Emerging Approaches. *Bioengineering (Basel)* **6**, doi:10.3390/bioengineering6010007 (2019).
104 Chiang, C. Y. & Chen, C. Toward characterizing extracellular vesicles at a single-particle level. *J Biomed Sci* **26**, 9, doi:10.1186/s12929-019-0502-4 (2019).
105 Linares, R., Tan, S., Gounou, C. & Brisson, A. R. Imaging and Quantification of Extracellular Vesicles by Transmission Electron Microscopy. *Methods Mol Biol* **1545**, 43-54, doi:10.1007/978-1-4939-6728-5_4 (2017).
106 Gurunathan, S., Kang, M. H., Jeyaraj, M., Qasim, M. & Kim, J. H. Review of the Isolation, Characterization, Biological Function, and Multifarious Therapeutic Approaches of Exosomes. *Cells* **8**, doi:10.3390/cells8040307 (2019).
107 Sharma, S., LeClaire, M. & Gimzewski, J. K. Ascent of atomic force microscopy as a nanoanalytical tool for exosomes and other extracellular vesicles. *Nanotechnology* **29**, 132001, doi:10.1088/1361-6528/aaab06 (2018).
108 Binnig, G., Quate, C. F. & Gerber, C. Atomic force microscope. *Phys Rev Lett* **56**, 930-933, doi:10.1103/PhysRevLett.56.930 (1986).
109 Sharma, S. *et al.* Structural-mechanical characterization of nanoparticle exosomes in human saliva, using correlative AFM, FESEM, and force spectroscopy. *ACS Nano* **4**, 1921-1926, doi:10.1021/nn901824n (2010).
110 Pospichalova, V. *et al.* Simplified protocol for flow cytometry analysis of fluorescently labeled exosomes and microvesicles using dedicated flow cytometer. *J Extracell Vesicles* **4**, 25530, doi:10.3402/jev.v4.25530 (2015).
111 Nolte-'t Hoen, E. N. *et al.* Quantitative and qualitative flow cytometric analysis of nanosized cell-derived membrane vesicles. *Nanomedicine* **8**, 712-720, doi:10.1016/j.nano.2011.09.006 (2012).
112 Gorgens, A. *et al.* Optimisation of imaging flow cytometry for the analysis of single extracellular vesicles by using fluorescence-tagged vesicles as biological reference material. *J Extracell Vesicles* **8**, 1587567, doi:10.1080/20013078.2019.1587567 (2019).
113 Shao, H. *et al.* New Technologies for Analysis of Extracellular Vesicles. *Chem Rev* **118**, 1917-1950, doi:10.1021/acs.chemrev.7b00534 (2018).
114 Zhang, P. *et al.* Ultrasensitive detection of circulating exosomes with a 3D-nanopatterned microfluidic chip. *Nat Biomed Eng* **3**, 438-451, doi:10.1038/s41551-019-0356-9 (2019).
115 Wang, C. *et al.* Droplet digital PCR improves urinary exosomal miRNA detection compared to real-time PCR. *Clin Biochem* **67**, 54-59, doi:10.1016/j.clinbiochem.2019.03.008 (2019).
116 Chen, W. W. *et al.* BEAMing and Droplet Digital PCR Analysis of Mutant IDH1 mRNA in Glioma Patient Serum and Cerebrospinal Fluid Extracellular Vesicles. *Mol Ther Nucleic Acids* **2**, e109, doi:10.1038/mtna.2013.28 (2013).
117 Yagi, Y. *et al.* Next-generation sequencing-based small RNA profiling of cerebrospinal fluid exosomes. *Neurosci Lett* **636**, 48-57, doi:10.1016/j.neulet.2016.10.042 (2017).
118 Rodriguez, M. *et al.* Identification of non-invasive miRNAs biomarkers for prostate cancer by deep sequencing analysis of urinary exosomes. *Mol Cancer* **16**, 156, doi:10.1186/s12943-017-0726-4 (2017).

119 Jin, X. *et al.* Evaluation of Tumor-Derived Exosomal miRNA as Potential Diagnostic Biomarkers for Early-Stage Non-Small Cell Lung Cancer Using Next-Generation Sequencing. *Clin Cancer Res* **23**, 5311-5319, doi:10.1158/1078-0432.CCR-17-0577 (2017).
120 Huang, X. *et al.* Characterization of human plasma-derived exosomal RNAs by deep sequencing. *BMC Genomics* **14**, 319, doi:10.1186/1471-2164-14-319 (2013).
121 Buschmann, D. *et al.* Evaluation of serum extracellular vesicle isolation methods for profiling miRNAs by next-generation sequencing. *J Extracell Vesicles* **7**, 1481321, doi:10.1080/20013078.2018.1481321 (2018).
122 Veldman-Jones, M. H. *et al.* Evaluating Robustness and Sensitivity of the NanoString Technologies nCounter Platform to Enable Multiplexed Gene Expression Analysis of Clinical Samples. *Cancer Res* **75**, 2587-2593, doi:10.1158/0008-5472.CAN-15-0262 (2015).
123 Geiss, G. K. *et al.* Direct multiplexed measurement of gene expression with color-coded probe pairs. *Nat Biotechnol* **26**, 317-325, doi:10.1038/nbt1385 (2008).
124 Mitchell, J. D. & Borasio, G. D. Amyotrophic lateral sclerosis. *Lancet* **369**, 2031-2041, doi:10.1016/S0140-6736(07)60944-1 (2007).
125 Hardiman, O., van den Berg, L. H. & Kiernan, M. C. Clinical diagnosis and management of amyotrophic lateral sclerosis. *Nat Rev Neurol* **7**, 639-649, doi:10.1038/nrneurol.2011.153 (2011).
126 Blackhall, L. J. Amyotrophic lateral sclerosis and palliative care: where we are, and the road ahead. *Muscle & nerve* **45**, 311-318, doi:10.1002/mus.22305 (2012).
127 Chen, S., Sayana, P., Zhang, X. & Le, W. Genetics of amyotrophic lateral sclerosis: an update. *Mol Neurodegener* **8**, 28, doi:10.1186/1750-1326-8-28 (2013).
128 Paez-Colasante, X., Figueroa-Romero, C., Sakowski, S. A., Goutman, S. A. & Feldman, E. L. Amyotrophic lateral sclerosis: mechanisms and therapeutics in the epigenomic era. *Nat Rev Neurol* **11**, 266-279, doi:10.1038/nrneurol.2015.57 (2015).
129 Hoye, M. L. *et al.* MicroRNA Profiling Reveals Marker of Motor Neuron Disease in ALS Models. *J Neurosci* **37**, 5574-5586, doi:10.1523/JNEUROSCI.3582-16.2017 (2017).
130 Rothstein, J. D. Current hypotheses for the underlying biology of amyotrophic lateral sclerosis. *Ann Neurol* **65 Suppl 1**, S3-9, doi:10.1002/ana.21543 (2009).
131 Bensimon, G., Lacomblez, L. & Meininger, V. A controlled trial of riluzole in amyotrophic lateral sclerosis. ALS/Riluzole Study Group. *N Engl J Med* **330**, 585-591, doi:10.1056/NEJM199403033300901 (1994).
132 Figueroa-Romero, C. *et al.* Expression of microRNAs in human post-mortem amyotrophic lateral sclerosis spinal cords provides insight into disease mechanisms. *Mol Cell Neurosci* **71**, 34-45, doi:10.1016/j.mcn.2015.12.008 (2016).
133 Khairoalsindi, O. A. & Abuzinadah, A. R. Maximizing the Survival of Amyotrophic Lateral Sclerosis Patients: Current Perspectives. *Neurol Res Int* **2018**, 6534150, doi:10.1155/2018/6534150 (2018).
134 Boukouris, S. & Mathivanan, S. Exosomes in bodily fluids are a highly stable resource of disease biomarkers. *Proteomics Clin Appl* **9**, 358-367, doi:10.1002/prca.201400114 (2015).
135 Lee, Y., El Andaloussi, S. & Wood, M. J. Exosomes and microvesicles: extracellular vesicles for genetic information transfer and gene therapy. *Hum Mol Genet* **21**, R125-134, doi:10.1093/hmg/dds317 (2012).

136 Soria, F. N. *et al.* Exosomes, an Unmasked Culprit in Neurodegenerative Diseases. *Front Neurosci* **11**, 26, doi:10.3389/fnins.2017.00026 (2017).
137 Basso, M. & Bonetto, V. Extracellular Vesicles and a Novel Form of Communication in the Brain. *Front Neurosci* **10**, 127, doi:10.3389/fnins.2016.00127 (2016).
138 Chiasserini, D. *et al.* Proteomic analysis of cerebrospinal fluid extracellular vesicles: a comprehensive dataset. *J Proteomics* **106**, 191-204, doi:10.1016/j.jprot.2014.04.028 (2014).
139 Rak, J. & Guha, A. Extracellular vesicles--vehicles that spread cancer genes. *Bioessays* **34**, 489-497, doi:10.1002/bies.201100169 (2012).
140 Datta Chaudhuri, A. *et al.* Stimulus-dependent modifications in astrocyte-derived extracellular vesicle cargo regulate neuronal excitability. *Glia*, doi:10.1002/glia.23708 (2019).
141 Ramirez, S. H., Andrews, A. M., Paul, D. & Pachter, J. S. Extracellular vesicles: mediators and biomarkers of pathology along CNS barriers. *Fluids Barriers CNS* **15**, 19, doi:10.1186/s12987-018-0104-7 (2018).
142 Andras, I. E. & Toborek, M. Extracellular vesicles of the blood-brain barrier. *Tissue Barriers* **4**, e1131804, doi:10.1080/21688370.2015.1131804 (2016).
143 Liu, C. G., Song, J., Zhang, Y. Q. & Wang, P. C. MicroRNA-193b is a regulator of amyloid precursor protein in the blood and cerebrospinal fluid derived exosomal microRNA-193b is a biomarker of Alzheimer's disease. *Mol Med Rep* **10**, 2395-2400, doi:10.3892/mmr.2014.2484 (2014).
144 Blandford, S. N., Galloway, D. A. & Moore, C. S. The roles of extracellular vesicle microRNAs in the central nervous system. *Glia* **66**, 2267-2278, doi:10.1002/glia.23445 (2018).
145 Bartel, D. P. MicroRNAs: genomics, biogenesis, mechanism, and function. *Cell* **116**, 281-297 (2004).
146 Lagos-Quintana, M., Rauhut, R., Lendeckel, W. & Tuschl, T. Identification of novel genes coding for small expressed RNAs. *Science* **294**, 853-858, doi:10.1126/science.1064921 (2001).
147 Vella, L. J. *et al.* A rigorous method to enrich for exosomes from brain tissue. *J Extracell Vesicles* **6**, 1348885, doi:10.1080/20013078.2017.1348885 (2017).
148 Lee, S., Mankhong, S. & Kang, J. H. Extracellular Vesicle as a Source of Alzheimer's Biomarkers: Opportunities and Challenges. *Int J Mol Sci* **20**, doi:10.3390/ijms20071728 (2019).
149 Brooks, B. R., Miller, R. G., Swash, M., Munsat, T. L. & World Federation of Neurology Research Group on Motor Neuron, D. El Escorial revisited: revised criteria for the diagnosis of amyotrophic lateral sclerosis. *Amyotrophic lateral sclerosis and other motor neuron disorders : official publication of the World Federation of Neurology, Research Group on Motor Neuron Diseases* **1**, 293-299 (2000).
150 Banigan, M. G. *et al.* Differential expression of exosomal microRNAs in prefrontal cortices of schizophrenia and bipolar disorder patients. *PLoS One* **8**, e48814, doi:10.1371/journal.pone.0048814 (2013).
151 Valeri, N. *et al.* MicroRNA-135b promotes cancer progression by acting as a downstream effector of oncogenic pathways in colon cancer. *Cancer Cell* **25**, 469-483, doi:10.1016/j.ccr.2014.03.006 (2014).

152 Wang, H. *et al.* NanoStringDiff: a novel statistical method for differential expression analysis based on NanoString nCounter data. *Nucleic Acids Res* **44**, e151, doi:10.1093/nar/gkw677 (2016).
153 Vlachos, I. S. *et al.* DIANA-miRPath v3.0: deciphering microRNA function with experimental support. *Nucleic Acids Res* **43**, W460-466, doi:10.1093/nar/gkv403 (2015).
154 Tsang, H. F. *et al.* NanoString, a novel digital color-coded barcode technology: current and future applications in molecular diagnostics. *Expert Rev Mol Diagn* **17**, 95-103, doi:10.1080/14737159.2017.1268533 (2017).
155 Su, G., Morris, J. H., Demchak, B. & Bader, G. D. Biological network exploration with Cytoscape 3. *Curr Protoc Bioinformatics* **47**, 8 13 11-24, doi:10.1002/0471250953.bi0813s47 (2014).
156 Bader, G. D. & Hogue, C. W. An automated method for finding molecular complexes in large protein interaction networks. *BMC Bioinformatics* **4**, 2 (2003).
157 Pulliam, L., Sun, B., Mustapic, M., Chawla, S. & Kapogiannis, D. Plasma neuronal exosomes serve as biomarkers of cognitive impairment in HIV infection and Alzheimer's disease. *J Neurovirol*, doi:10.1007/s13365-018-0695-4 (2019).
158 Katsuda, T., Kosaka, N. & Ochiya, T. The roles of extracellular vesicles in cancer biology: toward the development of novel cancer biomarkers. *Proteomics* **14**, 412-425, doi:10.1002/pmic.201300389 (2014).
159 Tomlinson, P. R. *et al.* Identification of distinct circulating exosomes in Parkinson's disease. *Ann Clin Transl Neurol* **2**, 353-361, doi:10.1002/acn3.175 (2015).
160 Silva, J. *et al.* Analysis of exosome release and its prognostic value in human colorectal cancer. *Genes Chromosomes Cancer* **51**, 409-418 (2012).
161 Eitan, E. *et al.* Age-Related Changes in Plasma Extracellular Vesicle Characteristics and Internalization by Leukocytes. *Sci Rep* **7**, 1342, doi:10.1038/s41598-017-01386-z (2017).
162 Frampton, A. E. *et al.* Glypican-1 is enriched in circulating-exosomes in pancreatic cancer and correlates with tumor burden. *Oncotarget* **9**, 19006-19013, doi:10.18632/oncotarget.24873 (2018).
163 Hosaka, T., Yamashita, T., Tamaoka, A. & Kwak, S. Extracellular RNAs as Biomarkers of Sporadic Amyotrophic Lateral Sclerosis and Other Neurodegenerative Diseases. *Int J Mol Sci* **20**, doi:10.3390/ijms20133148 (2019).
164 Saucier, D. *et al.* Identification of a circulating miRNA signature in extracellular vesicles collected from amyotrophic lateral sclerosis patients. *Brain Res* **1708**, 100-108, doi:10.1016/j.brainres.2018.12.016 (2019).
165 Varcianna, A. *et al.* Micro-RNAs secreted through astrocyte-derived extracellular vesicles cause neuronal network degeneration in C9orf72 ALS. *EBioMedicine* **40**, 626-635, doi:10.1016/j.ebiom.2018.11.067 (2019).
166 Volonte, C., Apolloni, S. & Parisi, C. MicroRNAs: newcomers into the ALS picture. *CNS Neurol Disord Drug Targets* **14**, 194-207 (2015).
167 Freischmidt, A., Muller, K., Ludolph, A. C. & Weishaupt, J. H. Systemic dysregulation of TDP-43 binding microRNAs in amyotrophic lateral sclerosis. *Acta Neuropathol Commun* **1**, 42, doi:10.1186/2051-5960-1-42 (2013).
168 Guo, D., Ma, J., Li, T. & Yan, L. Up-regulation of miR-122 protects against neuronal cell death in ischemic stroke through the heat shock protein 70-dependent NF-kappaB pathway by targeting FOXO3. *Exp Cell Res* **369**, 34-42, doi:10.1016/j.yexcr.2018.04.027 (2018).

169 Aryal, B., Singh, A. K., Rotllan, N., Price, N. & Fernandez-Hernando, C. MicroRNAs and lipid metabolism. *Curr Opin Lipidol* **28**, 273-280, doi:10.1097/MOL.0000000000000420 (2017).
170 Tracey, T. J., Steyn, F. J., Wolvetang, E. J. & Ngo, S. T. Neuronal Lipid Metabolism: Multiple Pathways Driving Functional Outcomes in Health and Disease. *Front Mol Neurosci* **11**, 10, doi:10.3389/fnmol.2018.00010 (2018).
171 Wen, Z. *et al.* Overexpression of miR185 inhibits autophagy and apoptosis of dopaminergic neurons by regulating the AMPK/mTOR signaling pathway in Parkinson's disease. *Mol Med Rep* **17**, 131-137, doi:10.3892/mmr.2017.7897 (2018).
172 Qadir, X. V., Han, C., Lu, D., Zhang, J. & Wu, T. miR-185 inhibits hepatocellular carcinoma growth by targeting the DNMT1/PTEN/Akt pathway. *Am J Pathol* **184**, 2355-2364, doi:10.1016/j.ajpath.2014.05.004 (2014).
173 Figueroa-Romero, C. *et al.* Identification of epigenetically altered genes in sporadic amyotrophic lateral sclerosis. *PLoS One* **7**, e52672, doi:10.1371/journal.pone.0052672 (2012).
174 Chan, M. *et al.* Identification of circulating microRNA signatures for breast cancer detection. *Clin Cancer Res* **19**, 4477-4487, doi:10.1158/1078-0432.CCR-12-3401 (2013).
175 Perera, N. D. & Turner, B. J. AMPK Signalling and Defective Energy Metabolism in Amyotrophic Lateral Sclerosis. *Neurochem Res* **41**, 544-553, doi:10.1007/s11064-015-1665-3 (2016).
176 Nieto-Gonzalez, J. L., Moser, J., Lauritzen, M., Schmitt-John, T. & Jensen, K. Reduced GABAergic inhibition explains cortical hyperexcitability in the wobbler mouse model of ALS. *Cereb Cortex* **21**, 625-635, doi:10.1093/cercor/bhq134 (2011).
177 Menon, P. *et al.* Cortical hyperexcitability and disease spread in amyotrophic lateral sclerosis. *Eur J Neurol* **24**, 816-824, doi:10.1111/ene.13295 (2017).
178 Libro, R., Bramanti, P. & Mazzon, E. The role of the Wnt canonical signaling in neurodegenerative diseases. *Life Sci* **158**, 78-88, doi:10.1016/j.lfs.2016.06.024 (2016).
179 Wang, S. *et al.* Role of Wnt1 and Fzd1 in the spinal cord pathogenesis of amyotrophic lateral sclerosis-transgenic mice. *Biotechnol Lett* **35**, 1199-1207, doi:10.1007/s10529-013-1199-1 (2013).
180 Chen, Y. *et al.* Activation of the Wnt/beta-catenin signaling pathway is associated with glial proliferation in the adult spinal cord of ALS transgenic mice. *Biochem Biophys Res Commun* **420**, 397-403, doi:10.1016/j.bbrc.2012.03.006 (2012).
181 Taguchi, Y. H. & Wang, H. Exploring microRNA Biomarker for Amyotrophic Lateral Sclerosis. *Int J Mol Sci* **19**, doi:10.3390/ijms19051318 (2018).
182 Peters, S. *et al.* The TGF-beta System As a Potential Pathogenic Player in Disease Modulation of Amyotrophic Lateral Sclerosis. *Front Neurol* **8**, 669, doi:10.3389/fneur.2017.00669 (2017).
183 Korner, S., Thau-Habermann, N., Kefalakes, E., Bursch, F. & Petri, S. Expression of the axon-guidance protein receptor Neuropilin 1 is increased in the spinal cord and decreased in muscle of a mouse model of amyotrophic lateral sclerosis. *Eur J Neurosci* **49**, 1529-1543, doi:10.1111/ejn.14326 (2019).
184 Van Battum, E. Y., Brignani, S. & Pasterkamp, R. J. Axon guidance proteins in neurological disorders. *Lancet Neurol* **14**, 532-546, doi:10.1016/S1474-4422(14)70257-1 (2015).

185 Freedman, D. M. *et al.* The association between cancer and amyotrophic lateral sclerosis. *Cancer Causes Control* **24**, 55-60, doi:10.1007/s10552-012-0089-5 (2013).
186 Klus, P., Cirillo, D., Botta Orfila, T. & Gaetano Tartaglia, G. Neurodegeneration and Cancer: Where the Disorder Prevails. *Sci Rep* **5**, 15390, doi:10.1038/srep15390 (2015).
187 Baade, P. D., Fritschi, L. & Freedman, D. M. Mortality due to amyotrophic lateral sclerosis and Parkinson's disease among melanoma patients. *Neuroepidemiology* **28**, 16-20, doi:10.1159/000097851 (2007).
188 Han, Y. Analysis of the role of the Hippo pathway in cancer. *J Transl Med* **17**, 116, doi:10.1186/s12967-019-1869-4 (2019).
189 Wang, Y. *et al.* Comprehensive Molecular Characterization of the Hippo Signaling Pathway in Cancer. *Cell Rep* **25**, 1304-1317 e1305, doi:10.1016/j.celrep.2018.10.001 (2018).
190 Lee, J. K. *et al.* MST1 functions as a key modulator of neurodegeneration in a mouse model of ALS. *Proc Natl Acad Sci U S A* **110**, 12066-12071, doi:10.1073/pnas.1300894110 (2013).
191 Wang, S. P. & Wang, L. H. Disease implication of hyper-Hippo signalling. *Open Biol* **6**, doi:10.1098/rsob.160119 (2016).
192 Kim, E. K. & Choi, E. J. Compromised MAPK signaling in human diseases: an update. *Arch Toxicol* **89**, 867-882, doi:10.1007/s00204-015-1472-2 (2015).
193 Ackerley, S. *et al.* p38alpha stress-activated protein kinase phosphorylates neurofilaments and is associated with neurofilament pathology in amyotrophic lateral sclerosis. *Mol Cell Neurosci* **26**, 354-364, doi:10.1016/j.mcn.2004.02.009 (2004).
194 Jan, A. T. *et al.* Perspective Insights of Exosomes in Neurodegenerative Diseases: A Critical Appraisal. *Front Aging Neurosci* **9**, 317, doi:10.3389/fnagi.2017.00317 (2017).
195 S, E. L. A., Mager, I., Breakefield, X. O. & Wood, M. J. Extracellular vesicles: biology and emerging therapeutic opportunities. *Nat Rev Drug Discov* **12**, 347-357, doi:10.1038/nrd3978 (2013).
196 van Balkom, B. W. *et al.* Endothelial cells require miR-214 to secrete exosomes that suppress senescence and induce angiogenesis in human and mouse endothelial cells. *Blood* **121**, 3997-4006, S3991-3915, doi:10.1182/blood-2013-02-478925 (2013).
197 Barros, F. M., Carneiro, F., Machado, J. C. & Melo, S. A. Exosomes and Immune Response in Cancer: Friends or Foes? *Front Immunol* **9**, 730, doi:10.3389/fimmu.2018.00730 (2018).
198 Xu, R. *et al.* Extracellular vesicles in cancer - implications for future improvements in cancer care. *Nat Rev Clin Oncol* **15**, 617-638, doi:10.1038/s41571-018-0036-9 (2018).
199 Candelario, K. M. & Steindler, D. A. The role of extracellular vesicles in the progression of neurodegenerative disease and cancer. *Trends Mol Med* **20**, 368-374, doi:10.1016/j.molmed.2014.04.003 (2014).
200 Yang, F. *et al.* Exosomal miRNAs and miRNA dysregulation in cancer-associated fibroblasts. *Mol Cancer* **16**, 148, doi:10.1186/s12943-017-0718-4 (2017).
201 Cazzoli, R. *et al.* microRNAs derived from circulating exosomes as noninvasive biomarkers for screening and diagnosing lung cancer. *J Thorac Oncol* **8**, 1156-1162, doi:10.1097/JTO.0b013e318299ac32 (2013).
202 Fabbri, M. *et al.* MicroRNAs bind to Toll-like receptors to induce prometastatic inflammatory response. *Proc Natl Acad Sci U S A* **109**, E2110-2116, doi:10.1073/pnas.1209414109 (2012).

203 Fujita, Y., Yoshioka, Y. & Ochiya, T. Extracellular vesicle transfer of cancer pathogenic components. *Cancer Sci* **107**, 385-390, doi:10.1111/cas.12896 (2016).
204 Salido-Guadarrama, I., Romero-Cordoba, S., Peralta-Zaragoza, O., Hidalgo-Miranda, A. & Rodriguez-Dorantes, M. MicroRNAs transported by exosomes in body fluids as mediators of intercellular communication in cancer. *Onco Targets Ther* **7**, 1327-1338, doi:10.2147/OTT.S61562 (2014).
205 Vinaiphat, A. & Sze, S. K. Clinical implications of extracellular vesicles in neurodegenerative diseases. *Expert Rev Mol Diagn* **19**, 813-824, doi:10.1080/14737159.2019.1657407 (2019).
206 Croese, T. & Furlan, R. Extracellular vesicles in neurodegenerative diseases. *Mol Aspects Med* **60**, 52-61, doi:10.1016/j.mam.2017.11.006 (2018).
207 Momen-Heravi, F. Isolation of Extracellular Vesicles by Ultracentrifugation. *Methods Mol Biol* **1660**, 25-32, doi:10.1007/978-1-4939-7253-1_3 (2017).
208 Witwer, K. W. *et al.* Standardization of sample collection, isolation and analysis methods in extracellular vesicle research. *J Extracell Vesicles* **2**, doi:10.3402/jev.v2i0.20360 (2013).
209 Kowal, J. *et al.* Proteomic comparison defines novel markers to characterize heterogeneous populations of extracellular vesicle subtypes. *Proc Natl Acad Sci U S A* **113**, E968-977, doi:10.1073/pnas.1521230113 (2016).
210 Koliha, N. *et al.* A novel multiplex bead-based platform highlights the diversity of extracellular vesicles. *J Extracell Vesicles* **5**, 29975, doi:10.3402/jev.v5.29975 (2016).
211 Sharma, P. *et al.* Immunoaffinity-based isolation of melanoma cell-derived exosomes from plasma of patients with melanoma. *J Extracell Vesicles* **7**, 1435138, doi:10.1080/20013078.2018.1435138 (2018).
212 Vaidyanathan, R. *et al.* Detecting exosomes specifically: a multiplexed device based on alternating current electrohydrodynamic induced nanoshearing. *Anal Chem* **86**, 11125-11132, doi:10.1021/ac502082b (2014).
213 Luka, G. *et al.* Microfluidics Integrated Biosensors: A Leading Technology towards Lab-on-a-Chip and Sensing Applications. *Sensors (Basel)* **15**, 30011-30031, doi:10.3390/s151229783 (2015).
214 Yoon, H. J. *et al.* Sensitive capture of circulating tumour cells by functionalized graphene oxide nanosheets. *Nat Nanotechnol* **8**, 735-741, doi:10.1038/nnano.2013.194 (2013).
215 Hirsch, J. D. *et al.* Easily reversible desthiobiotin binding to streptavidin, avidin, and other biotin-binding proteins: uses for protein labeling, detection, and isolation. *Anal Biochem* **308**, 343-357, doi:10.1016/s0003-2697(02)00201-4 (2002).
216 Holmberg, A. *et al.* The biotin-streptavidin interaction can be reversibly broken using water at elevated temperatures. *Electrophoresis* **26**, 501-510, doi:10.1002/elps.200410070 (2005).
217 Ansari, A., Lee-Montiel, F. T., Amos, J. R. & Imoukhuede, P. I. Secondary anchor targeted cell release. *Biotechnol Bioeng* **112**, 2214-2227, doi:10.1002/bit.25648 (2015).
218 Murlidhar, V. *et al.* A radial flow microfluidic device for ultra-high-throughput affinity-based isolation of circulating tumor cells. *Small* **10**, 4895-4904, doi:10.1002/smll.201400719 (2014).
219 Murlidhar, V. *et al.* Poor Prognosis Indicated by Venous Circulating Tumor Cell Clusters in Early-Stage Lung Cancers. *Cancer Res* **77**, 5194-5206, doi:10.1158/0008-5472.CAN-16-2072 (2017).

220 Zhu, Z. *et al.* Macrophage-derived apoptotic bodies promote the proliferation of the recipient cells via shuttling microRNA-221/222. *J Leukoc Biol* **101**, 1349-1359, doi:10.1189/jlb.3A1116-483R (2017).
221 Crescitelli, R. *et al.* Distinct RNA profiles in subpopulations of extracellular vesicles: apoptotic bodies, microvesicles and exosomes. *J Extracell Vesicles* **2**, doi:10.3402/jev.v2i0.20677 (2013).
222 Zhang, L., Jamaluddin, M. S., Weakley, S. M., Yao, Q. & Chen, C. Roles and mechanisms of microRNAs in pancreatic cancer. *World J Surg* **35**, 1725-1731, doi:10.1007/s00268-010-0952-z (2011).
223 Mindell, J. A. Lysosomal acidification mechanisms. *Annu Rev Physiol* **74**, 69-86, doi:10.1146/annurev-physiol-012110-142317 (2012).
224 Ferri, K. F. & Kroemer, G. Organelle-specific initiation of cell death pathways. *Nat Cell Biol* **3**, E255-263, doi:10.1038/ncb1101-e255 (2001).
225 Metro, G. & Crino, L. Advances on EGFR mutation for lung cancer. *Transl Lung Cancer Res* **1**, 5-13, doi:10.3978/j.issn.2218-6751.2011.12.01 (2012).
226 Wu, C. P., Wu, P., Zhao, H. F., Liu, W. L. & Li, W. P. Clinical Applications of and Challenges in Single-Cell Analysis of Circulating Tumor Cells. *DNA Cell Biol* **37**, 78-89, doi:10.1089/dna.2017.3981 (2018).
227 Dong, X., Alpaugh, K. R. & Cristofanilli, M. Circulating tumor cells (CTCs) in breast cancer: a diagnostic tool for prognosis and molecular analysis. *Chin J Cancer Res* **24**, 388-398, doi:10.3978/j.issn.1000-9604.2012.11.03 (2012).
228 Cohen, S. J. *et al.* Relationship of circulating tumor cells to tumor response, progression-free survival, and overall survival in patients with metastatic colorectal cancer. *J Clin Oncol* **26**, 3213-3221, doi:10.1200/JCO.2007.15.8923 (2008).
229 Hayes, D. F. *et al.* Circulating tumor cells at each follow-up time point during therapy of metastatic breast cancer patients predict progression-free and overall survival. *Clin Cancer Res* **12**, 4218-4224, doi:10.1158/1078-0432.CCR-05-2821 (2006).
230 de Bono, J. S. *et al.* Circulating tumor cells predict survival benefit from treatment in metastatic castration-resistant prostate cancer. *Clin Cancer Res* **14**, 6302-6309, doi:10.1158/1078-0432.CCR-08-0872 (2008).
231 Wang, C. *et al.* Longitudinally collected CTCs and CTC-clusters and clinical outcomes of metastatic breast cancer. *Breast Cancer Res Treat* **161**, 83-94, doi:10.1007/s10549-016-4026-2 (2017).
232 Haber, D. A. & Velculescu, V. E. Blood-based analyses of cancer: circulating tumor cells and circulating tumor DNA. *Cancer Discov* **4**, 650-661, doi:10.1158/2159-8290.CD-13-1014 (2014).
233 Wang, W., Song, Z. & Zhang, Y. A Comparison of ddPCR and ARMS for detecting EGFR T790M status in ctDNA from advanced NSCLC patients with acquired EGFR-TKI resistance. *Cancer Med* **6**, 154-162, doi:10.1002/cam4.978 (2017).
234 Odogwu, L. *et al.* FDA Benefit-Risk Assessment of Osimertinib for the Treatment of Metastatic Non-Small Cell Lung Cancer Harboring Epidermal Growth Factor Receptor T790M Mutation. *Oncologist* **23**, 353-359, doi:10.1634/theoncologist.2017-0425 (2018).
235 U.S. Food and Drug Administration. Summary of safety and effectiveness data: cobas EGFR Mutation Test v2 (2016) [cited December 8, 2019] Available from: <http://www.accessdata.fda.gov/cdrh_docs/pdf15/P150044B.pdf>.

236 Lianidou, E. S. & Markou, A. Circulating tumor cells in breast cancer: detection systems, molecular characterization, and future challenges. *Clin Chem* **57**, 1242-1255, doi:10.1373/clinchem.2011.165068 (2011).
237 Patil, P., Madhuprasad, Kumeria, T., Losic, D. & Kurkuri, M. Isolation of circulating tumour cells by physical means in a microfluidic device: a review. *Rsc Adv* **5**, 89745-89762, doi:10.1039/c5ra16489c (2015).
238 Esmaeilsabzali, H., Beischlag, T. V., Cox, M. E., Parameswaran, A. M. & Park, E. J. Detection and isolation of circulating tumor cells: principles and methods. *Biotechnol Adv* **31**, 1063-1084, doi:10.1016/j.biotechadv.2013.08.016 (2013).
239 Mostert, B., Sleijfer, S., Foekens, J. A. & Gratama, J. W. Circulating tumor cells (CTCs): detection methods and their clinical relevance in breast cancer. *Cancer Treat Rev* **35**, 463-474, doi:10.1016/j.ctrv.2009.03.004 (2009).
240 Sharma, S. *et al.* Using single cell analysis for translational studies in immune mediated diseases: Opportunities and challenges. *Mol Immunol* **103**, 191-199, doi:10.1016/j.molimm.2018.09.020 (2018).
241 Whale, A. S., Huggett, J. F. & Tzonev, S. Fundamentals of multiplexing with digital PCR. *Biomol Detect Quantif* **10**, 15-23, doi:10.1016/j.bdq.2016.05.002 (2016).
242 Zonta, E. *et al.* Multiplex Detection of Rare Mutations by Picoliter Droplet Based Digital PCR: Sensitivity and Specificity Considerations. *PLoS One* **11**, e0159094, doi:10.1371/journal.pone.0159094 (2016).
243 Lin, E. *et al.* High-Throughput Microfluidic Labyrinth for the Label-free Isolation of Circulating Tumor Cells. *Cell Syst* **5**, 295-304 e294, doi:10.1016/j.cels.2017.08.012 (2017).
244 Suda, K., Onozato, R., Yatabe, Y. & Mitsudomi, T. EGFR T790M mutation: a double role in lung cancer cell survival? *J Thorac Oncol* **4**, 1-4, doi:10.1097/JTO.0b013e3181913c9f (2009).
245 Wang, Y. & Ellis, P. EGFR mutation positive non-small cell lung cancer: can we identify predictors of benefit from immune checkpoint inhibitors. *Ann Transl Med* **5**, 424, doi:10.21037/atm.2017.08.14 (2017).
246 Jiang, X. W., Liu, W., Zhu, X. Y. & Xu, X. X. Evaluation of EGFR mutations in NSCLC with highly sensitive droplet digital PCR assays. *Mol Med Rep* **20**, 593-603, doi:10.3892/mmr.2019.10259 (2019).
247 Sun, H. B. *et al.* Association between hormone receptor expression and epidermal growth factor receptor mutation in patients operated on for non-small cell lung cancer. *Ann Thorac Surg* **91**, 1562-1567, doi:10.1016/j.athoracsur.2011.02.001 (2011).
248 Hsu, L. H., Chu, N. M. & Kao, S. H. Estrogen, Estrogen Receptor and Lung Cancer. *Int J Mol Sci* **18**, doi:10.3390/ijms18081713 (2017).
249 Hargadon, K. M. Dysregulation of TGFbeta1 Activity in Cancer and Its Influence on the Quality of Anti-Tumor Immunity. *J Clin Med* **5**, doi:10.3390/jcm5090076 (2016).